

**ELECTRICAL CONDUCTIVITY OF SEGREGATED NETWORK POLYMER
NANOCOMPOSITES**

A Dissertation

by

YEON SEOK KIM

Submitted to the Office of Graduate Studies of
Texas A&M University
in partial fulfillment of the requirements for the degree of

DOCTOR OF PHILOSOPHY

May 2007

Major Subject: Mechanical Engineering

**ELECTRICAL CONDUCTIVITY OF SEGREGATED NETWORK POLYMER
NANOCOMPOSITES**

A Dissertation

by

YEON SEOK KIM

Submitted to the Office of Graduate Studies of
Texas A&M University
in partial fulfillment of the requirements for the degree of

DOCTOR OF PHILOSOPHY

Approved by:

Chair of Committee,
Committee Members,

Head of Department,

Jaime C. Grunlan
Hung-Jue Sue
Roger J. Morgan
Zoubeida Ounaies
Dennis L. O'Neal

May 2007

Major Subject: Mechanical Engineering

ABSTRACT

Electrical Conductivity of Segregated Network Polymer

Nanocomposites . (May 2007)

Yeon Seok Kim, B.S., Chung-Ang University;

M.S., Purdue University

Chair of Advisory Committee: Dr. Jaime C. Grunlan

A set of experiments was designed and performed to gain a fundamental understanding of various aspects of the segregated network concept. The electrical and mechanical properties of composites made from commercial latex and carbon black are compared with another composite made from a polymer solution. The percolation threshold of the emulsion-based composite is nearly one order of magnitude lower than that of the solution-based composite. The segregated network composite also shows significant improvement in both electrical and mechanical properties with low carbon black loading, while the solution-based composite achieves its maximum enhancement at higher carbon black loading (~25wt%). The effect of the particle size ratio between the polymer particle and the filler was also studied. In order to create a composite with an extremely large particle size ratio ($> 80,000$), layer-by-layer assembly was used to coat large polyethylene particles with the carbon black. Hyper-branched polyethylenimine was covalently grafted to the surface of polyethylene to promote the film growth. The resulting composite has a percolation threshold below 0.1 wt%, which is the lowest percolation threshold ever reported for a carbon-filled composite.

Theoretical predictions suggest that the actual percolation threshold may be lower than 0.002 wt%.

Finally, the effect of the emulsion polymer modulus on the segregated network was studied. Monodispersed emulsions with the different glass transition temperature were used as the matrix. The composites made using the emulsion with higher modulus show lower percolation threshold and higher conductivity. Higher modulus causes tighter packing of carbon black between the polymer particles. When the drying temperature was increased to 80°C, the percolation thresholds became closer between some systems because their moduli were very close. This work suggests modulus is a variable that can be used to tailor percolation threshold and electrical conductivity, along with polymer particle size.

*To
My beloved wife, Jahee,
My daughter, Katie, and
My Lord Jesus*

ACKNOWLEDGEMENTS

I would like to express my sincere gratitude to my academic advisor, Dr. Jaime C. Grunlan, for his inspiration, advice, and encouragement. He helped me to be a productive researcher and earn my Ph. D. degree in less than three years. I also thank my committee members, Dr. Sue, Dr. Morgan, and Dr. Ounaies. Special thanks are also given to Dr. Bergbreiter and his Ph. D. student, Kang-Shyang Liao, in the Chemistry Department for providing functionalized polyethylene particles and participating in many helpful discussions for a journal paper that was published at *Chemistry of Materials*. I am grateful to Dr. Wei and his student, Kun Tao, at Texas Southern University for their help in DMA and DSC testing. I appreciate the assistance of Mr. Tom Stephan at the Microscopy & Imaging Center at Texas A&M University for SEM work. I would like to thank my former and current colleagues: Woong Jae Boo, Lei Liu, Woo-sik Jang, Maricela Lizcano, Thomas Dawidczyk, Sethu Miriyala, Jason Jan, John Wright, and many others who helped me in many ways. Finally, I thank my family who has supported me throughout my studies. Without them, not any of my work would have been possible.

TABLE OF CONTENTS

	Page
ABSTRACT	iii
DEDICATION	v
ACKNOWLEDGEMENTS	vi
TABLE OF CONTENTS	vii
LIST OF TABLES	x
LIST OF FIGURES.....	xi
 CHAPTER	
I INTRODUCTION.....	1
1.1 Background	1
1.2 Objectives and Dissertation Outline.....	3
II LITERATURE REVIEW.....	7
2.1 Percolation Theory and Models	7
2.2 Composites with Randomly Dispersed Filler.....	12
2.3 Segregated Network Composites	15
III EFFECT OF MICROSTRUCTURE ON THE ELECTRICAL AND MECHANICAL PROPERTIES OF THE POLYMER COMPOSITES WITH CARBON BLACK.....	21
3.1 Introduction	21
3.2 Experimental	22
3.2.1 Materials.....	22
3.2.2 Emulsion-Based Composite Preparation.....	22
3.2.3 Solution-Based Composite Preparation	23
3.2.4 Composite Characterization	23
3.2.4.1 Electrical Conductivity	23
3.2.4.2 Thermomechanical Properties	24
3.2.4.3 Composite Microstructure	25
3.3 Results and Discussion.....	25

CHAPTER	Page
3.3.1 Composite Microstructure.....	25
3.3.2 Electrical Conductivity.....	29
3.3.3 Storage Modulus.....	32
3.4 Conclusion.....	33
 IV CONDUCTIVE THIN FILMS ON FUNCTIONALIZED POLYETHYLENE PARTICLES.....	 35
4.1 Introduction.....	35
4.2 Experimental.....	40
4.2.1 Materials.....	40
4.2.2 Preparation of PEI/Gantrez Hyperbranched Grafts on Oxidized PE Particle.....	40
4.2.3 Preparation of PEI/Gantrez Oxidized PE Particles.....	41
4.2.4 Carbon Black Mixture Preparation.....	42
4.2.5 Film Deposition.....	42
4.2.6 Characterizations of the Particle and Coating.....	42
4.3 Results and Discussion.....	43
4.3.1 PEI-Grafted Polyethylene.....	43
4.3.2 Carbon Black Coated Particles.....	48
4.3.3 Segregated Network Films.....	53
4.4 Conclusion.....	61
 V TAILORING PERCOLATION THRESHOLD WITH EMULSION POLYMER MODULUS.....	 62
5.1 Introduction.....	62
5.2 Experimental.....	63
5.2.1 Materials.....	63
5.2.2 Emulsion Polymer Synthesis.....	63
5.2.3 Composite Preparation.....	64
5.2.4 Characterization of Emulsion and Composites.....	66
5.3 Results and Discussion.....	66
5.3.1 Monodispersed Latex Characterization.....	66
5.3.2 Composite Microstructure.....	71
5.3.3 Electrical Conductivity.....	76
5.4 Conclusion.....	79
 VI CONCLUSION AND FUTURE RESEARCH PLAN.....	 81
6.1 Segregated Network vs. Random Dispersion.....	81
6.2 Polymer-Filler Particle Size Ratio.....	82

	Page
6.3 Polymer Matrix Modulus	83
6.4 Future Work.....	84
6.4.1 Influence of Emulsion Particle Size on Composite Properties.....	84
6.4.2 Influence of Particle Size Distribution on Composite Properties.....	85
6.4.3 Transparent Conductive Polymer Composite.....	85
REFERENCES	87
APPENDIX A	94
VITA	124

LIST OF TABLES

TABLE	Page
3.1 Percolation parameters for solution and emulsion-based composites.....	31
4.1 Carbon black concentration and sheet resistance result.....	56
4.2 Percolation threshold prediction calculated by Malliaris and Turner Model.....	59
5.1 Recipe for the latexes with various ratio of BA/MMA.....	65
5.2 Composition, particle size, and theoretical and actual T_g of latexes.....	68

LIST OF FIGURES

FIGURE	Page
1.1 Schematic illustration of producing a polymer nanocomposite with a segregated network from an aqueous mixture of carbon black and a polymer emulsion	3
1.2 Overview of the segregated network polymer nanocomposite research.....	4
2.1 Schematic of electrical conductivity as a function of filler concentration. The cartoon images at the top highlight how the filler microstructure is changing with concentration.....	8
2.2 Schematic of adjoining insulating particles uniformly covered by conducting particles (reproduced from [37])	11
2.3 SEM micrographs of nylon (a) and PP (b) with 4 phr CB (reproduced from [14]).....	13
2.4 Volume resistivity of PP and Engage with CB (reproduced from [43])	14
2.5 Formation of a segregated network of small filler with large polymer particles (a). Photomicrograph of 7 vol% nickel in polyvinyl chloride (b) (reproduce from [28]).....	16
2.6 Resistivity of PE-L/TiN (■) and PE-S/TiN (□) (a). Average particle size of PE-L is nearly five times bigger than that of PE-S. Microstructure of PE-L/TiN (b). (reproduced from [24]).....	17
2.7 Micrographs of HDPE/PP/CB (a) (reproduced from [51]), and 45/55 PE/PS blend with 1wt% CB (b) (reproduced from [52])	18
2.8 Electrical conductivity as a function of carbon black concentration for three different matrices: PVAc latex (●), PNVP solution (◇), and PVAc water dispersible powder (○) (reproduced from [17]).....	20
3.1 Schematic of a four-point-probe apparatus	24
3.2 SEM images of emulsion-based composites containing 4 wt% (a), 8wt% (b), and 10 wt% (c) carbon black.....	26

FIGURE	Page
3.3 SEM images of solution-based composites containing 4 wt% (a), 8 wt% (b), 10 wt% (c), and 22.5 wt% (d) carbon black.....	27
3.4 Electrical conductivity of emulsion and solution-based composites as a function of carbon black concentration.....	30
3.5 Storage modulus of emulsion and solution-based composites as a function of carbon black concentration.....	33
4.1 Schematic of the LbL self-assembly procedure for creating functional thin films. The cycle is repeated until the desired number of bilayers is deposited to create a multilayer film on the substrate.....	38
4.2 Procedure for covalent layer-by-layer deposition of PEI/Gantrez on oxidized PE particle surface.....	46
4.3 ATR-IR spectra of oxidized PE and PEI/ Gantrez PE derivatives.....	47
4.4 Titrimetric results of PEI/ Gantrez PE powders based on three individual experiments.....	48
4.5 SEM images of neat, acid-oxidized, and PEI-grafted PE particles coated with varying numbers of bilayers of CB stabilized with PAA and PEI.....	50
4.6 Carbon black concentration as a function of the number of bilayers on PEI-grafted, oxidized, and neat PE particles.....	52
4.7 Optical microscope cross sections of compressed films made with neat, acid-oxidized, and PEI-grafted PE particles containing two and eight bilayers of CB stabilized with PAA and PEI.....	54
4.8 Electrical conductivity as a function of the number of the bilayers for films made by compression molding PE particles following LbL deposition of CB.....	55
4.9 Electrical conductivity as a function of CB concentration for films made by compression molding PE particles following LbL deposition of CB.....	57
4.10 Comparison of Slupkowski's model with the electrical conductivity data for PEI grafted PE.....	60

FIGURE	Page
5.1 Particle size distribution of the three P(BA-co-MMA) latexes. The number after BA refers to the weight fraction of butyl acrylate in the copolymer (i.e., “5” means 50 wt%)	67
5.2 Glass transition temperature of P(MMA-n-BA) copolymers, measured experimentally and predicted by the Fox equation, as a function of the weight fraction of methyl methacrylate.....	69
5.3 Storage modulus (E') of neat acrylic latexes as a function of temperature	71
5.4 SEM images of BA 5 with 5 wt% (a) and 10 wt% (b), BA6 with 5 wt% (c) and 10 wt% (d), and BA7 with 5 wt% (e) and 10wt% (f) carbon black. These composites were dried at room temperature	73
5.5 SEM images of BA 5 with 10 wt% (a) and 15 wt% (b), BA6 with 10 wt% (c) and 15 wt% (d), and BA7 with 10 wt% (e) and 15wt% (f) carbon black. These composites were dried at 80 °C	75
5.6 Electrical conductivity of latex-based composites, dried at room temperature, as a function of carbon black concentration	77
5.7 Electrical conductivity of latex-based composites, dried at 80°C, as a function of carbon black concentration.....	78

CHAPTER I

INTRODUCTION

1. 1. Background

Composites consisting of an electrically conductive filler and a polymer matrix exhibit beneficial properties inherited from the polymer matrix (good toughness, flexibility, light weight) combined with electrical conductivity. These materials are suited for many applications such as thermal resistors [1,2], chemical sensors [3,4], electromagnetic interference (EMI) shielding [5,6], and electrostatic dissipation (ESD) [6,7]. These electrically conductive composites are typically prepared using melt mixing [8,9] or solution processing [10,11]. A high concentration of conductive filler is often required for randomly dispersed composites to achieve reasonable conductivity. In many cases, the high filler concentrations required to achieve significant electrical conductivity is accompanied by high mixing viscosity and brittle composite films with extensive porosity due to aggregated filler [12,13]. Segregated network composites, made with a polymer blend or a particulate polymer matrix solve this problem by reducing the percolation threshold concentration (PTC) [14-17]. The PTC is the amount of filler at which the conductivity of a composite significantly increases due to the formation of an interconnected network [18]. It has been reported that the PTC for spherical, randomly dispersed filler is around 15 vol% [10,12]. Previous studies have shown that

Dissertation style and format follow those of Polymer.

this concentration can be reduced by an order of magnitude (or more) by creating a segregated network [17,19-26]

The segregated network concept relies on a polymer matrix with an exclusionary microstructure [27]. In essence, the conductive filler is given a restricted volume in which to reside that leads to network formation at very low concentration. Large polymer particle or domain size relative to conductive particle size yields lower PTC [28]. There are a variety of matrices used to produce segregated network polymer composites. The first method to create a segregated network composite involved compressing a mixture of polymer powder with a conductive filler [24,25,28,29]. These powder-based composites exhibit percolation thresholds from 0.3~6 vol%. Using polymer blends is another technique that can produce a segregated network. In this case, the conductive filler resides predominantly within one polymer that is immiscible in the other polymer [14,15] or it can be distributed at the interface between different polymers phases [16]. These blends produce lower PTC than powder-based systems, but neither concept is expected to have good mechanical integrity.

One of the most recent methods to reduce PTC is using a polymer emulsion to create the segregated network. As an emulsion-filler mixture is drying, the filler is retained within the interstitial space between the polymer particles [17,26]. Relatively large polymer particles (100nm-1 μ m) compared to the size of filler (1-40nm) efficiently lower the PTC of the composite. Figure 1.1 shows how a polymer emulsion mixed with carbon black generates a segregated network during drying. The emulsion-based system is similar to using polymer powder in terms of forcing filler into the interstitial space.

Unlike using polymer blends or powders, this emulsion method can be done under ambient conditions, thereby using less energy to process. Furthermore, the coalescence of the polymer particles during drying results in mechanically robust films [30].

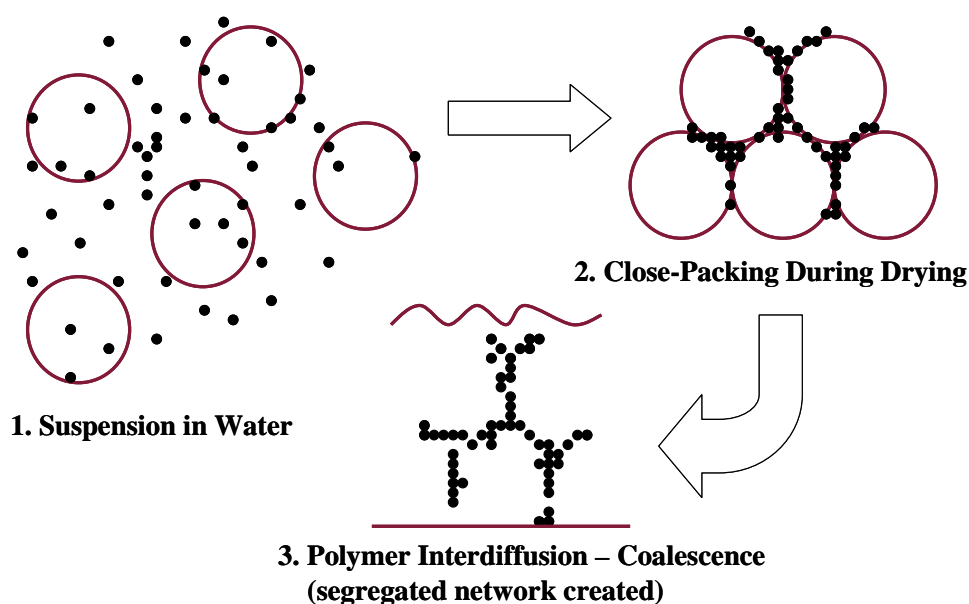


Figure 1.1. Schematic illustration of producing a polymer nanocomposite with a segregated network from an aqueous mixture of carbon black and a polymer emulsion.

1.2 Objectives and Dissertation Outline

The overall goal of the present work is to improve the electrical properties of polymer nanocomposites, while maintaining the intrinsic properties of the polymer matrix. A related goal of this project is to synthesize polymer nanocomposites with very

low PTC and high maximum conductivity with carbon black (CB). An overview of this research is shown in Figure 1.2. The key objectives are:

1. To study the microstructure and properties of polymer composites with a segregated network of filler in comparison to composites with randomly dispersed filler.
2. To understand the effect of very large particle size ratio, between polymer and filler on the electrical properties of the final composites.
3. To analyze the effect of the polymer matrix modulus on PTC and conductivity, using a series of acrylic polymer emulsions.

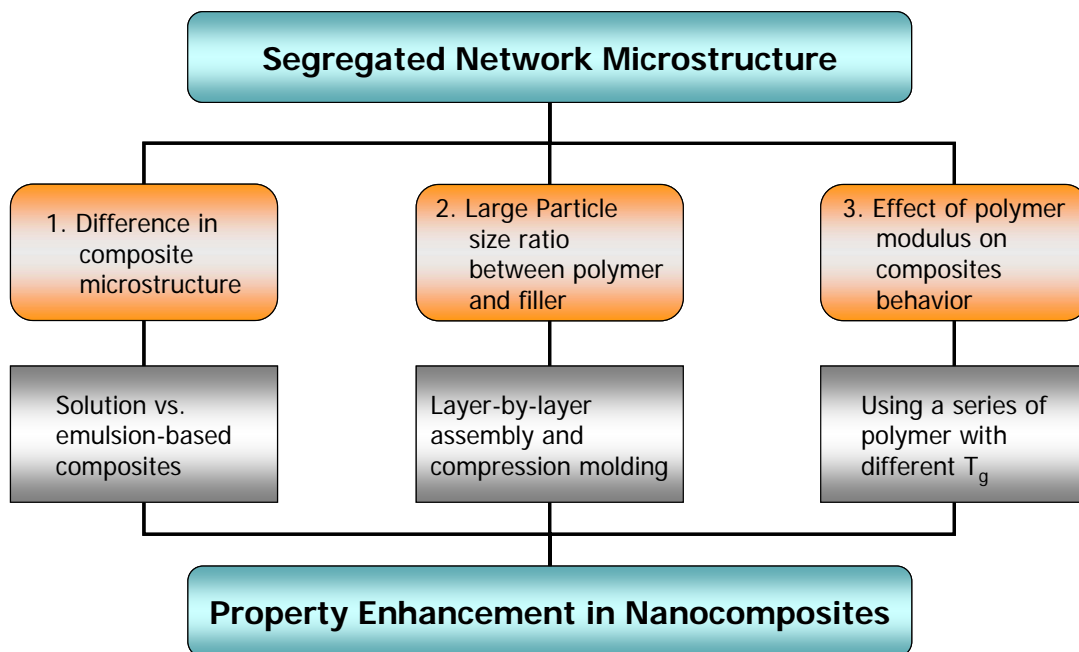


Figure 1.2. Overview of the segregated network polymer nanocomposite research.

Chapter II is a review of the literature about electrically conducting polymer composites. This chapter provides further understanding about the importance and effectiveness of the segregated network in creating conducting polymer composites with low PTC and high maximum electrical conductivity. It also contains a brief review of composites with randomly dispersed filler.

Chapter III examines the effect of polymer microstructure on the final properties of composites without altering composition. Two composites having identical chemical composition but different microstructure were synthesized and characterized. One system was prepared using CB and a poly(vinyl acetate) (PVAc) emulsion to create segregated network composites, while a randomly dispersed composite was made by dispersing CB in PVAc dissolved in a solvent. Random and segregated microstructures lead to differences in the final properties of composites even though both systems have similar chemical compositions.

Chapter IV examines the significance of particle size ratio between polymer particles and filler on lowering the PTC. The importance of uniform surface coverage of CB on the polymer particles was also investigated. Hyper-branched polyethylenimine (PEI) was covalently grafted to the surface of polyethylene (PE) particles in an effort to promote the growth of conductive thin films deposited using layer-by-layer (LbL) assembly. To show the effectiveness of PEI grafting, three composites were synthesized and compared. The final composite, made by compressing the coated particles, has a particle size ratio over 80,000 and a PTC below 0.01 wt%.

Chapter V explores the effect of polymer emulsion modulus on the PTC of final composites. A series of emulsions with different glass transition temperature were synthesized using butyl acrylate (BA) and methyl methacrylate (MMA) monomers. The glass transition temperature was controlled by changing the ratio of BA and MMA. Since they have very different glass transition temperatures (pure PBA has $T_g = -50^\circ\text{C}$, while the T_g of PMMA is 105°C), they exhibit different room temperature modulus. This chapter will provide an understanding of how the change in polymer modulus affects the segregated network.

In Chapter VI, concluding remarks are presented to summarize the findings of this work and future research directions are proposed.

CHAPTER II

LITERATURE REVIEW

2.1. Percolation Theory and Models

Polymers are usually an insulating material. By adding electrically conductive fillers, the composites will exhibit electrical conductivity and can be used in a variety of applications (some examples were mentioned in Chapter I). The electrical conductivity of the mixture increases dramatically at a critical filler concentration called the percolation threshold. Below this concentration the filler particles are not interconnected within the polymer matrix. With no contact between the filler particles the composite remains an insulator. Once the concentration reaches the percolation threshold concentration (PTC), the filler particles are able to contact each other, and form a conducting network. Figure 2.1 shows typical electrical conductivity behavior of a polymer filled with conductive filler as a function of filler concentration. It is worthwhile to note that the theoretically predicted percolation threshold for a randomly dispersed system is around 15 vol% [31]. Many models and equations have been proposed to understand this behavior. Some of these models are reviewed in this section.

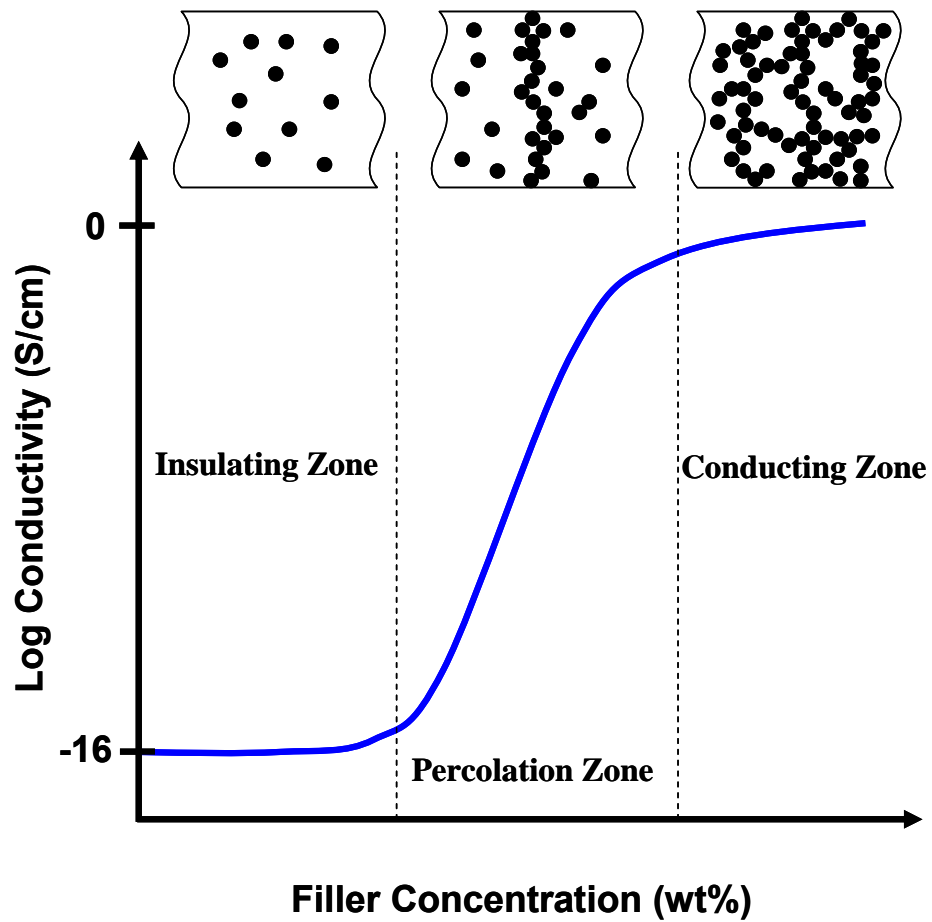


Figure 2.1. Schematic of electrical conductivity as a function of filler concentration. The cartoon images at the top highlight how the filler microstructure is changing with concentration.

Kirkpatrick formalized percolation theory to predict conductivity above the PTC [18]. He showed that electrical conductivity follows the power-law relationship:

$$\sigma = \sigma_0 (V - V_c)^s \quad (2.1)$$

where σ is the conductivity of the composite, σ_0 is the intrinsic conductivity of the filler, V is the volume fraction of the filler, V_c is the percolation threshold, and s is the power-law exponent. The value of s is typically between 1.5 and 3 for three-dimensional percolation. Many experimental studies have shown that this model works with results for carbon nanotubes [32], CB [33], metal particles [34], and intrinsically conductive polymers [35] in an insulating matrix

Malliaris and Turner proposed a theoretical model to predict the percolation threshold based on the assumption of incipient formation of infinitely long chains of metallic powder [28]:

$$V_A = 50P_C [1 + (\phi/4)(R_p / R_f)]^{-1} \quad (2.2)$$

where P_C is the first nonzero probability for infinitely long sequences of adjacent lattice sites occupied by conductive elements (e.g., $P_C = 1/3$ for hexagonal, $1/2$ for square, and $2/3$ for triangular), ϕ is a factor that depends in the mode of packing of the conducting fillers (e.g. $\phi = 1.11$ for hexagonal), R_p is the polymer particle size, and R_f is the filler particle size. They assumed that the surface of large polymer particles is uniformly covered by the conductive fillers. As a result, a double layer of the filler is formed when the particles are compressed.

Janzen developed a percolation model based on the concept of the mean number of contacts between filler particles [36]. He used 1.5 as the mean contact number based on the result of Kirkpatrick and proposed following equation:

$$V_c = \frac{1}{1 + 0.67z\rho\varepsilon} \quad (2.3)$$

where V_c is the percolation threshold, z is the coordination number (number of nearest neighbors) in a specific lattice, ρ is the density of the filler particles, and ε is the specific pore volume of the filler particles. He found that this prediction agrees well with experimental results.

Slupkowski proposed an electrical conductivity model for mixtures of conducting and insulating powders [37]. He considered the diameters of both powders as significant parameters. This model includes three assumptions. First, the diameter of insulating particles is much larger than that of conducting particles. Large insulating particles are in contact with each other and form a simple cubic network. Finally, the conducting particles uniformly cover the surface of the insulating particles. Figure 2.2 shows the model based on these assumptions. These assumptions lead following equation:

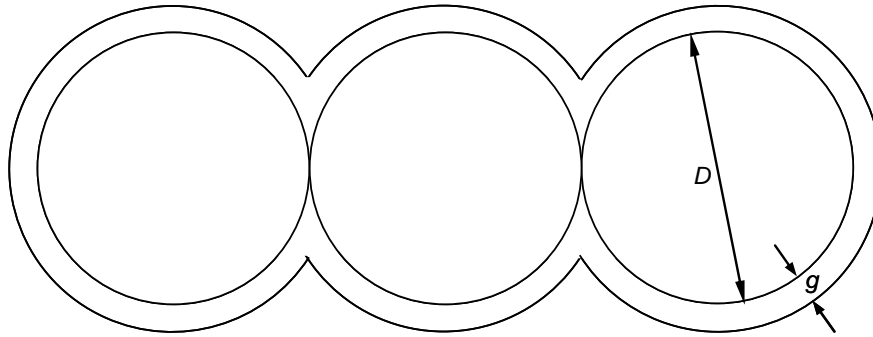
$$\sigma = 2\pi\sigma_c \frac{d([x] + P)}{D \ln\left(1 + \frac{D}{([x] + 1)d}\right)} \quad (2.4)$$

where σ is the conductivity of the mixture, σ_c is the specific conductivity of the conducting particle, D is the diameter of the insulating particle, d is the diameter of the conductive particles, P is the probability of the formation of a network of adjoining

particles, and x is the number of totally filled sublayers of thickness d and is defined by the following equation:

$$[x] = \left(\sqrt[3]{\frac{1}{1-V}} - 1 \right) \frac{D}{2d} \quad (2.5)$$

where V is the volume fraction of the conductive particle.



$$g = ([x] + 1) d$$

Figure 2.2. Schematic of adjoining insulating particles uniformly covered by conducting particles (reproduced from [37]).

Other than the models introduced in this section, there are many approaches to explain the percolation behavior of the conducting composites [38-42], but no model is able to explain all of the different experimental results. In addition to inconsistency with

experimental results, no model is able to reflect the significant effects of various processing parameters.

2.2. Composites with Randomly Dispersed Filler

Carbon-based fillers are the most common materials used to create electrically conductive polymer composites, even though metallic fillers have higher intrinsic conductivity. Metallic fillers are less useful due to stabilization problems and oxidation that creates an insulating layer on their surfaces during processing [24,43]. It is for this reason that composites with carbon-based fillers are the focus of this review.

Tchoudakov et al. studied the electrical behavior of polypropylene/CB and nylon/CB composites [14]. Composites were prepared using melt mixing. The PTC of the PP composites was observed at 2.5 phr (per hundred resins), while the conductivity of the nylon/CB system did not increase in conductivity until 13 phr. The authors claimed that the interfacial energy difference between PP/CB and nylon/CB caused this difference in the PTC. The nylon has better interaction with CB than PP, causing the formation of the conducting network to be impeded by better dispersion in the nylon matrix. In this case, a higher loading of CB is required to reach the PTC. Figure 2.3 shows the microstructure difference between nylon/CB and PP/CB composites. Dispersion of CB in nylon is qualitatively more uniform. A variety of other melt-mixed, conductive composites have also been studied with thresholds ranging from 2 to 27 vol% [8,9,39,44,45]. This wide range is due to factors such as polymer crystallinity and surface energy that influence network formation.

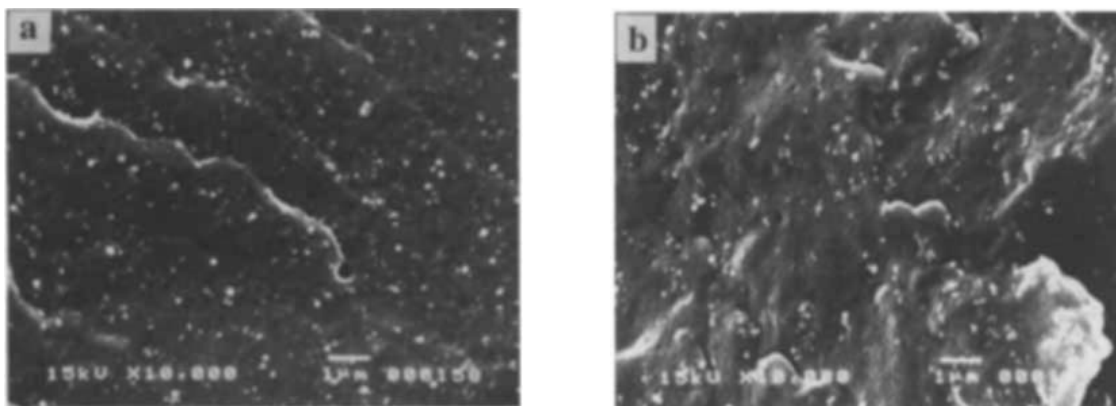


Figure 2.3. SEM micrographs of nylon (a) and PP (b) with 4 phr CB (reproduced from [14]).

Schueler et al. studied the percolation behavior of CB in epoxy resin [11]. When the CB is dispersed in the liquid polymer, the coulombic force between CB particles can cause a potential barrier that hinders agglomeration, resulting in a conducting pathway. The authors examined the effect of external shear force and ionic strength to overcome this potential barrier. It was shown that applying external shear force before curing or adding salt to increase the ionic strength can accelerate the agglomeration process of CB, leading to lower PTC for the conducting composites. PTC was lowered to 0.06 vol % CB by adding a chloride-methanol solution with maximum conductivity near 0.001 S/cm. Many other groups have studied conductive epoxy composites [46-48] and other solution-processed systems with PTC ranging from 0.9 to 3 vol% [10,12].

Huang examined the effect of polymer crystallinity on the PTC of CB [43]. The resistivity of CB-filled PP was compared to the CB-filled ethylene-octane copolymer (Engage). Ethylene-octane copolymer has about 10-15 wt% crystallinity, while PP has

more than 80 wt% crystallinity. CB cannot reside in the crystalline regions and the PTC was decreased in PP as a result. The PTC of CB was reduced from 5 to 2 vol % by changing the polymer matrix from ethylene-octane to PP, as shown in Figure 2.4. Several other studies have shown this effect of crystallinity on PTC [14,44,49].

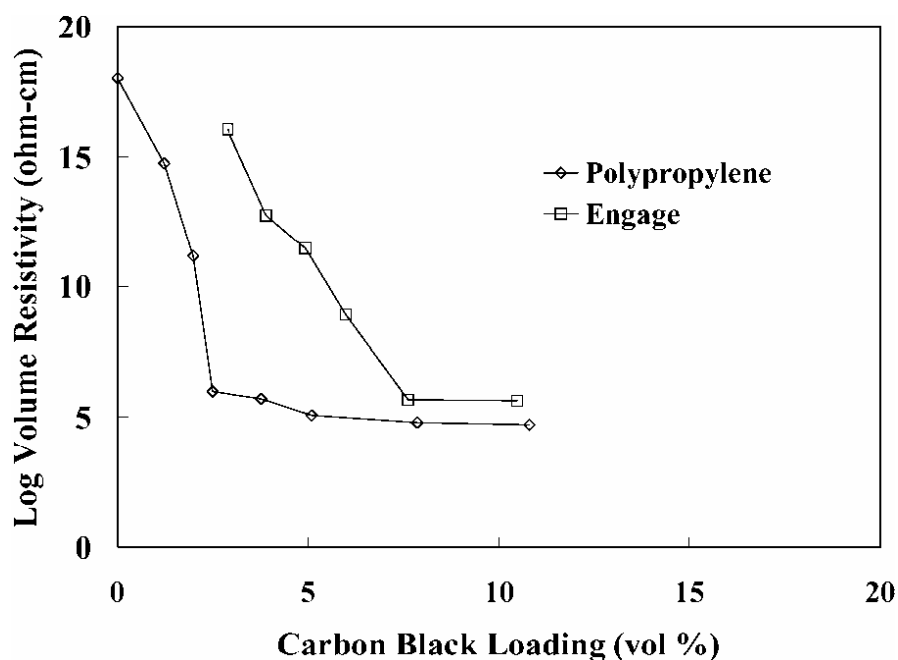


Figure 2.4. Volume resistivity of PP and Engage with CB (reproduced from [43]).

The molecular weight of the polymer matrix can also influence the PTC. Sumita et al. compared CB-filled composites with different polymer molecular weights [45]. The authors showed that higher molecular weight led to an increase in the PTC due to the difficulty of CB dispersion. Huang and Wu studied the effect of the melt flow index

using three different ethylene-vinyl acetate copolymers. Higher melt flow index along with high crystallinity resulted in a decrease in the PTC [50].

2.3. Segregated Network Composites

The term segregated network was originally formalized by Kusy in 1977 when discussing the effect of particle size ratio of polymer and metal powders [27]. He defined a segregated network as the dispersion of metallic particles restricted by the presence of much larger polymeric particles. Several methods have since been used to create segregated networks with conductive fillers in a polymer matrix.

Compacting a mixture of polymer powder and conductive filler was the first approach to create a segregated network. Malliaris and Turner used compression molding to prepare polyethylene (PE)/nickel blends [28]. They reported that the PTC decreases as the size ratio of polymer to metal particle size increases. Figure 2.5 shows a schematic illustration of compacting the particles and a micrograph of the compacted sample. Yacubowicz et al. studied the electrical and dielectric behavior of CB/PE systems prepared by compression molding [25]. The authors reported that the PTC is in the range of 0.3 – 0.7 vol%. The dielectric constant increased sharply up to the PTC. Bouchet et al. used ceramic particles as the conductive filler to create segregated network composites [24], as shown in Figure 2.6. Ceramic powder (titanium carbide or titanium nitride (TiN)) and ultrahigh molecular weight polyethylene were combined with a sintering technique. They reported the effects of various parameters such as pressure, temperature, time, and particle size ratio on PTC. High pressure and temperature

increased the maximum conductivity of composites at higher concentration, but the PTC was also increased. The lowest PTC achieved was about 6 vol%.

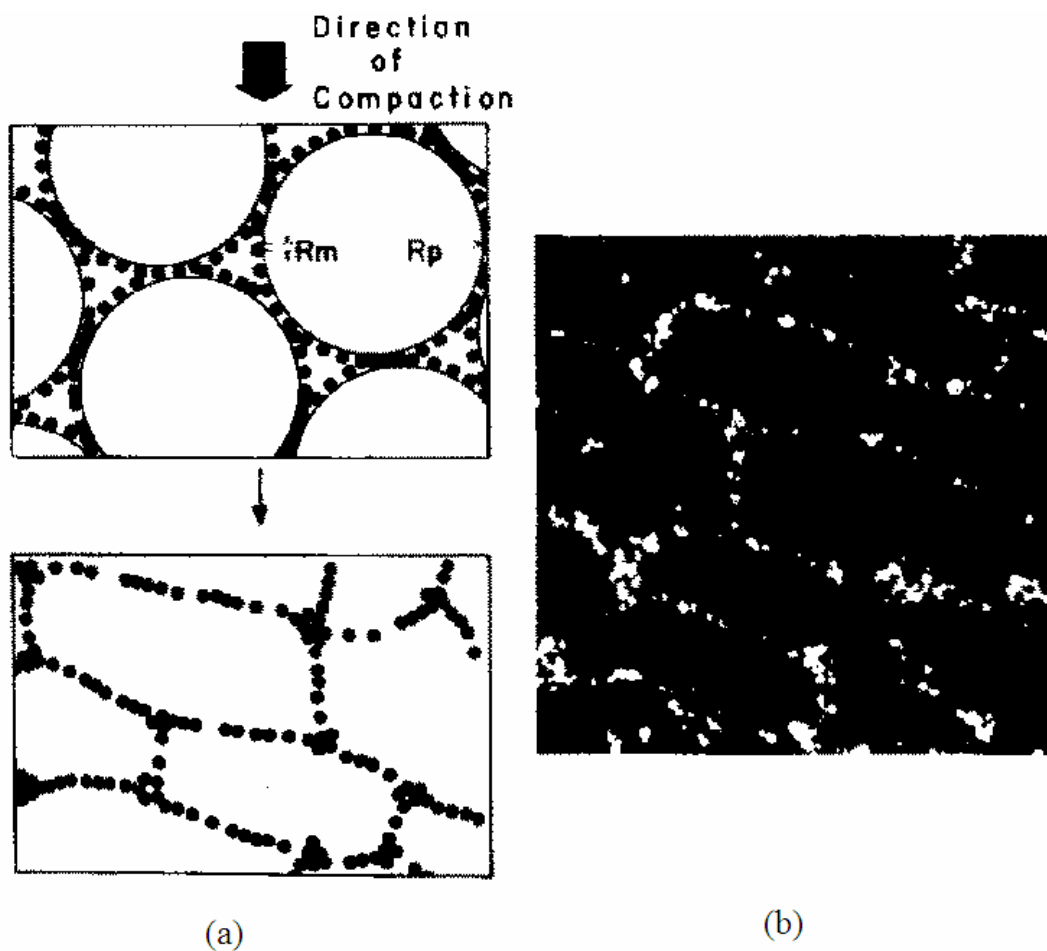


Figure 2.5. Formation of a segregated network of small filler with large polymer particles (a). Photomicrograph of 7 vol% nickel in polyvinyl chloride (b) (reproduce from [28]).

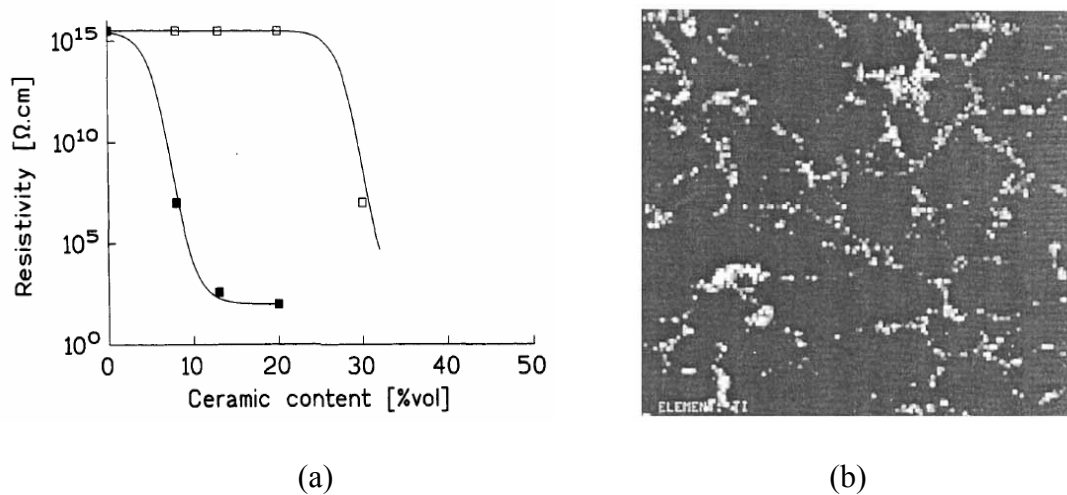


Figure 2.6 Resistivity of PE-L/TiN (■) and PE-S/TiN (□) (a). Average particle size of PE-L is nearly five times bigger than that of PE-S. Microstructure of PE-L/TiN (b). (reproduced from [24]).

Another important method used to create a segregated network is with a polymer blend. The uneven dispersion of the filler due to the phase separation of the polymer blend can make conducting composites with low filler concentration. Sumita et al. studied composite systems with segregated CB in three kinds of polymer blends: HDPE/PP, PP/PMMA and HDPE/PMMA [51], as shown in Figure 2.7. Two types of distribution of CB in polymer blends were reported. In one case, CB is distributed in one of the two polymers and is relatively homogeneously dispersed in this phase. In another instance, CB is located preferentially at the interface of the two polymers. The distribution of CB was verified by plotting the conductivity as a function of the effective concentration in one of the phases. The plot of CB/HDPE was found to be similar to the plot of the CB/HDPE/PP blend, which suggests that the CB was predominantly

dispersed in HDPE phase. The reported PTC of this polymer blend system was around 0.1 vol% with a maximum conductivity near 0.001S/cm ($1000 \Omega \cdot \text{cm}$). Gubbels et al. studied the selective localization of CB in PE/PS blends [52]. HDPE, PS, and CB were mixed at 200 °C, and then compressed. When CB was mixed with pure PE only, percolation was observed at 5 wt%. After CB was selectively dispersed in PE, the percolation threshold of the blend system (10/90 PE/PS system) decreased to 1.5 wt%. Carbon black was dispersed at the interface by mixing with PS first and then adding PE. After annealing, the PTC was reduced to 0.4 wt% for a 45/55 PE/PS blend.

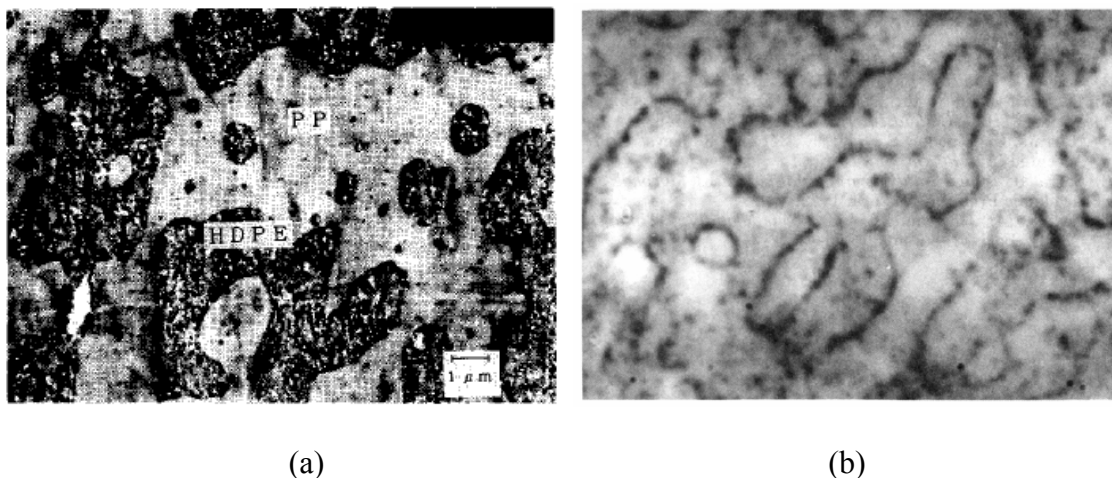


Figure 2.7. Micrographs of HDPE/PP/CB (a) (reproduced from [51]), and 45/55 PE/PS blend with 1wt% CB (b) (reproduced from [52]).

More recently, polymer emulsions have been used as the matrix to create conductive polymer composites with a segregated network of filler. In a polymer emulsion, solid polymer particles are suspended in water. When they are mixed with conductive fillers they create excluded volume during drying. As a result, the filler is pushed into interstitial space between the polymer particles and form a segregated network (see Figure 1.1). Grunlan et al. showed the effectiveness of emulsion-based composites compared to those that were solution-processed [17]. Figure 2.8 shows composites with three different polymer matrixes: poly(vinyl acetate) (PVAc) latex, water-dispersible PVAc powder, and solution-based poly(*N*-vinylpyrrolidone) (PNVP). The PTC for the CB/PNVP composite was near 15 vol% and it decreased to 3.44 vol% with PVAc powder. It was further reduced to 2.39 vol% when PVAc latex was used. In a later study, Grunlan et al. showed that the PTC could be further reduced to 0.038 wt% (~0.035 vol%) by replacing CB with single-walled carbon nanotubes due to the high aspect ratio and high intrinsic conductivity of SWNT [32].

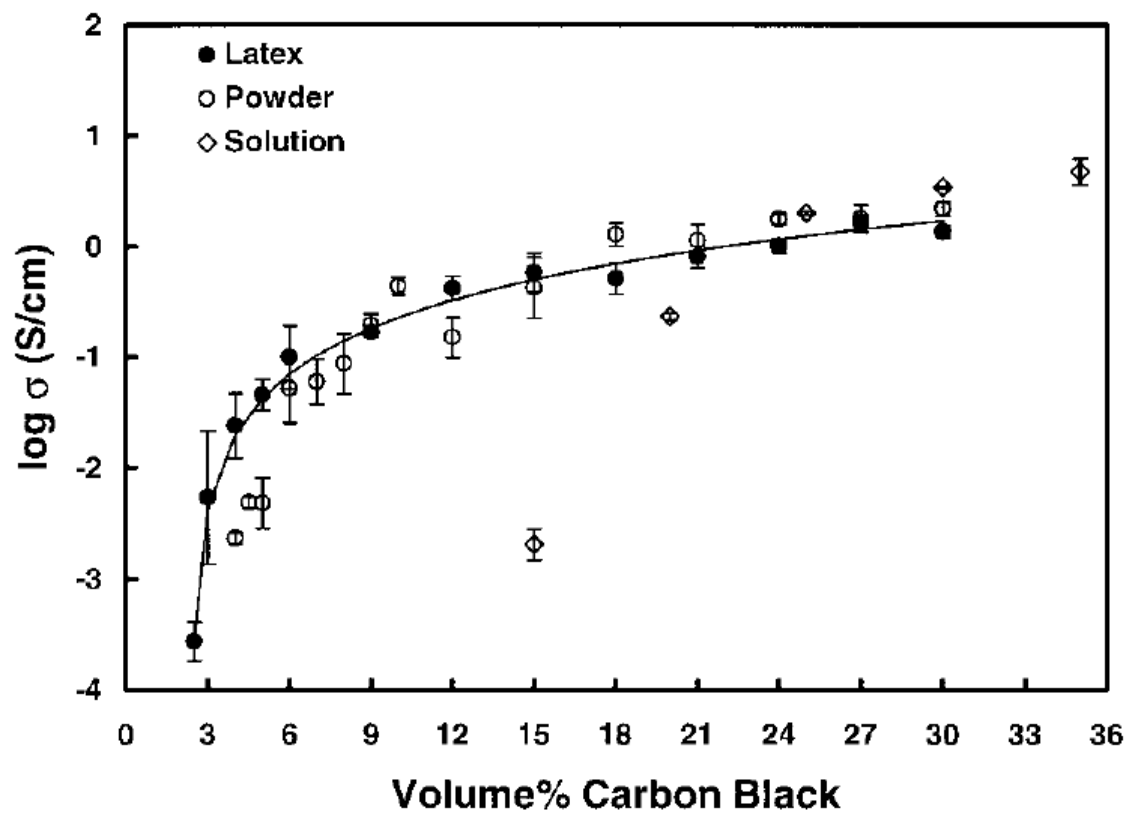


Figure 2.8. Electrical conductivity as a function of carbon black concentration for three different matrices: PVAc latex (●), PNVP solution (◇), and PVAc water dispersible powder (○) (reproduced from [17]).

CHAPTER III

**EFFECT OF MICROSTRUCTURE ON THE ELECTRICAL AND
MECHANICAL PROPERTIES OF THE POLYMER COMPOSITES WITH
CARBON BLACK**

3. 1. Introduction

The literature review in Chapter II (Section 2.3) showed that a segregated network of conductive filler in a polymer matrix could reduce the percolation threshold concentration (PTC). This microstructure's influence on electrical conductivity has been well studied [17,21,27,30,53], but direct comparison of a segregated network and randomly dispersed composite, with the same matrix, has not been explicitly performed. To clarify the influence of microstructure only, two composites with the same chemical composition were prepared. One system was prepared using carbon black (CB) and a poly(vinyl acetate) (PVAc) emulsion to create segregated network composites and randomly dispersed composites were prepared by dispersing CB in PVAc dissolved in dimethylformamide (DMF). Electrical and mechanical properties of these two composites are evaluated here. The PTC of the emulsion-based composite is almost an order of magnitude lower than that of the solution-based composite. Significant differences in mechanical behavior are also observed.

3. 2. Experimental

3.2.1. Materials

The PVAc emulsion (Vinac XX210), supplied by Air Products (Allentown, PA), was 55.53 wt% solid in water. The average particle size of this emulsion is approximately 650 nm with a broad distribution. PVAc pellets, with a molecular weight of 101,600 g/mol, were purchased from Acros Organics (Morris Plains, NJ). Dimethylformamide (DMF) used to dissolve the PVAc pellets was also purchased from Acros Organics. Carbon Black (Conductex 7055 Ultra) was supplied by Columbian Chemicals (Marietta, GA). This grade of CB has a nitrogen surface area (NSA) of 55 m²/g and a primary particle size of 42 nm.

3.2.2. Emulsion-Based Composite Preparation

The pre-composite mixture with the highest loading of CB was prepared first. To begin, deionized water was added to the emulsion to reduce the viscosity. CB black was then added to the diluted emulsion and stirred at 3600 rpm for 15 min using a high speed impeller blade. Upon completion of mixing, some portion was removed to make a film. Subsequent compositions were made by adding more emulsion and deionized water. These mixtures were kept at a constant 15 wt% solids during mixing. Composites were made by pouring 12g of mixture into 4 in² polystyrene molds. These mixtures were dried at 80 °C for two hours followed by one day in a vacuum desiccator.

3.2.3. Solution-Based Composite Preparation

DMF was chosen to dissolve the PVAc pellets due to its high boiling point (156 °C) and polarity. CB is quite polar, so it is possible to mix it into a DMF-based solution without using a dispersing agent. DMF's high boiling temperature prevents evaporation during mixing. A solution containing 10 wt% of PVAc in DMF was rolled for one day on a Cell-Production Roller Apparatus manufactured by BELCO Biotechnology (Vineland, NJ) with a rotation speed of approximately 10 rpm to achieve equilibrium. The preparation of composite mixtures followed the procedure of the emulsion-based composites (see section 3.2.1). After mixing, the solution-based mixtures were poured into 4 in² aluminum molds (DMF dissolves polystyrene molds) and dried at 120 °C for two hours (80 °C is not high enough to evaporate DMF completely). Finally, these films were dried in a vacuum desiccator for one day.

3.2.4. Composite Characterization

3.2.4.1. Electrical Conductivity

Electrical conductivity was measured with a custom built four-point probe system. The schematic illustration of a four-point probe is shown in Figure 3.1. Four-point probe measurement is a well known technique to measure the electrical resistance of a thin layer or sheet by passing a current between the outside probes and measuring the drop in voltage between the two inside probes. Sheet resistance (R_s) is obtained with:

$$R_s = 4.53 \times V/I \quad (3.1)$$

where 4.53 is the shape factor. The bulk resistivity (in $\Omega\cdot\text{cm}$) of a film can be calculated by multiplying the R_s by thickness in centimeters. The four-point probe system consists of Keithley 2000 multimeter, Agilent E3644A power supply, four-point probe and probe mount from Signatone (Gilroy, CA). Current is measured by the multimeter and voltage is recorded by a LabView program.

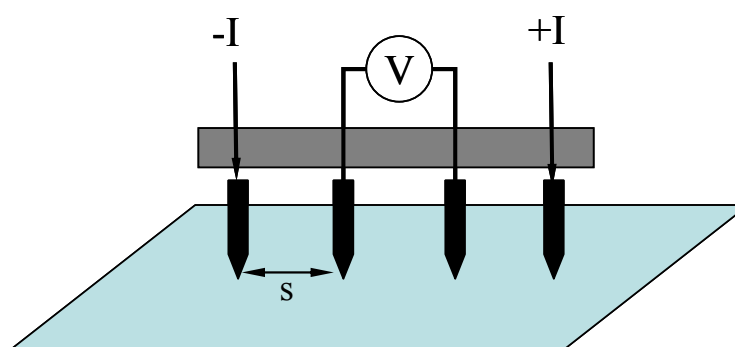


Figure 3.1. Schematic of a four-point-probe apparatus.

3.2.4.2. Thermomechanical Properties

Dynamic mechanical analysis (DMA) was used to measure the glass transition temperature and storage modulus of the composite films. The Q-800 DMA by TA Instruments (New Castle, DE) was used in this study. In most cases, tests were run at 1

Hz and temperature was ramped at 3°C/min from -50 – 100 °C. The amplitude of strain was fixed at 0.1% and T_g was taken as the peak in the loss modulus curve.

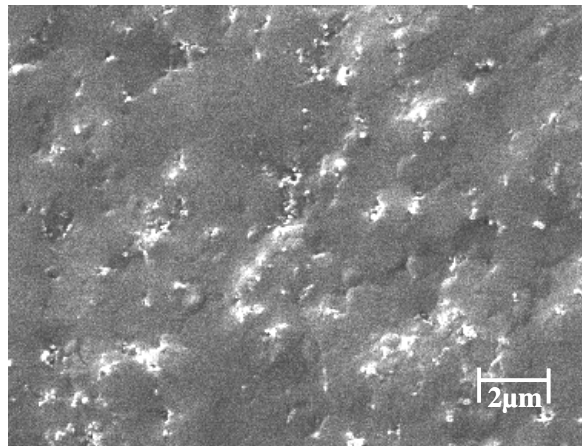
3.2.4.3. Composite Microstructure

The cross-sections of the composite films were imaged with a Tescan VEGA-II SEM (Cranberry Township, PA). Films were soaked in liquid nitrogen and fractured by hand. The surfaces were sputter coated with 4nm of platinum prior to SEM imaging.

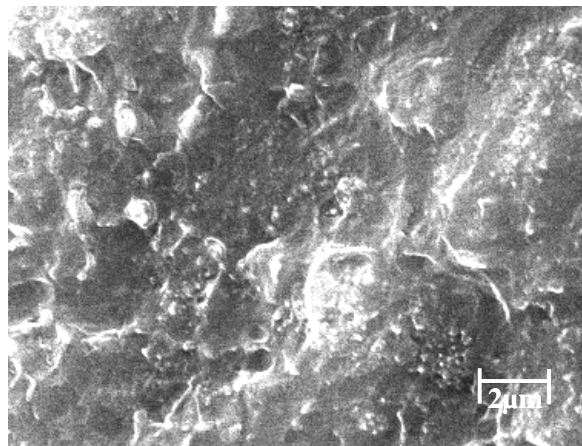
3.3. Results and Discussion

3.3.1. Composite Microstructure

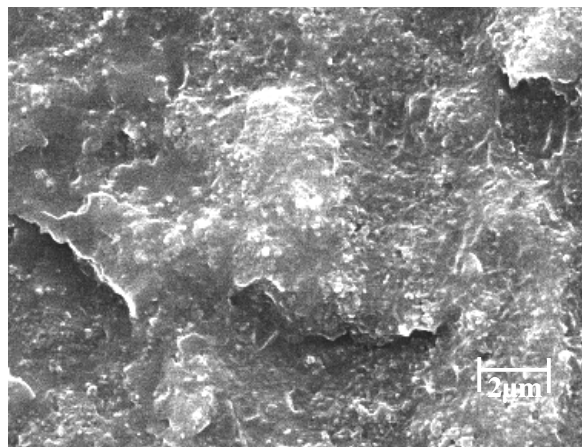
Once the mixtures are completely dried, the solution and emulsion-based composites have a nearly identical chemical composition (CB in PVAc), but they have significantly different microstructure. Figure 3.2 shows cross sectional images of emulsion-based composites with 4, 8, and 10 wt% CB and Figure 3.3 shows the cross sections of solution-based composites with 4, 8, 10, and 22.5 wt% CB. In both images, CB appears as white nanoparticles embedded in the darker polymer matrix. The emulsion-based system results in a segregated network of CB at low concentration (Fig. 3.2(a)), while the solution-based system shows no conducting pathway until a higher concentration. This difference in microstructure produces significant differences in electrical and mechanical behavior, which will be discussed in following sections.



(a)



(b)



(c)

Figure 3.2. SEM images of emulsion-based composites containing 4 wt% (a), 8wt% (b), and 10 wt% (c) carbon black.

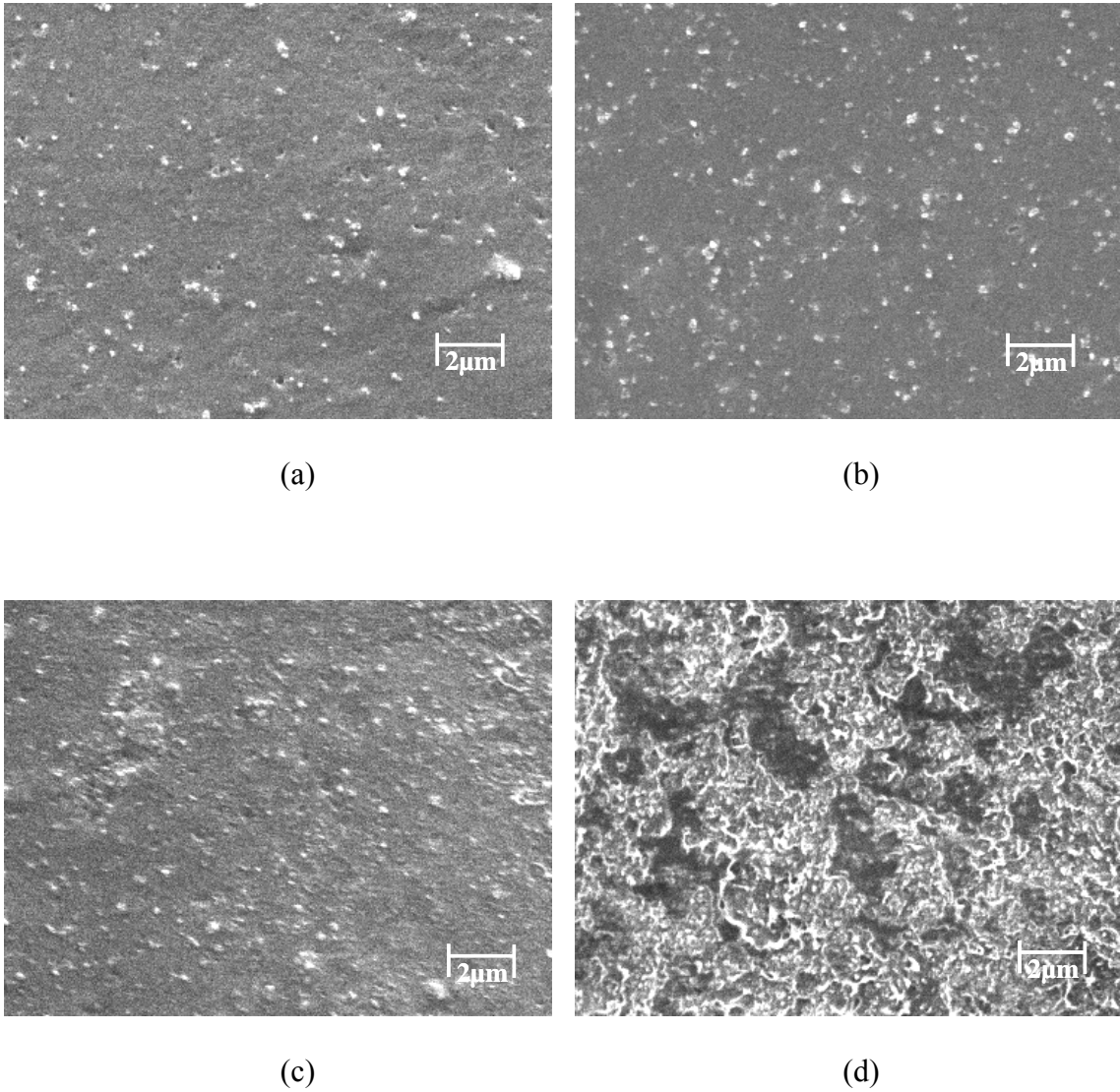


Figure 3.3. SEM images of solution-based composites containing 4 wt% (a), 8 wt% (b), 10 wt% (c), and 22.5 wt% (d) carbon black.

The cross-section image of an emulsion-based composite with 4 wt% CB (Fig. 3.2 (a)) reveals that the emulsion is not perfectly coalesced. The shape of the polymer particles can be weakly discerned in some spots. The dried neat emulsion film, however, is completely transparent and its modulus matches literature values, which indicates it is sufficiently coalesced. At 4 wt% CB there are few voids or strong aggregation of CB present because this system is below the critical pigment volume concentration (CPVC) [54]. CPVC is the point at which there is just sufficient polymer to hold all of the filler. Above the CPVC, filler particles are not sufficiently surrounded by polymer and voids begin to form. Many properties of composites such as modulus, permeability, and fracture toughness change at the CPVC [30,55]. The fractured surface of the emulsion-based composite with 8 wt% CB (Fig. 3.2 (b)) is quite rough and shows some voids indicating the CB concentration is close the CPVC. At 10 wt% (Fig. 3.2. (c)), the CB is strongly aggregated, creating many voids in the composite structure and indicating that the CB concentration has reached or surpassed the CPVC.

Carbon black is more randomly dispersed in the solution-based composites (Fig. 3.3). Up to 10 wt%, composite cross sections are very smooth and CB is very uniformly dispersed. The particles are separated by the polymer matrix, causing the composite to be insulating. It is clear that the CPVC for the solution-based composite is higher than that of the emulsion-based system because no voids are observed at this point. The image of the composite containing 22.5 wt% CB shows significant aggregation of CB that is accompanied by nano-porosity.

3.3.2. Electrical Conductivity

Conductivity as a function of CB concentration for both composites, fitted with percolation curves, is shown in Figure 3.4. It is clear that the microstructural differences, observed with SEM, result in significant conductivity differences. The concentration of CB was converted to volumetric concentration to fit the data with the classical percolation power law (Equation 2.1). The distinction between the two composites' microstructure occurs during the drying process. For the randomly dispersed composite, CB can be placed anywhere within the polymer matrix. The small size of CB requires it to create a conducting pathway throughout the composite thickness. Unlike the solution-based system, CB in the emulsion has only limited space to situate during the drying process. Selective distribution of CB within the polymer matrix leads to the formation of a segregated network at lower CB concentration. This early formation of a conducting pathway results in very low PTC for emulsion-based composites. The maximum conductivity of both systems also shows similar behavior with the PTC. To reach the highest conductivity, the solution-based composite requires about twice the loading of CB than the emulsion-based system. The solution-based composite, however, achieves a higher value of maximum conductivity at high CB loading. As shown in SEM images (see Figures 3.2 and 3.3), the CVPC for the solution-based composite is much higher than that of the emulsion-based system. Once reaching the CVPC, the porosity of the composite increases and further CB loading does not contribute to the formation of additional conductive pathways. Beyond the CVPC, the conductivity remains nearly constant and eventually decreases. The CVPC for the solution-based composites is

higher, which allows them to hold more CB without creating voids. As a result, the maximum conductivity of the solution-based composites is higher.

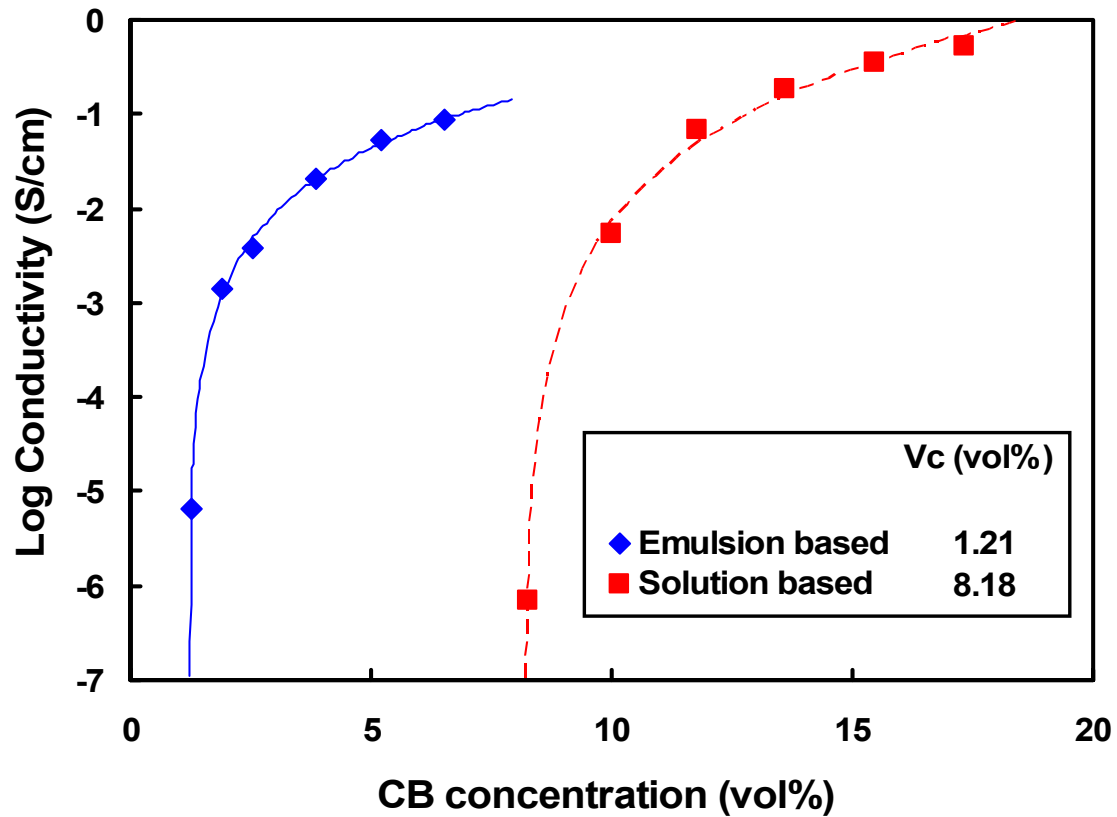


Figure 3.4. Electrical conductivity of emulsion and solution-based composites as a function of carbon black concentration.

The solid lines in Figure 3.4 represent the percolation power law (Equation 2.1) fitted to the experimental data and the fitting parameters are summarized in Table 3.1. The percolation threshold decreases from 8.18 to 1.21 vol% by changing the microstructure of the composites. This significant decrease in the PTC shows the effectiveness of the segregated network. The solution-based composite value is lower than the theoretically predicted value for randomly dispersed composites (around 15 vol%). This is because the interaction between CB particles is stronger than that between CB and the polymer matrix. When the filler-filler interaction is stronger, particle aggregation results in the formation of a conductive pathway at lower concentration. Many studies have shown this behavior with a variety of polymers [11,14,39,44].

Table 3.1. Percolation parameters for solution and emulsion-based composites

	σ_0 (S/cm)	s	V_c
Emulsion	43.4	2.11	1.21
Solution	593.4	2.83	8.18

3.3.3. Storage Modulus

Figure 3.5 shows the storage modulus of emulsion and solution-based composites as a function of carbon black concentration. The overall trend of modulus behavior of both systems is very similar to the electrical conductivity behavior. Modulus of the emulsion-based system increases fast at low CB concentration, while the solution-based composite achieves a higher maximum modulus at high concentration. Both systems show initial increase in the storage modulus with CB concentration. The moduli of composites decrease once the CB concentration exceeds the CVPC. The storage modulus of the solution-based system never decreases within this experiment, indicating that the CVPC is above 25 wt% CB. The modulus of the neat emulsion film is 2.27 GPa and a composite with 2 wt% CB already exhibits a 12% increase (2.55GPa). The modulus increases up to 2.88 GPa as the CB concentration increases to 8 wt%. Beyond this concentration, the modulus starts to drop due to severe aggregation of CB, as shown in Figure 3.2 (c). For the solution-based system, the modulus increases slowly until 15wt% CB. The solution-based composite requires 15wt% CB to achieve a 9% improvement in modulus, which corresponds to 2 wt% CB for the emulsion-based composite. At 15 wt% CB, the slope of modulus increase changes abruptly in the solution-based system due to the carbon black networking.

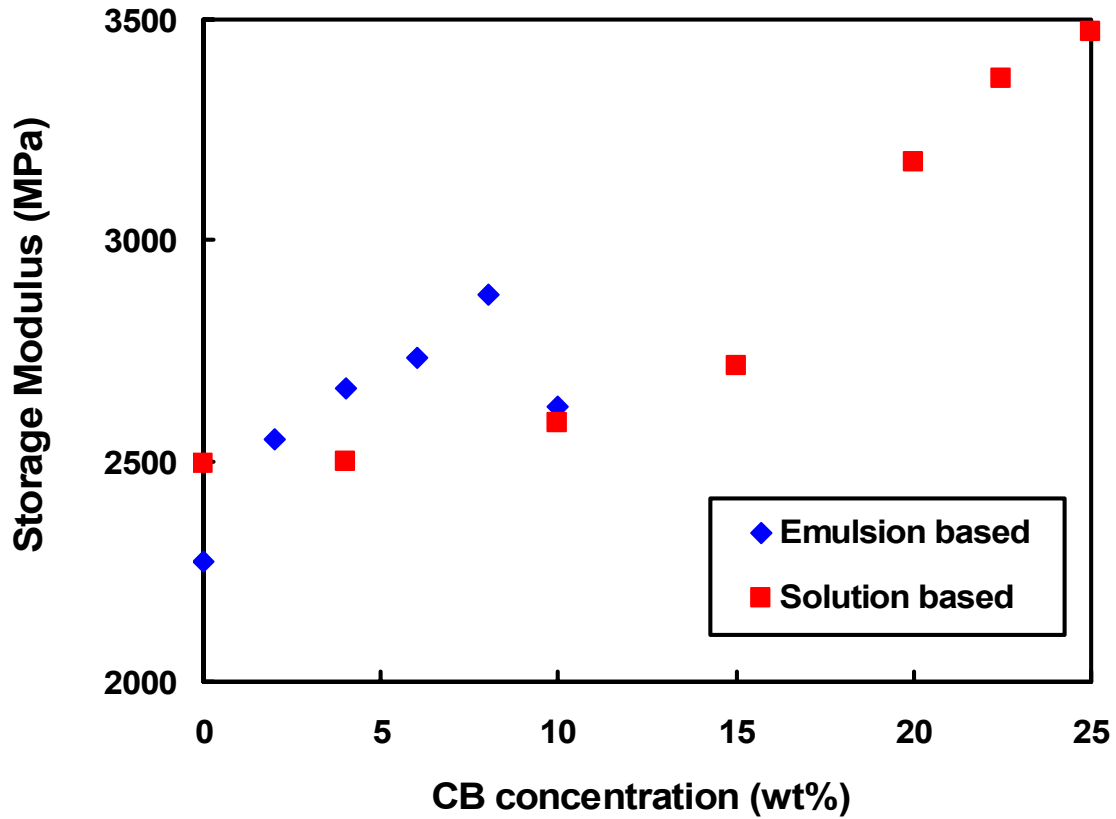


Figure 3.5. Storage modulus of emulsion and solution-based composites as a function of carbon black concentration.

3.4. Conclusion

The effect of microstructure on the electrical and mechanical properties of carbon black filled poly(vinyl acetate) has been investigated. The emulsion-based composite shows a fast response to the CB loading, while the solution-based composite exhibits greater maximum enhancement in both electrical and mechanical behavior. Because CB particles cannot penetrate into the emulsion particles, they situate in the interstitial space between CB particles during drying and create a segregated network at low

concentration. SEM images reveal the significant difference in microstructure between emulsion and solution-based systems. The emulsion-based composite forms a strong segregated network at 4 wt% CB, while no conducting pathway is found until 10 wt% for the solution-based system. The percolation threshold for the emulsion-based composite is 1.21 vol%, which is nearly one order of magnitude lower than that of the solution-based composite. A similar trend is also found in the storage modulus of both systems. The emulsion-based system reaches a maximum enhancement of 26% at 8 wt% CB, while the solution-based system shows only a small increase at this concentration. Even though the solution-based system accomplishes higher maximum enhancement of both electrical and mechanical properties, it requires 25 wt% CB to accomplish this. These results show that the emulsion-based system is very effective at enhancing the electrical and mechanical properties of composites with low filler loading.

CHAPTER IV
CONDUCTIVE THIN FILMS ON FUNCTIONALIZED POLYETHYLENE
PARTICLES*

4.1. Introduction

In Chapter II, several methods to form a segregated network were described. One of the simplest methods to create a composite with a segregated network is mixing the polymer particles with much smaller filler particles [24,25,28,29]. The particle size ratio between a polymer matrix and conductive filler has a critical effect on the formation of a segregated network and the percolation threshold. When the polymer and conductive filler have similar size, a large concentration is necessary to form a continuous network of filler within the polymer matrix. It is desirable for composites to have extremely large particle size ratio to achieve very low PTC, but no one ever succeeded to make composites with an extremely large particle size ratio (>1000) due to processing difficulty and uneven surface coverage of filler on the polymer particles. In the present work, we have created composites having a particle size ratio over 80,000 using layer-by-layer (LbL) assembly in order to create a uniform coating of the polymer particle surface [56].

* Reprinted with permission from “Conductive Thin Films on Functionalized Polyethylene Particles” by Y.-S. Kim *et al.*, 2006. *Chemistry of Materials*, 18, 2997-3004. ©2006 American Chemical Society

LbL assembly is a method used to impart functionality to the surface of nearly any type of substrate [57,58]. Thin films are deposited by alternately exposing a substrate to aqueous mixtures (or solutions) of mutually attractive molecules or particles. In most cases the attraction between species is provided by charge and each combination of a positively and negatively-charged layer is referred to as a bilayer. Each deposited layer is typically 1 – 100 nm thick depending on charge-density [59,60], counterion [59], molecular weight [61], temperature [62], deposition time [63,64], and pH [65,66] of the species being deposited. Concentration [64] and ionic strength [64,67] of the deposition mixture will also influence layer thickness. LbL-based thin films can impart chemical sensing [68-70], electrically conductive [71,72], super-hydrophobic [73], electrochromic [74,75], magnetic [76], and antimicrobial behavior [77,78] to a given substrate. Figure 4.1 shows the process used to apply small carbon black particles (~ 21nm) to the surface of large PE particles (> 100 μ m). Many materials can be used as a substrate for LbL deposition without the need for surface modification, but there is difficulty building layers on polyolefins [79,80]. It is difficult to get water-based coatings to adhere well to polyolefins, such as polyethylene and polypropylene, due to low surface energy and lack of polarity. Corona or plasma treatments can be used to increase the surface energy of polyolefin films [81-84]. Both of these techniques generate polar functionalities on the film surface that will improve wetting and subsequent adhesion of an aqueous coating. Oxidative acid etching is another method that generates hydroxyl and carboxylic acid species to create surface polarity [85]. However, these surface modification techniques

only produce monolayer of functionality that can disappear upon surface reorganization.

A more recent technique, used here to promote stable layer-by-layer film growth and stronger adhesion, is the growth or graft of polyelectrolytes on polyolefin [86-89]. In the present study, a hyper-branched polyethylenimine (PEI) surface was generated on polyethylene particles in a similar manner to that done previously on a silica support [89]. Hyper-branching yields a uniform surface coverage of polyelectrolyte down to the microscopic level, despite initial growth occurring only sparsely over the PE particle surface. The presence of PEI on the polyethylene particle then facilitates near perfect surface coverage by alternate deposition of carbon black stabilized with poly(acrylic acid) [PAA] and PEI in a layer-by-layer fashion. Untreated PE exhibits very poor acceptance of the LbL film growth under the same conditions, while oxidative acid etching exhibits intermediate behavior. The carbon black-coated particles so formed produce highly conductive composites when compression molded.

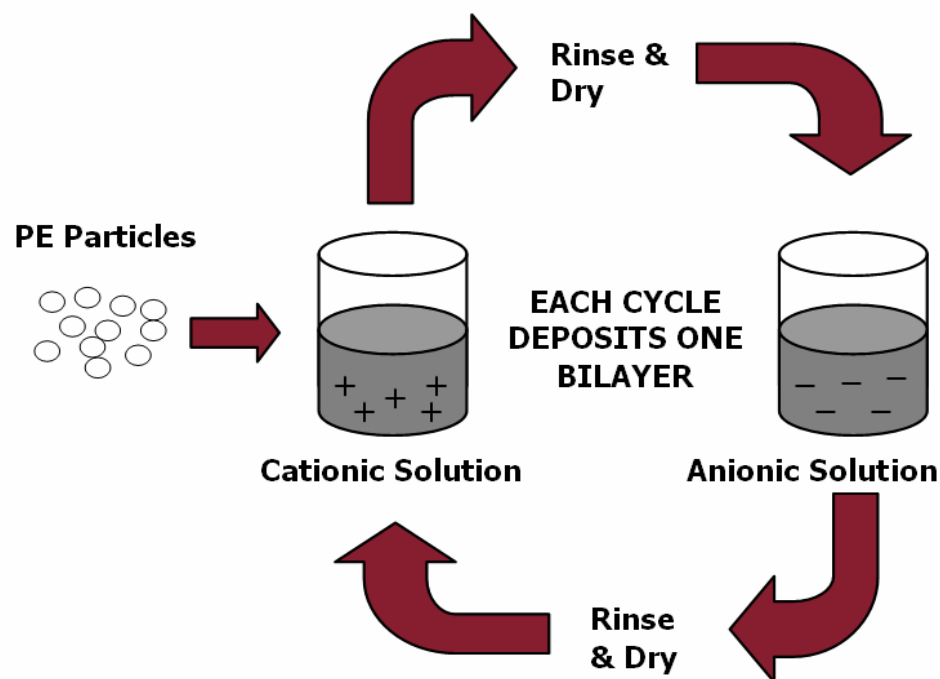


Figure 4.1 Schematic of the LbL self-assembly procedure for creating functional thin films. The cycle is repeated until the desired number of bilayers is deposited to create a multilayer film on the substrate.

In many cases, the high carbon black concentrations required to achieve significant electrical conductivity is often accompanied by high mixing viscosity and brittle composite films with extensive porosity due to aggregated filler [12,13]. Layer-by-layer deposition circumvents high viscosity processing by using dilute mixtures (< 1 wt% solids) to deposit layers of carbon black that are pre-stabilized with polyethylenimine (PEI) and poly(acrylic acid) (PAA) to impart basic and acidic surface chemistry, respectively. The resulting films are thin (< 1 μm), flexible, and dense, with a high concentration of carbon black (> 45 wt %) [72]. When applied to PEI-treated

polyethylene particles, with an average particle size of 1.7 μm , highly conductive composites were produced that have a very small weight fraction of carbon black following compaction.

In this work, a comparison is made between untreated polyethylene particle, oxidative acid etched particle and particle that has hyper-branched PEI on its surface. Infrared spectroscopy and electron microscopy are used to characterize the three types of particle prior to layer-by-layer deposition of carbon black. The PEI-treated and unmodified PE particles are then compared with respect to LbL film growth using electron microscopy and thermogravimetric analysis. PE particles containing 2 – 8 bilayers of carbon black, stabilized with PEI and PAA to provide positive and negative surface charge, were studied. The results indicate that deposition on unmodified or acid etched polyethylene does not produce uniform carbon black films and the material that does deposit has variable thickness and poor interfacial adhesion. PEI-grafted polyethylene promotes uniform deposition of carbon black thin films as evidenced by gravimetric analyses that show a linear increase in weight per bilayer. Composite films, made using compression molding, exhibited a percolation threshold below 0.01 wt% carbon black and a maximum electrical conductivity of 0.2 S/cm with a concentration of only 6.2 wt% carbon black. These segregated network composites have among the lowest percolation threshold ever reported with carbon black as the conductive filler. This combination of surface functionalization and layer-by-layer assembly could be used to deposit other types of conductive material or to impart other properties, such as antimicrobial or flame suppression.

4.2. Experimental

4.2.1 Materials

Polyethylenimine (PEI, M_n 10,000), poly(methyl vinyl ether-*alt*-maleic anhydride) (Gantrez, M_n 1,130,000), ethyl chloroformate (97%) and *N*-methylmorpholine (ReagentPlus, 99%) were purchased from Sigma-Aldrich (Milwaukee, WI) and used as received. Ethylenediamine was purchased from EM SCIENCE (Gibbstown, NJ) and distilled before used. Triethylamine (Reagent Grade) was purchased from Fisher Scientific (Fair Lawn, NJ) and used as received. Poly(acrylic acid) (PAA M_n 25,000) and polyethyleneimine (PEI, M_n 100,000) which were used for CB stabilization were also purchased from Sigma-Aldrich (Milwaukee, WI) and used as received. Conductex 975 Ultra carbon black was supplied by Columbian Chemicals (Marietta, GA). This grade of CB has a nitrogen surface area (NSA) of 242 m²/g, density of 1.89 g/cm³, and a primary particle size of 21 nm. The PE powder used in this study is Fortiflex HDPE J60-800-178, which has a density of 0.96 g/cm³ and an average particle size of 1.7 mm with a very wide size distribution.

4.2.2 Preparation of PEI/ Gantrez Hyperbranched Grafts on Oxidized PE Particle

The PE particle was extracted 12hours with CH₂Cl₂ in a Soxhlet apparatus and dried at reduced pressure. The PE particle was then oxidized using CrO₃/ H₂SO₄/ H₂O (1:1:2 by weight) at 90°C for 1 h, washed with water and acetone, and allowed to air dry.

The oxidized PE particle was then extracted 12 hours with CH_2Cl_2 in a Soxhlet apparatus and dried at reduced pressure.

4.2.3 Preparation of PEI/ Gantrez Oxidized PE Particles

Oxidized PE particle (10 g) was first activated by treatment with a mixture of ethyl chloroformate (5 mL) and N-methylmorpholine (5 mL) in 60 mL of DMF for 15 min. Next, the particle was isolated by filtration, solution washed with CH_2Cl_2 , and allowed to air dry. The activated PE particle was then placed into a 60 mL solution of CH_2Cl_2 and polyethylenimine (PEI, branched, $M_n=10,000$) (1.5 g) for 1h. After isolating the PE particle by filtration and washing it with CH_2Cl_2 and MeOH, the PEI treated PE particle was placed into a solution of triethylamine (10 mL) and of MeOH (60 ml) for 5 min to ensure that any surface ammonium salts were neutralized. The aminated PE particle was again isolated by filtration, washed with MeOH, and allowed to air dry. This PEI treated PE particle was then, placed into a 60 mL of THF solution of poly(methyl vinyl ether-alt-maleic anhydride) (Gantrez, $M_n=1,130,000$) (1.5 g) containing ethylenediamine (28 μL) for 1 h, and isolated by filtration, washed with THF, and allowed to air dry. The Gantrez treated PE particle could then be placed into the PEI solution to reform a nucleophilic aminated surface. This cycle of PEI treatment followed by Gantrez treatment was repeated 5 times to obtain the PEI-6/ Gantrez-5 PE particle.

4.2.4 Carbon Black Mixture Preparation

PEI and PAA were added to de-ionized water to produce 0.05 wt% solutions. These solutions were rolled for 12 hours on a Cell-Production Roller Apparatus manufactured by BELCO Biotechnology (Vineland, NJ) with a rotation speed of approximately 10 rpm to achieve equilibrium. Carbon black was then added to the solution at a concentration of 0.25wt% using a high speed impeller for 15 minutes at 3600 rpm, followed by rolling for 12 hours to achieve equilibrium.

4.2.5 Film Deposition

Polyethylene particles were alternately immersed into CB-PEI and CB-PAA aqueous mixtures. The initial immersion in each mixture was for five minutes followed by one minute immersions to deposit additional bilayers. Following each immersion the particles were filtered to remove water and excess material. For the PEI grafted PE particles, the CB-PAA mixture was used first since they were already covered by PEI, but normally CB-PEI would be deposited first. After the deposition was complete, the coated particles were vacuum dried for more than 24 hours to remove residual moisture. Once dried, the particles were compacted in an aluminum mold at 90 °C for 30 minutes with a pressure of 150 kg/cm². The resulting films are 1.5 mm thick.

4.2.6 Characterizations of the Particle and Coating

Attenuated total reflection-infrared (ATR-IR) spectroscopy was used to confirm growth of the PEI/ Gantrez graft on the PE surface. A Bruker Tensor 27 series FT-IR,

with a Pike MIRacle ATR accessory at an angle of 45° using a ZnSe crystal, was used. In these spectra, the integrated intensity of the amide peak (1640 cm^{-1} - 1650 cm^{-1}) and carboxylate peak (1550 cm^{-1} - 1560 cm^{-1}) is shown to increase in comparison with the intensity of the underlying bulk polymer C-H absorption (2910 and 2850 cm^{-1}). Titrimetric analysis was carried out by first suspending a weighed amount of the PEI/ Gantrez PE particle in a 0.01M HCl solution and shaking the mixture for 1h. An aliquot of the resulting HCl solution was titrated with 0.01M NaOH solution. In this way, the amount of HCl consumed by basic groups (amine and carboxylate) on the PEI/ Gantrez PE particle could then be determined. The average numbers of millimoles of basic groups of PE particle for PEI-1, PEI-2/ Gantrez-1, PEI-3/ Gantrez-2, PEI-4/ Gantrez-3, PEI-5/ Gantrez-4, PEI-6/ Gantrez-5 PE particle were 0.0380 , 0.2332 , 0.3613 , 0.5089 , 0.6545 , and 0.8896 mmol/g of particle, respectively. The concentration of the CB on the particle surface was determined using thermogravimetric analysis (TGA) operated from 25°C to 900°C at a rate of 10°C per minute. The conductivities of the compacted films were measure by a home-built four-point-probe system.

4.3. Results and Discussion

4.3.1 PEI-Grafted Polyethylene

In order to create a surface amenable to layer-by-layer assembly, polyethylene particle was modified according to the steps shown in Figure 4.2. First, the PE particle was oxidized by chromic acid. The carboxylic acid groups formed in that oxidation were

then activated by ethyl chloroformate to form anhydride groups. A nucleophilic polymer, polyethylenimine (PEI), was then allowed to react with the anhydrides to form a product where some amine groups of the PEI formed covalent amide bonds and some amine groups of the PEI formed ammonium carboxylates. At this point, the surface was treated with an excess of Et_3N in MeOH. This produced an amine-rich surface that was in turn allowed to react with an electrophilic polymer, poly(methyl vinyl ether-alt-maleic anhydride) (Gantrez) to form a new graft with amic acid linkages. This step produced an anhydride-rich surface because of the excess of anhydride groups that did not react. These steps were repeated several times to yield a hyperbranched hydrophilic surface covered by a network of the PEI and Gantrez polymers with a high functional group loading. Repetition of these steps alternately 6 times with PEI and 5 times with Gantrez produced a grafted product PEI 6/Gantrez 5. This was experimentally a rather simple process much like layer-by-layer deposition. The entire surface modification procedure took approximately 12h.

This covalent step-by-step assembly process is schematically shown in Figure 4.2. This artistic picture is not necessarily correct and it is suspicious that, for example, amine groups from the PEI 1 stage can and do react with Gantrez polymer introduced when forming the PEI 3/ Gantrez 3 stage. ATR-IR spectroscopy was used to follow the progress of the grafting chemistry as shown in Figure 4.3. The oxidized PE had a relatively small peak due to carbonyl groups at 1710 cm^{-1} . After activation and PEI treatment, the acid carbonyl peak disappeared and an amide peak (1650 cm^{-1}) appeared. The Gantrez stages showed anhydride peaks at 1790 and 1730 cm^{-1} , and also a C-O peak

ascribed to the methoxyl group around 1100 cm^{-1} . The reaction of PEI and Gantrez to form a mixture of amic acids and ammonium carboxylate groups was confirmed by the disappearance of anhydride peaks and the appearance of amide and carboxylate peaks. Qualitatively, the growth of the grafting layers could be estimated by comparing the integral of amide and carboxylate region (1650 and 1560 cm^{-1}) with that of C-H region from PE itself (2910 and 2850 cm^{-1}). The final PEI 6 had a ratio of about 0.7, whereas the ratio was less than 0.05 with PEI 1. The PEI/ Gantrez covalent assembly process was also monitored by acid-base titration. The results, shown in Figure 4.4, reveal a linear growth of titratable groups. After 6 covalent stages of grafting with PEI as the nucleophilic polymer and a mixture of Gantrez with 1.6 wt% ethylenediamine as the electrophilic polymer, the surface loading of the last PEI 6 stage reached 0.89 mmol basic groups per gram of particle. The PEI grafted material has a nanoscale texture on the surface while the neat and oxidized PE have smooth surfaces, as shown by SEM images in Supporting Information. PEI is one of the two polymers used to stabilize CB for LbL assembly, so the grafted particle has an ideal surface.

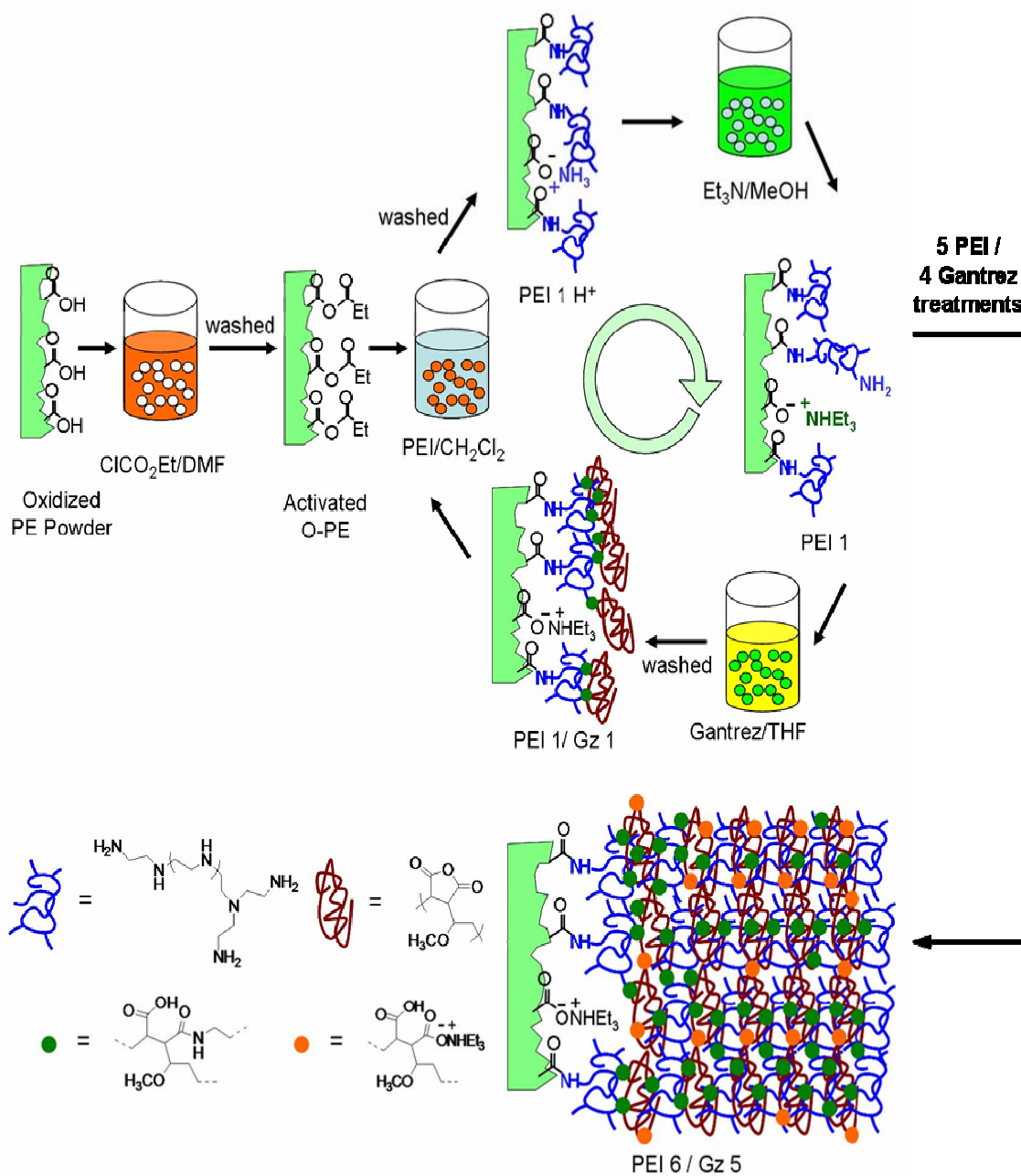


Figure 4.2. Procedure for covalent layer-by-layer deposition of PEI/Gantrez on oxidized PE particle surface.

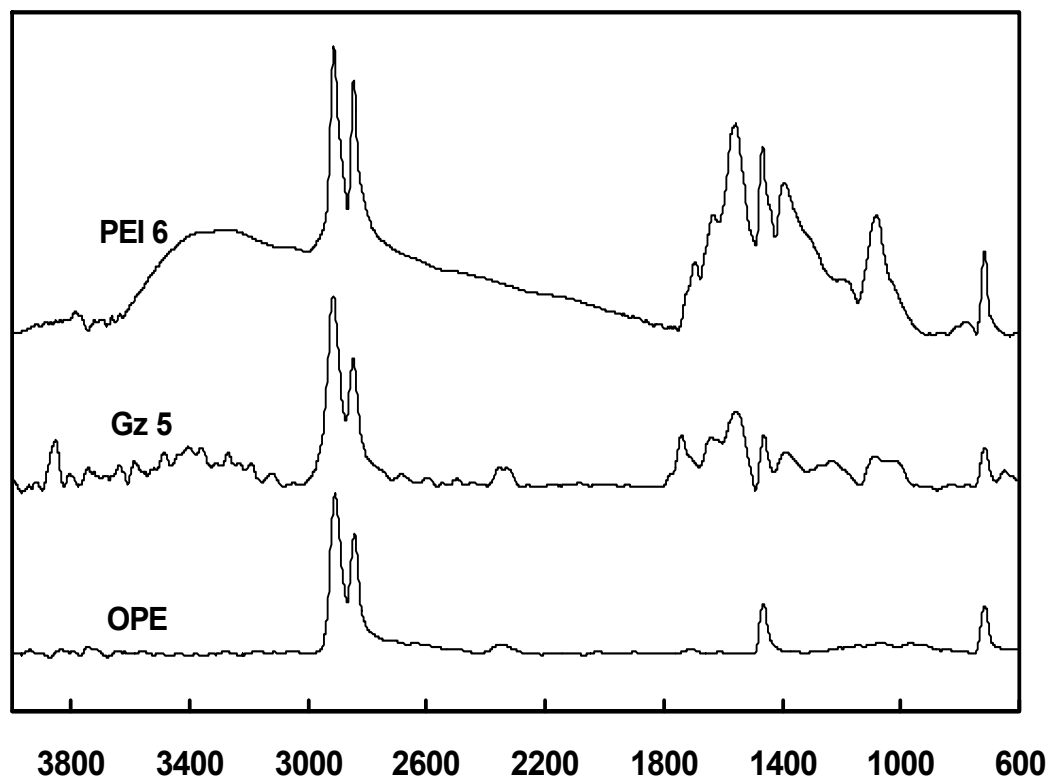


Figure 4.3. ATR-IR spectra of oxidized PE and PEI/ Gantrez PE derivatives.

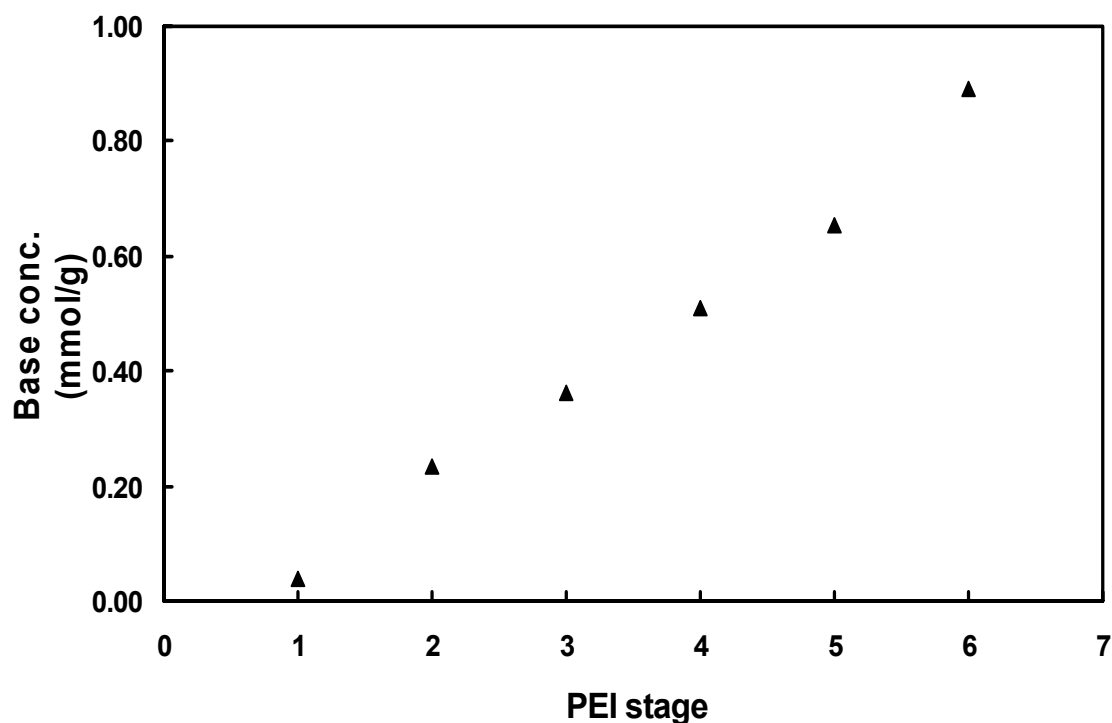


Figure 4.4. Titrimetric results of PEI/ Gantrez PE powders based on three individual experiments.

4.3.2 Carbon Black Coated Particles

Polyethylene is a relatively inert, non-polar polymer that is largely incompatible with the species used for LbL assembly [57]. As shown in Figure 4.5, carbon black deposition is very poor on neat PE after two full deposition cycles (i.e., 2-bilayers of PEI-CB and PAA-CB). The carbon black layer covers only a small area of an otherwise clean surface. Oxidized PE is not much better after 2-bilayers, whereas the PEI-grafted surface is completely coated by carbon black. After 4 bilayers the coating area increases significantly but the coating is non-uniform. Some areas are completely covered by the

coating while others are completely clean. It appears that spots coated in the previous step acts like nucleation sites for subsequent steps. This phenomenon is more clearly shown in once six bilayers are deposited, where the boundary of two coating pieces is observed. Each piece of the coating grows as the number of bilayers increases and eventually links together. After 8 bilayers, almost all of the area is covered by the carbon black coating, but boundaries between initial growth sites persist. In addition to poor growth, the CB exhibits poor bonding with the neat PE surface as evidenced by the interfacial gaps shown at eight bilayers. Only a small portion of the coating is weakly attached to the surface by van der Waals attractions and can be easily removed with a small amount of force. Some research groups are actually exploiting this behavior to produce free standing layer-by-layer assemblies [90].

Acid oxidation of the surface improves the deposition of carbon black to some degree. After two bilayers, the oxidized PE shows that the surface is more uniformly speckled with CB than the neat PE particles (see Figure 4.5). Oxidized PE shows significant improvement over neat PE after four bilayers are deposited. Furthermore, full surface coverage of the oxidized PE particles is achieved with six bilayers. Much like the situation with neat PE, poor bonding between the oxidized PE and the CB thin film is observed. The interfacial gap shown in Figure 4.5 at eight bilayers is similar to those seen on neat PE, although thin film uniformity is much improved. Lack of completely uniform growth is believed due to surface reorganization that eliminates much of the negative surface charge initially produced during the oxidation process [91].

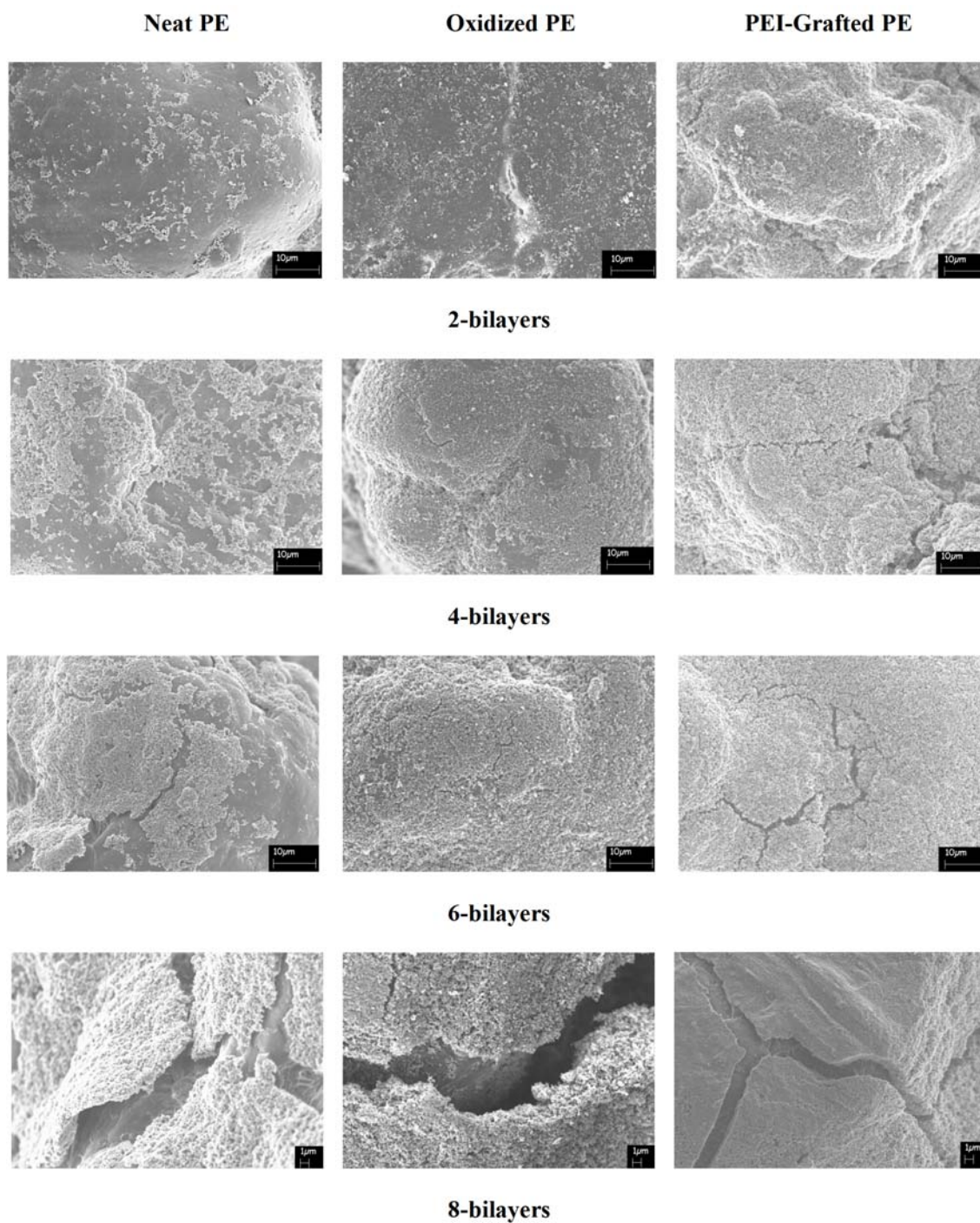


Figure 4.5. SEM images of neat, acid-oxidized, and PEI-grafted PE particles coated with varying numbers of bilayers of CB stabilized with PAA and PEI.

Only the PEI grafted particle demonstrates near perfect compatibility with the LbL process. Unlike the neat and oxidized PE, which show poor initial surface coverage, the PEI-grafted surface is completely covered with just two bilayers of PAA-CB/PEI-CB (see Figure 4.5). Good interfacial adhesion is also evidenced by the lack of an interfacial gap between the CB thin film and grafted PE. With improved adhesion comes an increase in cracking as the deposited film, containing ~45 wt % CB [72], attempts to relieve stress. The poor adhesion on the neat PE leads to buckling that is not observed on the PEI-grafted PE. The intermediate deposition and adhesion on the oxidized PE exhibit true cracking, but at six bilayers rather than the four needed on the grafted surface. A linear increase in CB concentration with the number of bilayer deposited suggests that cracking does not adversely affect film growth for the PEI-grafted PE. TGA, shown in Figure 4.6, qualitatively correlates with the SEM images in Figure 4.5.

The CB concentration of the PEI grafted particles increases linearly as the number of bilayers is increased, exceeding 6 wt% after eight bilayers are deposited. The CB concentration of neat PE is nearly undetectable at two and four bilayers, but increases suddenly at six bilayers. The increasing rate from six to eight bilayers is similar to that of the PEI-grafted case. This result suggests that the CB does not achieve good surface coverage until six bilayers, as shown in the SEM images (see Figure 4.5). Once the CB layer covers a significant fraction of the surface, additional CB layers can be uniformly deposited because the surface of the support is already covered with complementary material. The CB concentration of the oxidized PE falls in between the

grafted and neat samples. The initial growth is similar to the neat PE, but at six bilayers it becomes more like the PEI-grafted PE.

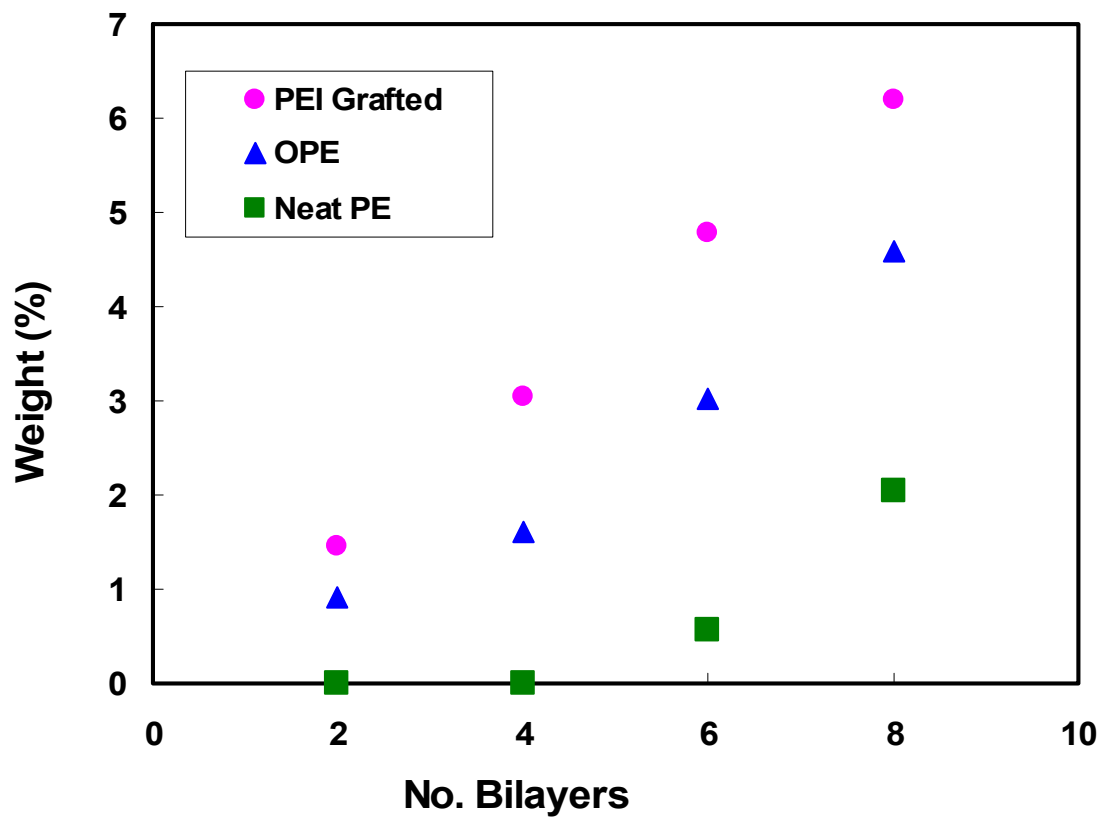


Figure 4.6. Carbon black concentration as a function of the number of bilayers on PEI-grafted, oxidized, and neat PE particles.

4.3.3 Segregated Network Films

After deposition, the coated polyethylene particles were compacted at 90 °C for 30 min. Figure 4.7 shows cross sections of all three films with two and eight bilayers deposited. These images show a segregated network of CB, which is expected to be electrically conductive despite its low concentration of conductive material. During compression, the PE particles lose their roughly spherical shape and become more oblong. The amount of CB, which appears black in these images, correlates well with SEM (see Figures 4.5) and TGA results (see Figure 4.6). For neat PE with two bilayers of CB, the network is incomplete due to poor surface coverage. The carbon black network is much more developed in the film made from oxidized PE, and still more enhanced in the film made with PEI-grafted PE. The microstructure shown for two bilayers on PEI-grafted PE is very comparable to that shown for the neat PE with eight bilayers of CB. Electrical conductivity of these films correlates very well with these microstructures, with better developed networks exhibiting higher conductivity.

During compaction, the large PE particles create excluded volume that keeps CB at the boundaries between them. As a result, the CB coatings create a segregated network structure that reduces the percolation threshold. Figure 4.8 shows the conductivity of compressed films as a function of the number of the bilayers deposited.

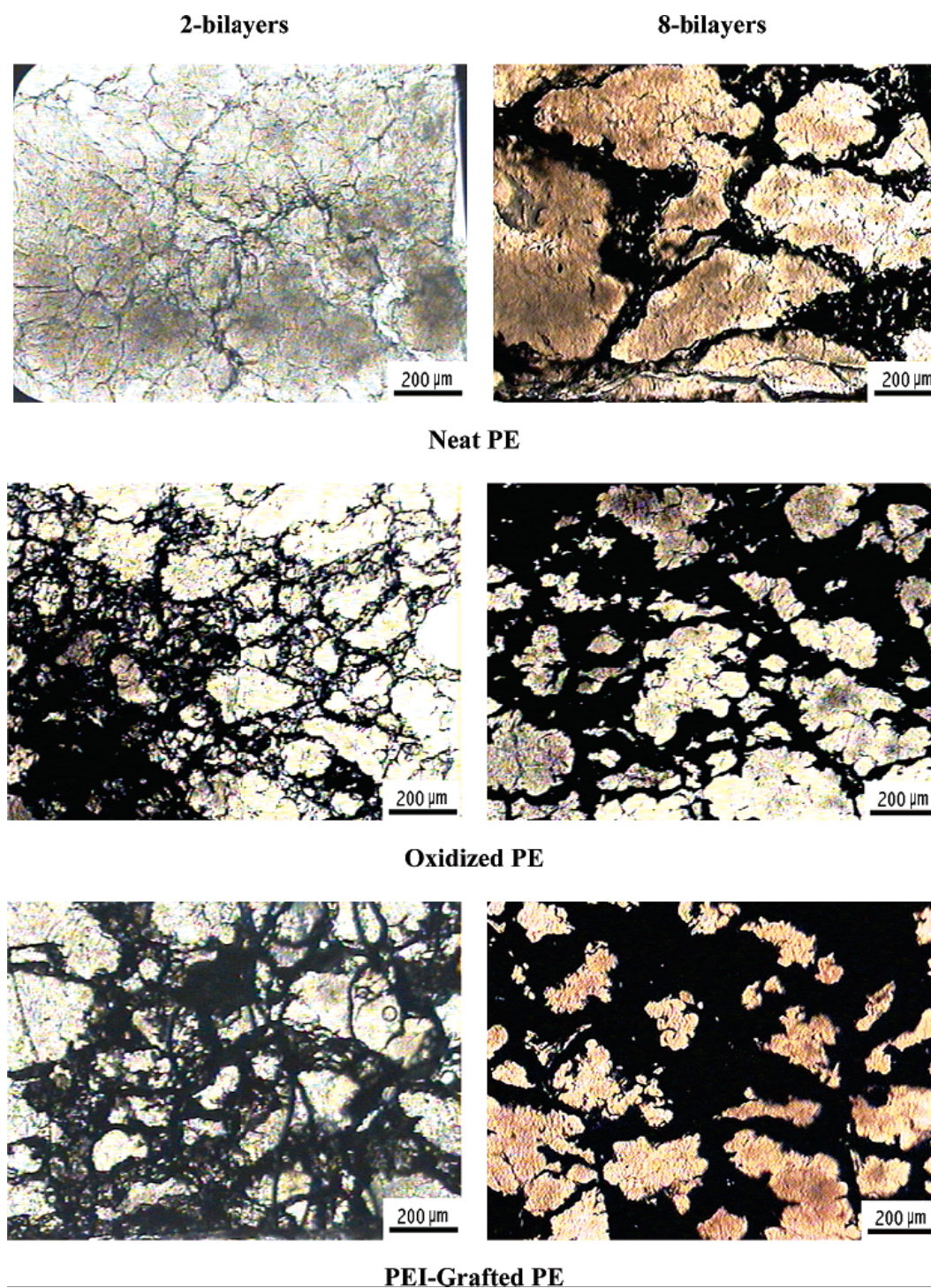


Figure 4.7. Optical microscope cross sections of compressed films made with neat, acid-oxidized, and PEI-grafted PE particles containing two and eight bilayers of CB stabilized with PAA and PEI.

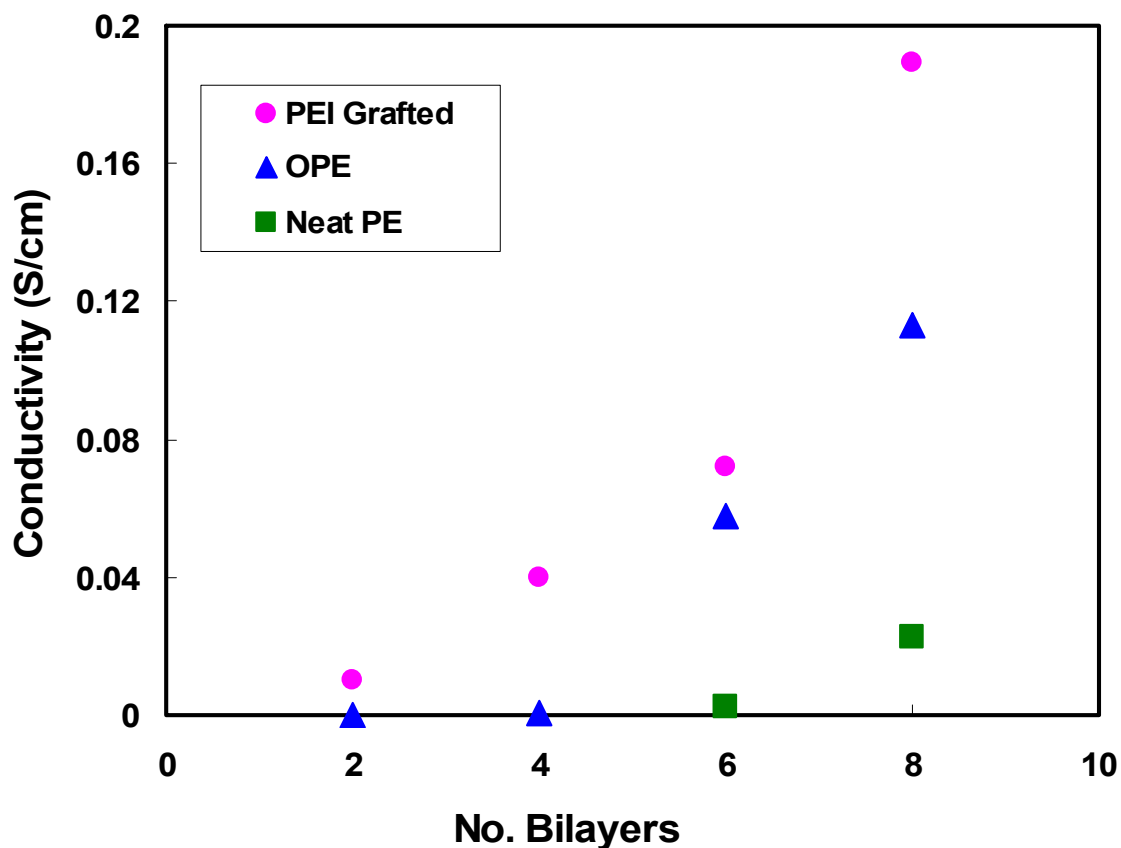


Figure 4.8. Electrical conductivity as a function of the number of the bilayers for films made by compression molding PE particles following LbL deposition of CB.

As expected, films made from PEI-grafted particles exhibit the greatest electrical conductivity. With eight bilayers deposited, conductivity near 0.2 S/cm is achieved. On the basis of TGA results (see Figure 4.6) this corresponds to a CB concentration of just 6 wt%. Composites made using traditional melt processing required more than 30 wt% of the same high structure carbon black to obtain a comparable resistivity in HDPE [92]. Films made with neat PE particles do not exhibit measurable conductivity until six bilayers of CB are deposited, and this value (~ 0.002 S/cm) is more than an order of

magnitude lower than the PEI-grafted film (~ 0.07 S/cm). The films made from oxidized PE particles show electrical conductivity that is more similar to the grafted particles than that of the neat PE, exhibiting measurable conductivity at all bilayers. Despite showing a similar trend of increasing conductivity with number of bilayers, the oxidized particle films are significantly less conductive than the grafted films at all bilayers (see Table 4.1).

Table 4.1. Carbon black concentration and sheet resistance result.

Particle	No. Bilayers	CB Concen. (wt %)	Thickness (mm)	Sheet Resistant (Ω /sq)
Neat	2	N/A	1.45	N/A
	4	N/A	1.64	N/A
	6	0.5737	1.49	3465.99
	8	2.923	1.21	293.13
Oxidzed	2	0.9216	1.69	1308272.89
	4	1.618	1.56	18614.45
	6	3.032	1.54	112.79
	8	4.59	1.47	55.99
Grafted	2	1.455	1.43	672.24
	4	3.05	1.69	168.99
	6	4.778	1.50	92.06
	8	6.1915	1.31	40.13

The difference in film behavior between oxidized PE and PEI-grafted PE is more pronounced when conductivity is shown as a function of carbon black concentration. Using the TGA data from Figure 4.6, the number of bilayers in Figure 4.8 can be converted to CB concentration to generate percolation-style curves for the films made with oxidized and PEI-grafted particles. Figure 4.9 shows these data fitted with the classical percolation power law [18].

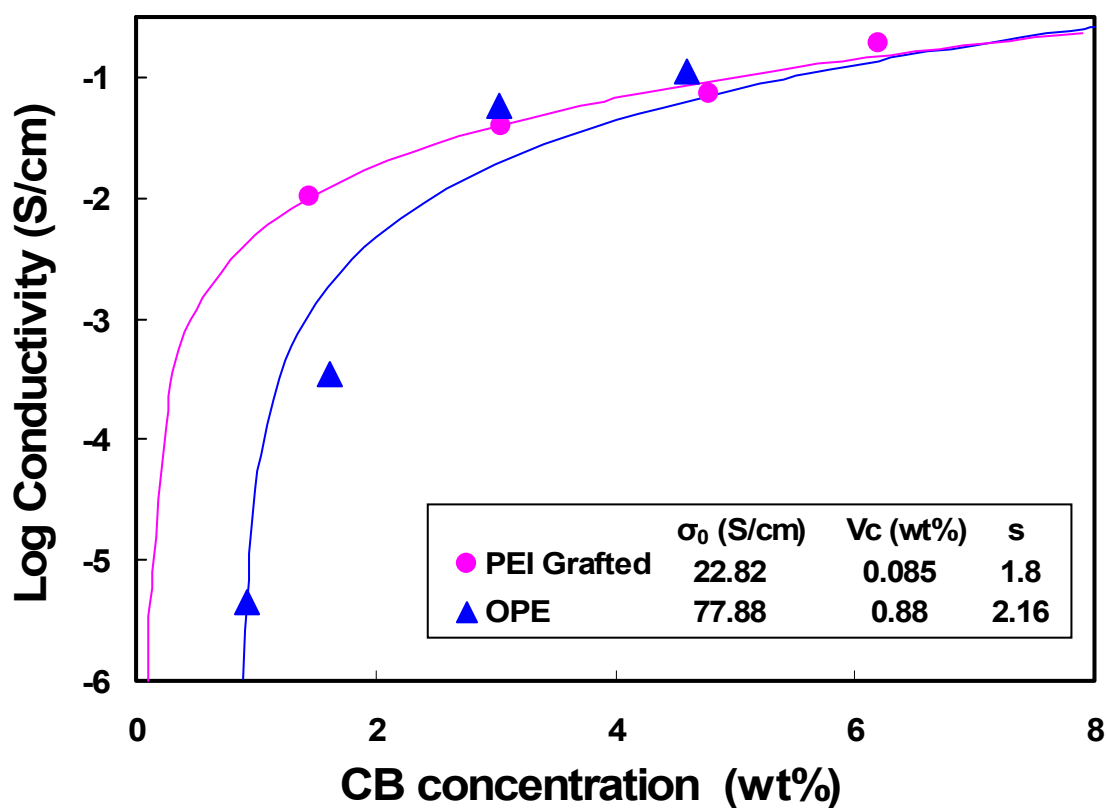


Figure 4.9. Electrical conductivity as a function of CB concentration for films made by compression molding PE particles following LbL deposition of CB.

The PEI-grafted polyethylene films have a PTC of 0.085 wt% CB, while the oxidized polyethylene films have a percolation threshold that is an order of magnitude higher (0.88 wt%). Melt processed composite films made with the same carbon black and polyethylene of the same density show a percolation threshold of 13.5 wt% [92]. It is clear that the segregated network microstructure is responsible for the large shift in percolation threshold. The order of magnitude difference between the two surface treatments suggests that the deposition is less uniform in the case of the oxidized PE particles, as evidenced by comparing the SEM images in Figure 4.5. Both systems converge near 3 wt% CB, but this concentration is achieved at four bilayers for the grafted particles and six bilayers for the oxidized particles. This combination of low percolation threshold and relatively high electrical conductivity, especially for the PEI-grafted system, is currently the best reported for a carbon black-filled polymer composite.

There are several models to predict the percolation threshold of segregated network composites, as summarized in Chapter II. The model proposed by Malliaris and Turner (Equation 2.2 in Chapter II) predicts the PTC based on the assumption that a monolayer of conductive particles covers the surface of each polymer particle [28]. Table 4.2 shows the calculated percolation thresholds using the Malliaris and Turner model with various packing modes. These results are about an order of magnitude lower than the PTC determined by fitting the experimental data with the classic percolation law (Equation 2.1 in Chapter II). Some of this discrepancy may be accounted for by the difference between the assumption of the model and the actual composite microstructure. This model is based on the formation of a monolayer of conductive filler, but carbon

black exists as aggregates of individual nanoparticles. Another possible source of inconsistency is that conductivity results may not reflect the percolation behavior of the composite sufficiently. As shown in Figure 4.9, all conductivity measurements were done in the conducting zone rather than in the percolation zone because the conductivity of two bilayers is already above percolation. It is quite possible that the actual PTC is lower than the PTC fitted with percolation power law. The model of Malliaris and Turner only predicts the PTC, so it is not possible to compare it with the entire conductivity trend of the composite.

Table 4.2. Percolation threshold prediction calculated by Malliaris and Turner model.

Mode of Packing	Triangular	Square	Hexagonal
Coordination Number	3	4	6
ϕ	1.11	1.27	1.375
P_c	2/3	1/2	1/3
V_A (wt%)	0.002	0.0018	0.0015

Slupkowski developed a model to predict the electrical conductivity at any filler concentration above the PTC [37] (Equation 2.4 in Chapter II). The comparison of Slupkowski's model with the experimental data is shown in Figure 4.10. The model's prediction is in reasonable agreement with the experimental data. Slupkowski's model

predicts that the PTC of the composite is lower than the fitted PTC using the empirical percolation power law (Equation 2.1). It is not certain whether Slupkowski's model can explain this composite system better than the classical percolation model, but it demonstrates the possibility that the PTC is actually lower than the fitted PTC, which is also predicted by the model of Malliaris and Turner.

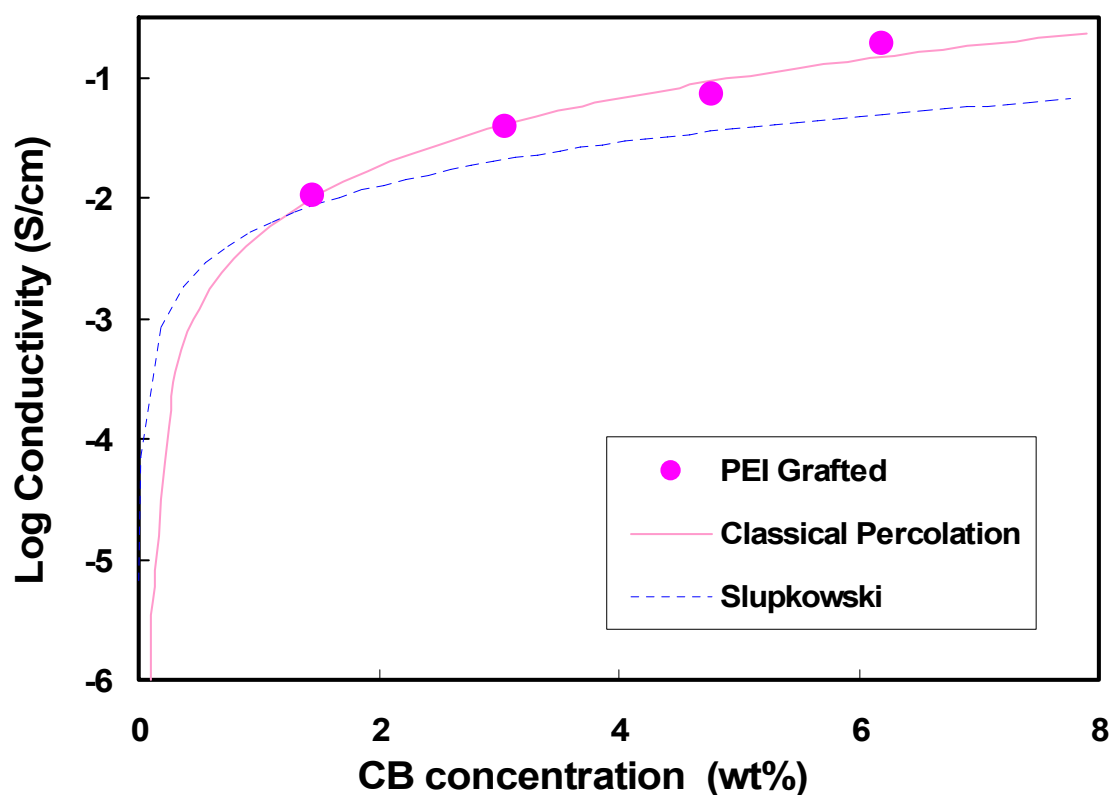


Figure 4.10. Comparison of Slupkowski's model with the electrical conductivity data for PEI grafted PE.

4.4. Conclusion

The effects of no treatment, surface oxidation, and covalent grafting of PEI on PE particles were compared with respect to growth and adhesion of CB thin films deposited using LbL assembly. In the absence of surface modification, LbL film growth is patchy and adhesion is very poor. Surface oxidation improves the rate of film growth; however, it still lacked uniformity at small numbers of bilayers, and adhesion remained weak. Grafting multiple layers of PEI to the PE particle surface provided excellent coverage and promoted stable LbL film growth and excellent adhesion. This CB coated powder was compression molded into films, and their conductivity was measured, which revealed a percolation threshold below 0.01 wt% CB for the PEI-grafted system. Electrical conductivity of 0.2 S/cm was achieved with only 6 wt% carbon black, which is exceptional for a CB-filled PE film. Modification of deposition parameters, such as the ratio of stabilizer to CB, may further increase conductivity and/or reduce the percolation threshold of these films. The use of surface grafting in combination with LbL deposition could be used to impart other useful properties to polyolefin films or particles, including antimicrobial or flame retardant behavior. These results demonstrate the ability to use LbL assembly on a substrate that is traditionally incompatible with this water-based technology.

CHAPTER V
TAILORING PERCOLATION THRESHOLD WITH EMULSION POLYMER
MODULUS

5. 1. Introduction

For segregated network composites, one of the most important parameter influencing the percolation threshold concentration (PTC) is the particle size ratio between the polymer and filler particles, as discussed in Chapter IV. Larger particle size ratio enables a conducting pathway to form at a much lower concentration. Many theories have been proposed to estimate the effect of the particle size ratio and many experimental studies have been performed to confirm them. Few studies have been done to examine other parameters affecting the PTC. In this chapter, the effect of the polymer matrix modulus on the composite's electrical and mechanical behavior is examined. Monodisperse P(MMA-co-BA) emulsion polymers with varying glass transition temperatures were prepared using a semicontinuous process. Differences in the glass transition temperature result in different room temperature moduli that influence composite microstructure formation and properties.

5.2. Experimental

5.2.1. Materials

Methyl methacrylate (MMA), n-butyl acrylate (BA), methacrylic acid (MAA), poly(vinyl alcohol) (PVOH, Mn 85,000-124,000), and sodium persulfate ($\text{Na}_2\text{S}_2\text{O}_8$) were purchased from Sigma-Aldrich (Milwaukee, WI) and used as received. Triton X-405 (70% in water solution), from Sigma-Aldrich, and sodium dodecyl sulfate (SDS, $\text{C}_{12}\text{H}_{25}\text{NaO}_4\text{S}$), from J. T. Baker (Phillipsburg, NJ), were used as surfactants. Sodium bicarbonate (NaHCO_3), from Sigma-Aldrich, was used as a buffer during the reaction and later used to adjust the pH of the final latexes. Sodium silicate ($\text{Na}_2\text{O}_7\text{Si}_3$), from Sigma-Aldrich, and Tamol 791 A, from Rohm and Hass (Philadelphia, PA) were used as dispersing agents. Conductex 7055 Ultra carbon black (CB) was provided by Columbian Chemicals (Marietta, GA). This grade of CB has a nitrogen surface area (NSA) of $55 \text{ m}^2/\text{g}$ and a primary particle size of 42 nm.

5.2.2 Emulsion Polymer Synthesis

Emulsions (or latexes) were synthesized using a semicontinuous polymerization process. Synthesis was carried out in a 1000 ml three-neck round bottom flask equipped with a mechanical stirrer, a Teflon stirring paddle, and a speed controller. To begin, 9.23 g of Triton X-405 was dissolved in 37.59 g of deionized water. Once dissolved, a mixture of BA, MMA, and MAA was continuously fed into the flask for 45 minutes at room temperature while the mixture was stirred at 355 rpm. This pre-emulsion, a highly viscous

white blend, was then moved into the addition funnel for polymerization. Triton-X 405, SDS, and sodium bicarbonate were dissolved in water in the reaction flask, fitted with a condenser, addition funnel and a nitrogen gas tube. The solution was stirred at 155 rpm and a mixture of BA and MMA (44.63 g) was added into the flask. Next, the flask was heated to 65°C using a water bath to keep the temperature constant during the reaction. Once at temperature, the polymerization was initiated by adding a sodium persulfate solution. After 5 minutes, the pre-emulsion was steadily dripped into the flask for 3.5 h. The reactor was held at 65°C for 15 min after the pre-emulsion feed was complete to reduce unreacted monomer. At the end of the polymerization, the latexes were filtered through 10 micron polyester filter bags to remove grit. Poly(vinyl alcohol) (PVOH) was then added to the latexes (2% by weight of acrylic polymer) in order to improve the shear stability during the mixing process [18] and sodium bicarbonate was used to increase the pH of the latexes to 7.5. Films for glass transition temperature and mechanical property testing were prepared by drying the latexes under ambient condition for two days, followed by drying in a vacuum desiccator for one day. Latex recipes are shown in Table 5.1.

5.2.3 Composite Preparation

Sodium silicate (0.05 wt%) and Tamol 731A (0.05 wt%) were added to de-ionized water, followed by carbon black at a concentration of 5 wt%. These ingredients were mixed using a high speed impeller for 20 minutes at 3600 rpm, followed by rolling for 12 hours to achieve equilibrium. This CB mixture was then added to each emulsion with

deionized water and mixed at 3600 rpm for 15 min. The mixture having the highest concentration of CB was made first, with lower concentrations produced by diluting with deionized water and emulsion. These aqueous pre-composite mixtures were kept at a constant 15 wt% solids during processing. After the mixing was complete, 12g of the liquid was poured into a 9 in² mold and allowed to dry under ambient conditions for 48 hours, followed by another 24 h drying period in a vacuum desiccator. The final composite films have a thickness of 185-230 μm .

Table 5.1. Recipe for the latexes with various ratio of BA/MMA.

Pre Emulsion

Latex	BA (g)	MMA (g)	MAA (g)	Triton X-405 (g)	Deionized Water (g)
BA5	101.64	101.64	5.05	9.23	37.59
BA6	121.97	81.31	5.05	9.23	37.59
BA7	142.30	60.99	5.05	9.23	37.59

Reactor Charge

Latex	BA (g)	MMA (g)	Triton X-405 (g)	SDS (g)	sodium persulfate (g)	Sodium Bicarbonate (g)	Deionized Water (g)
BA5	22.31	22.31	5.10	0.36	1.02	1.02	202.73
BA6	26.78	17.85	5.10	0.36	1.02	1.02	202.73
BA7	31.24	13.39	5.10	0.36	1.02	1.02	202.73

5.2.4. Characterization of Emulsion and Composites

Polymer particle size analysis was performed with a Zetasizer Nano-S Zen 1600 (Malvern Inc., Southborough, MA). A Q-800 Dynamic Mechanical Analyzer (DMA) (TA Instruments, New Castle, DE) was used to evaluate the glass transition temperature and storage modulus of the latex films. DMA testing was conducted with a tensile fixture at a frequency of 1 Hz. The temperature was ramped from -50 to 100 °C with a heating rate of 3 °C/min. The amplitude of the strain was fixed at 0.15 %. The maximum point on the loss modulus was taken to be the glass transition temperature (T_g) for each sample. The cross-sections of the composite films were imaged with a Tescan VEGA-II SEM (Cranberry Township, PA). Films were soaked in liquid nitrogen and fractured by hand and the surfaces were sputter coated with 4 nm of platinum prior to SEM imaging. Electrical conductivity was measured with a home-built four-point-probe system (see description in Chapter IV).

5.3. Results and Discussion

5.3.1 Monodispersed Latex Characterization

Following synthesis, the particle size and glass transition temperature of the latexes were characterized. Particle size, BA/MMA ratio, and glass transition temperature of these latexes are summarized in Table 5.2. Particle size distributions are shown in Figure 5.1. The average particle size is approximately 150nm for all three systems. The polydispersity indexes (PDI) are below 1.1 for all latexes, indicating they are

monodispersed. It has already been established that using ionic and nonionic surfactant yields emulsions with narrow particle size distributions [93].

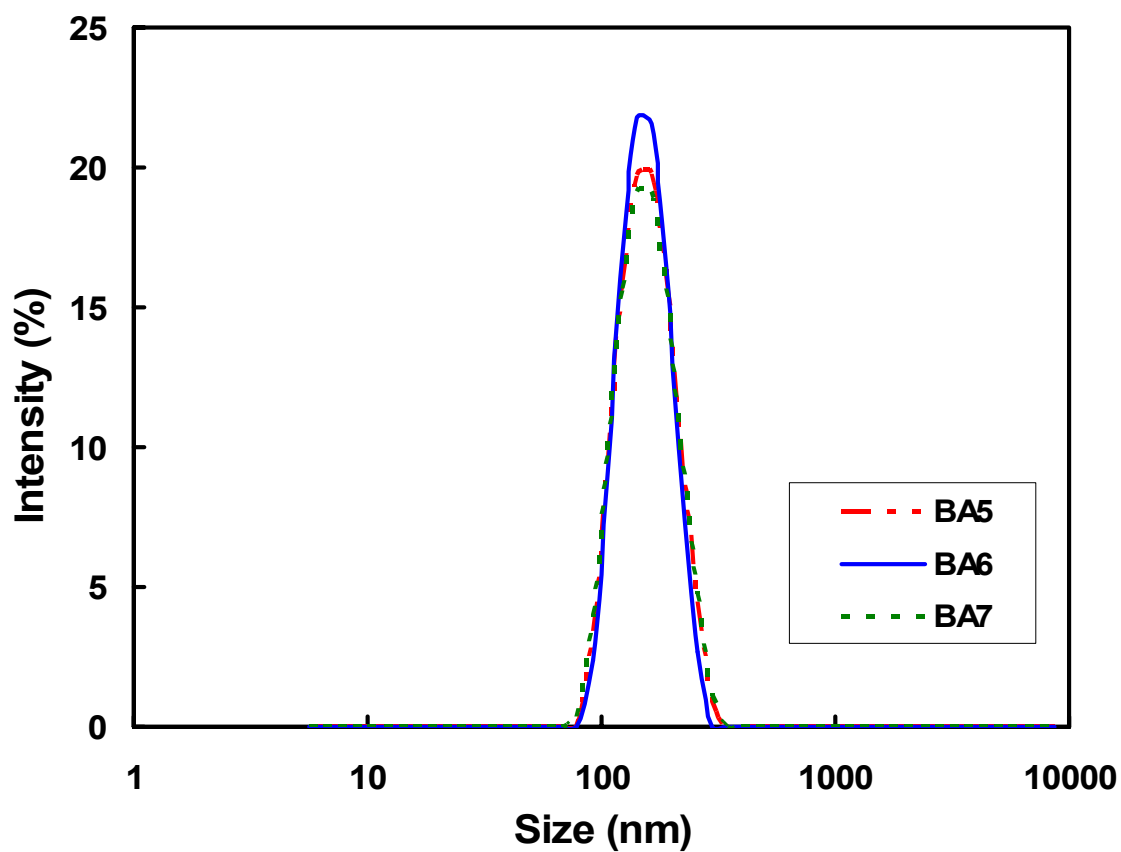


Figure 5.1. Particle size distribution of the three P(BA-co-MMA) latexes. The number after BA refers to the weight fraction of butyl acrylate in the copolymer (i.e., “5” means 50 wt%).

Table 5.2. Composition, particle size, and theoretical and actual T_g of latexes.

Latex	BA/MMA	Particle Size (nm)	PDI	T_g , FOX (°C)	T_g , DMA °C)
BA5	50:50	150	1.057	4.4	20.2
BA6	60:40	149	1.037	-9.3	0.4
BA7	70:30	149	1.061	-21.8	-8.7

The glass transition temperature of a copolymer can be approximated using the Fox equation [94]:

$$\frac{1}{T_g} = \frac{w_1}{T_{g1}} + \frac{w_2}{T_{g2}} = \frac{w_{BA}}{219} + \frac{w_{MMA}}{378} \quad (5.1)$$

where, w is the weight fraction of each component and T_g is the glass transition temperature of each homopolymer and copolymer in Kelvin. Figure 5.2 shows the experimental and theoretical glass transition temperatures for the latexes made here. The experimental data are qualitatively in good agreement with the Fox prediction, but experimentally determined glass transition temperature is consistently 12 – 15 °C higher. This is likely due non-random sequencing arrangements of MMA and BA repeat units. The Fox equation assumes that the two units are arranged in a completely random manner. In reality, MMA and BA have different reactivity ratios ($r_{MMA}= 0.920$ and $r_{BA}=0.130$) [95]. MMA has a higher ratio, so it tends to react with itself more than BA during

polymerization. This difference in reactivity will lead to longer sequences of MMA, making the glass transition temperature of the copolymer higher than expected.

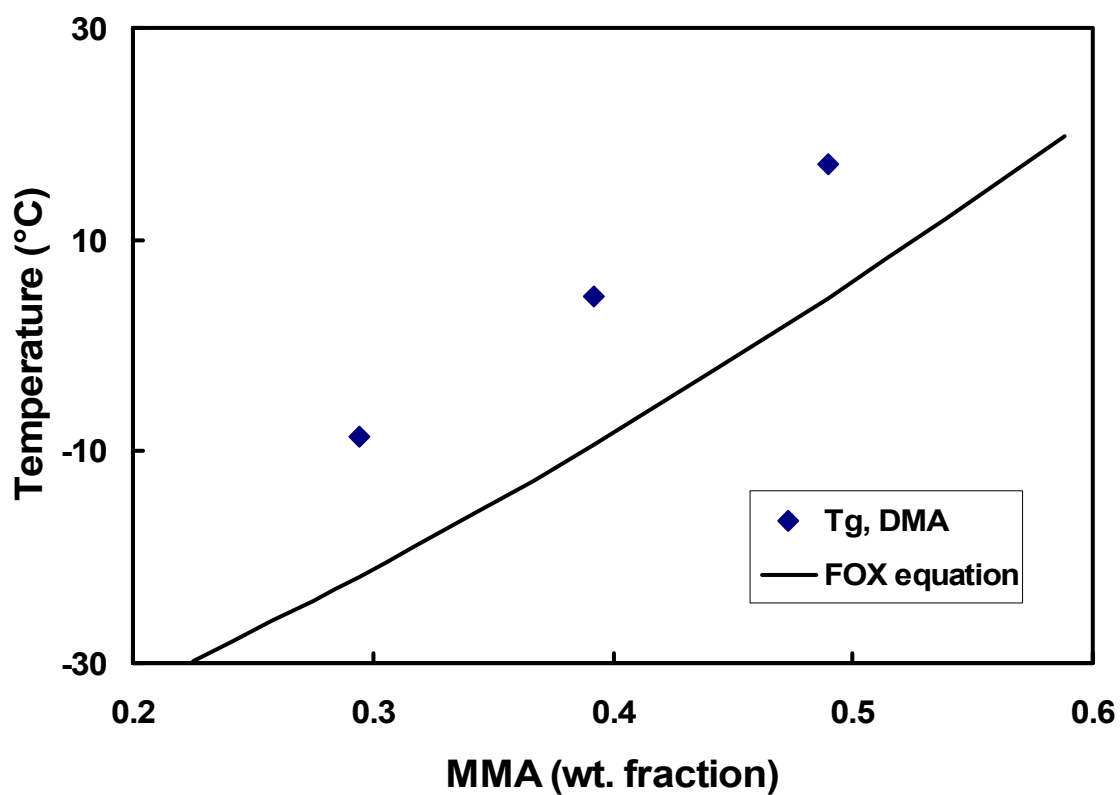


Figure 5.2. Glass transition temperature of P(MMA-n-BA) copolymers, measured experimentally and predicted by the Fox equation, as a function of the weight fraction of methyl methacrylate.

Figure 5.3 shows neat latex storage modulus as a function of temperature. The storage modulus is considered to be nearly the same as elastic modulus at room temperature [96]. The room temperature storage modulus increases with higher glass transition temperature. The storage modulus at 20 °C is 637.71 MPa for BA5, 18.35 MPa for BA6, and 3.57 MPa for BA7, respectively. The storage modulus at room temperature drops most significantly by changing the BA composition from 50 to 60 wt% due to the transition between the glassy and rubbery states of the polymer. It is worth noting that the overall shape of the storage modulus curve is similar for all of the latexes despite differences in chemical composition. This indicates that the thermo-mechanical response of all latexes to temperature is very similar regardless of the glass transition temperature. This data also provides another important trait of the latexes. The storage modulus curve drops only once for each polymer, suggesting that BA and MMA are completely miscible with each other, making one coherent phase.

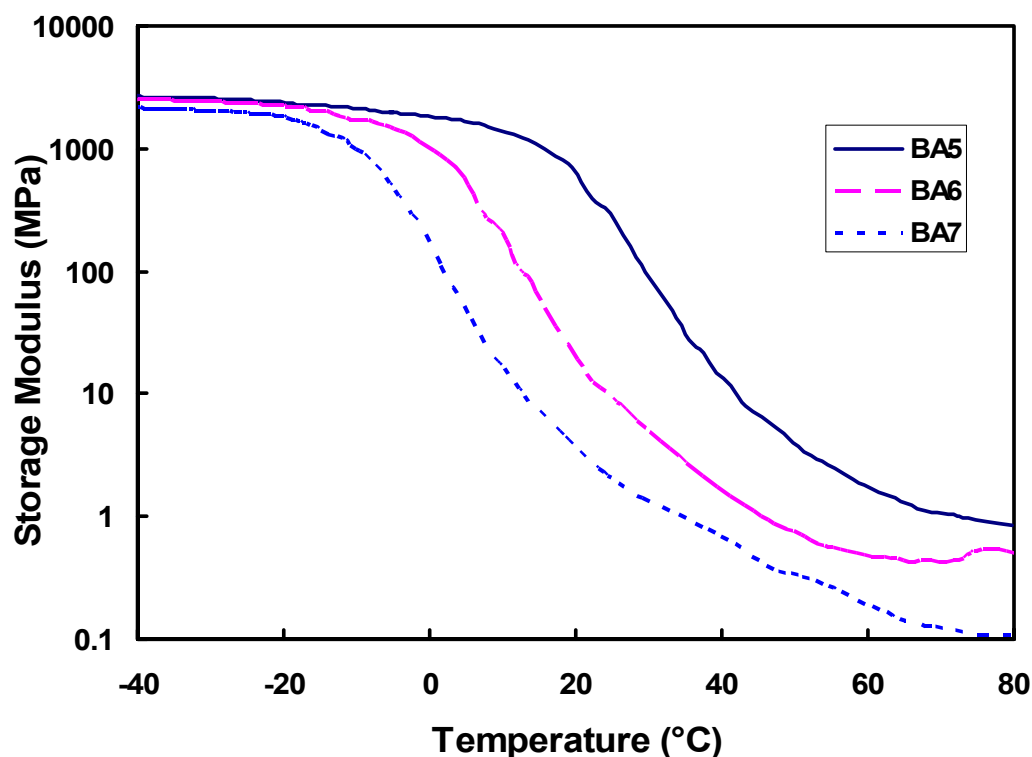


Figure 5.3. Storage modulus (E') of neat acrylic latexes as a function of temperature.

5.3.2 Composite Microstructure

After polymerization, CB was added to each emulsion to produce conducting composites. During drying, the polymer particles push the CB into the interstitial space between them and the segregated CB network is formed. The modulus of the polymer particle plays an important role in the formation of the segregated network. SEM images of composites dried at room temperature are shown in Figure 5.4. At this temperature, the storage modulus of BA5 is about 30 times higher than that of BA6 and two orders of magnitude higher than that of BA7. As shown in Figure 5.4(a), the BA5 composite

creates a strong network at 5 wt% CB. Carbon black is better dispersed in BA6 and BA7. Before drying, the dispersion level of CB in each emulsion should be similar because CB is pre-dispersed in water using dispersing agents. The mixture was stirred again during the composite preparation process, but this should not significantly alter the dispersion. The difference in CB distribution within the polymer matrix comes primarily from the different modulus.

The copolymer containing 50 wt% butyl acrylate (BA5) has a relatively high modulus at room temperature, so the polymer particles tend to maintain their original shape and more effectively force CB into the interstitial space during coalescence. The segregated network of CB is formed at lower concentration and the PTC is much lower than the other BA series, as will be discussed in following section. The modulus of BA6 and BA7 is very low at room temperature, so the polymer is more like a liquid and the emulsion particles tend to deform around CB particles rather than simply contact them. The polymer matrix penetrates into the gap between CB particles and hinders the formation of a conducting pathway. SEM images of BA6 and BA7 with 5 wt% CB (Fig. 5.4 (a) and (e)) show that the CB particles are separated by the polymer matrix more effectively. At this concentration, the electrical conductivity is not measurable for these systems. SEM images of composites with 10 wt% CB clearly show the distinction between BA5 (Fig. 5.4 (b)) and the other composites. For the BA5 system, CB is highly aggregated in the polymer matrix due to the lack of deformation of the polymer matrix around CB particles. For BA6 and BA7 (Figs. 5.4 (d) and (f)), the segregated network of CB grows stronger as the CB concentration increases from 5 to 10 wt%.

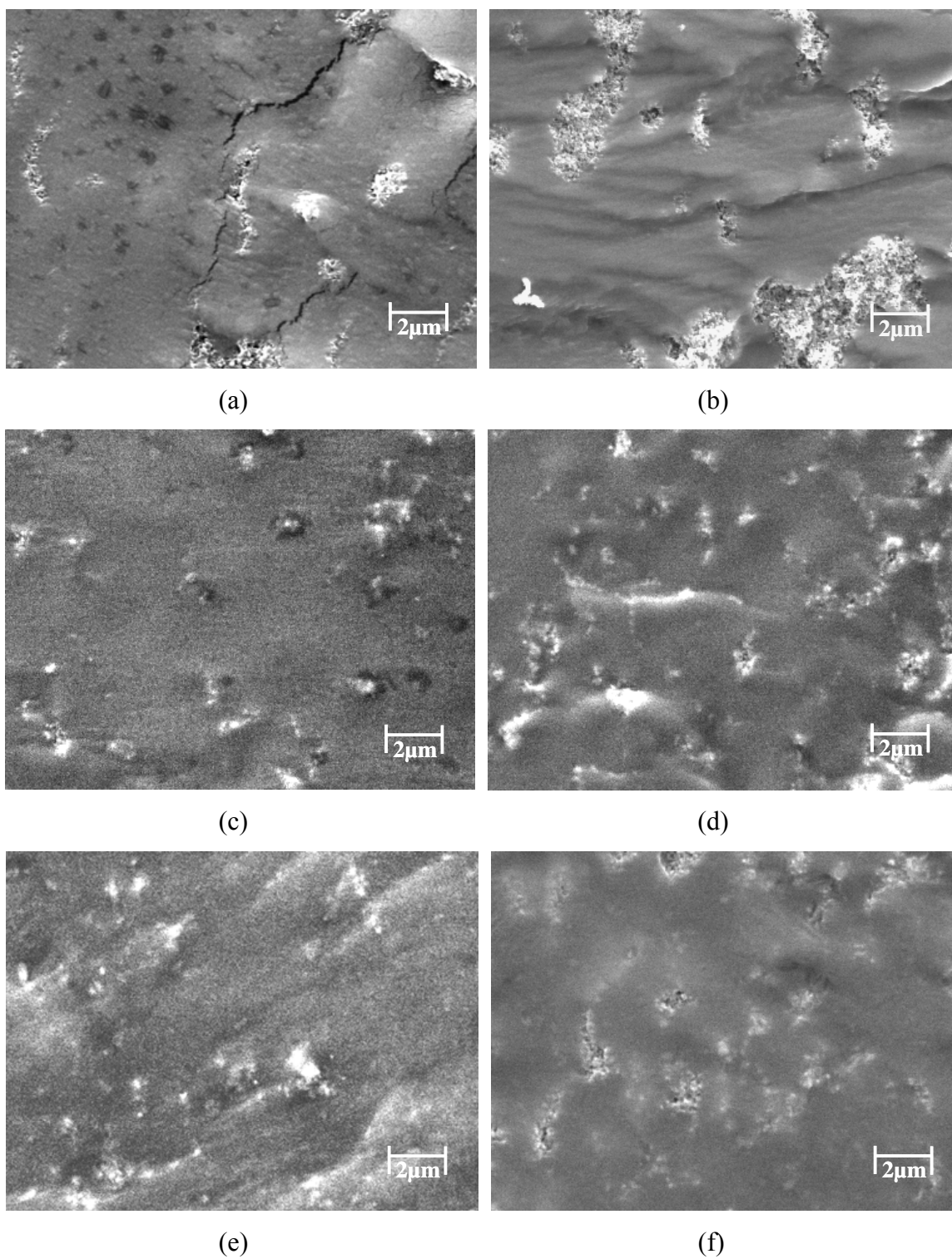


Figure 5.4. SEM images of BA 5 with 5 wt% (a) and 10 wt% (b), BA6 with 5 wt% (c) and 10 wt% (d), and BA7 with 5 wt% (e) and 10 wt% (f) carbon black. These composites were dried at room temperature.

To further examine the effect of the matrix modulus, composites were dried at 80°C. Figure 5.5 shows the cross sectional images of these composites. At this temperature, the storage modulus is 0.84 MPa for BA5, 0.51 MPa for BA6, and 0.1 MPa for BA7, respectively. The dispersion level of CB in each emulsion is similar due to more similar modulus. At 10 and 15 wt% CB, there is no difference in the SEM images of BA5 and BA6. The carbon black appears well dispersed within the polymer matrix and the segregated network is well defined. For the BA6 system, the dispersion level of CB at 10 wt% (Fig. 5.5 (c)) is comparable with that of the composites dried at room temperature (Fig. 5.4. (d)) with the same concentration. Unlike BA6, the BA5 system shows a dramatic difference in the distribution of CB between composites dried at room temperature and at 80°C. The composites dried at room temperature show a significant level of porosity due to CB aggregation. These pores are nearly eliminated when the drying temperature is increased to 80°C. The emulsion particles are much softer at this elevated temperature, so they easily deform around CB particles and fill the gaps between them.

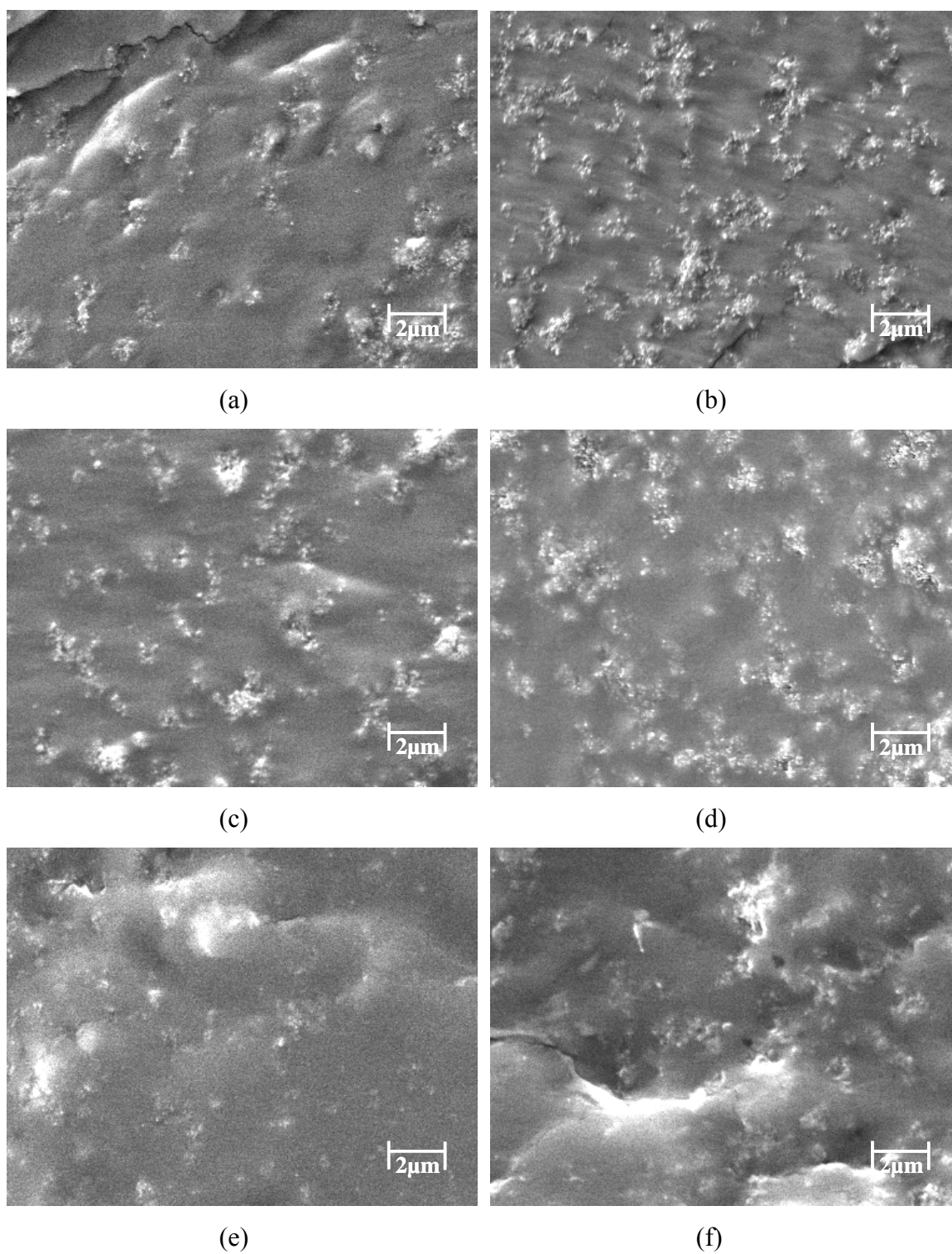


Figure 5.5. SEM images of BA 5 with 10 wt% (a) and 15 wt% (b), BA6 with 10 wt% (c) and 15 wt% (d), and BA7 with 10 wt% (e) and 15wt% (f) carbon black. These composites were dried at 80 °C.

The BA7 system shows somewhat different behavior relative to BA6. At room temperature, the dispersion level of CB is equivalent in BA6 and BA7. At 80°C, however, CB is almost randomly dispersed. At 10 wt% CB (Fig. 5.5 (e)) no network structure has formed and only a weak network with a few pores is observed at 15 wt% CB. With such a low glass transition temperature, the BA7 emulsion particles become extremely soft at 80°C. These low modulus particles behave more like a solution polymer, effectively separating CB particles and hindering the formation of a segregated network. The conductivity results in the next section reinforce this assessment.

5.3.3 Electrical Conductivity

Electrical conductivity was measured as a function of CB concentration for composite series dried at room temperature and at 80°C. These results are shown in Figure 5.6 (room temperature) and Figure 5.7 (80 °C). At room temperature, the PTC of BA5 is 1.5 vol%, while the PTCs for BA6 and BA7 are 4.28 and 4.93 vol%, respectively. Again, the higher modulus of BA5 particles forces the CB into the interstitial space more effectively and forms the segregated network at a much lower concentration. The conductivity values are also higher for BA5 at all concentrations. The stronger CB network in BA5, due to the lack of polymer deformation and aggregation of CB, results in higher conductivity for a given CB concentration. The difference in the electrical conductivity between BA5 and BA6 becomes smaller as CB concentration increases. The PTC for BA7 is close to that of BA6, but the conductivity value is much lower, due to greater polymer deformation that weakens contact between CB particles.

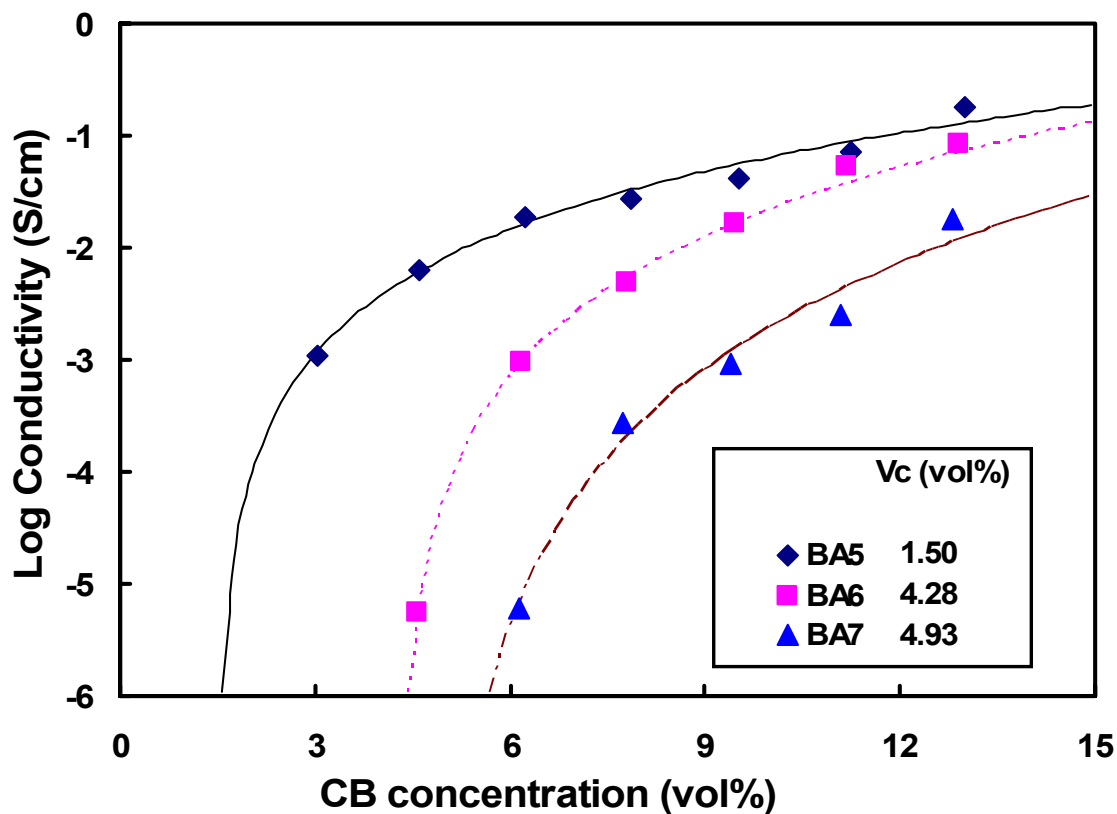


Figure 5.6. Electrical conductivity of latex-based composites, dried at room temperature, as a function of carbon black concentration.

Increasing the drying temperature yields dramatic changes in the electrical behavior of the BA5 system. The PTC increases from 1.5 to 3.56 vol%. The modulus of BA5 is reduced three orders of magnitude, from 610.8 to 0.84 MPa, by increasing the temperature from 20 to 80°C. The modulus of BA5 at 80°C is close to BA6, making both systems behave in a similar manner. At each concentration, the conductivity of BA5 is comparable to that of BA6. As expected from the microstructure (see Fig. 5.5), the electrical conductivity of BA7 shows dissimilar behavior with these other systems. The

conductivity of BA7 dried at 80°C is not measurable until 9.5 vol% CB and the measured values are much smaller than that of the other systems. This kind of conductivity behavior is often found in polymer composites with randomly dispersed filler. BA7 contains 70 wt% of BA, which means its melting point is much lower than the other systems. Low melting point makes BA7 act like a melt-based composite at 80°C and the conductivity trend of BA7 becomes more like that of a randomly dispersed composite.

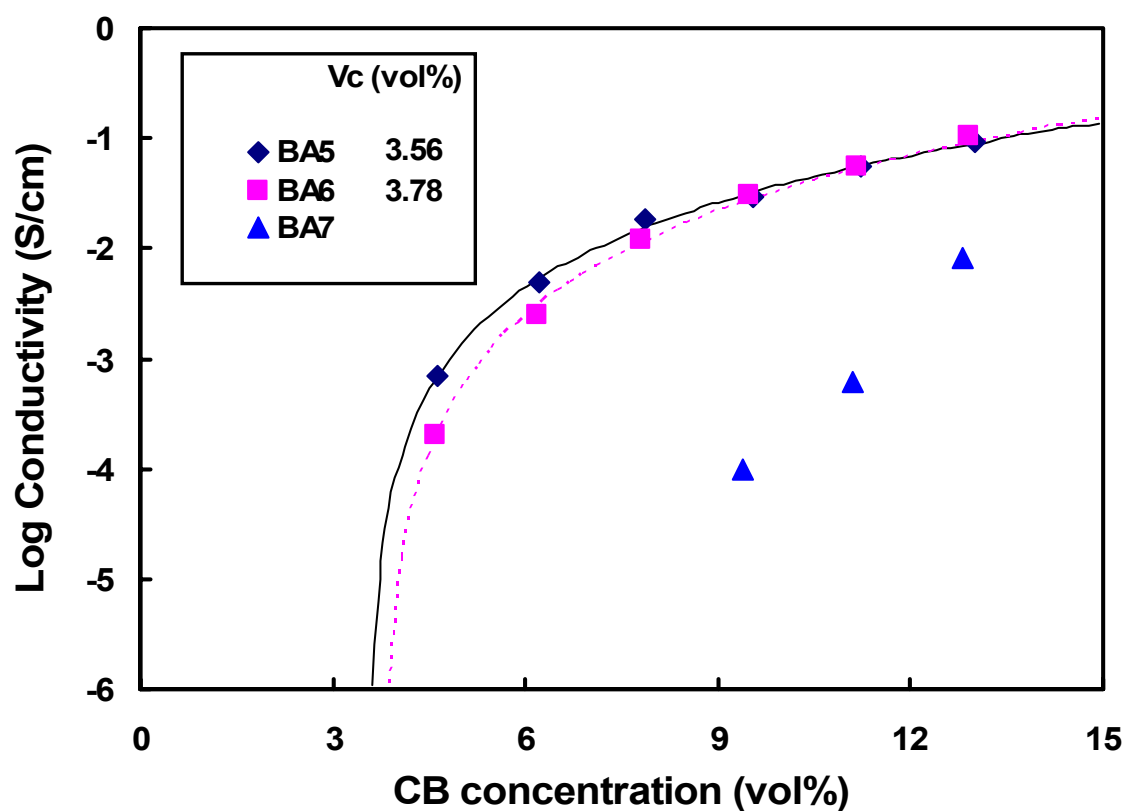


Figure 5.7. Electrical conductivity of latex-based composites, dried at 80°C, as a function of carbon black concentration.

5.4. Conclusion

A series of emulsions with different glass transition temperatures were synthesized by varying the concentration of butyl acrylate and methyl methacrylate repeat units. The glass transition temperatures of these latexes were higher than those predicted by the Fox equation due to greater MMA reactivity that likely increased its concentration in the copolymer. Composites made using the emulsion with higher room temperature modulus (due to higher T_g) shows lower PTC and higher conductivity. When the modulus of the polymer is high, the emulsion particles tend to maintain their original shape during the coalescence process. In this case, carbon black particles are more effectively forced into the interstitial space between polymer particles to form a segregated network at lower concentration. Lower modulus polymer particles easily deform around CB particles and separate them from one another. The BA5 system shows a stronger network of CB at room temperature with lower concentration. The electrical conductivity data reinforces this assumption. The PTC of BA5 at room temperature is significantly lower than those of the lower modulus systems and the conductivity values are higher. Disparity between BA5 and BA6 is eliminated by increasing the drying temperature to 80°C, where the modulus of BA5 is close to that of BA6. The dispersion level of CB in both BA5 and BA6 is qualitatively the same. When the emulsion contains 70 wt% of BA, the modulus of the copolymer is < 1 MPa at 80°C. CB is more uniformly dispersed in this very soft matrix without formation of a network until much higher concentration. The conductivity behavior of BA7 is close to that of a randomly dispersed composite produced from

solution or melt processing. This study clearly demonstrates the importance of polymer modulus on the electrical properties of emulsion-based composites.

CHAPTER VI

CONCLUSION AND FUTURE RESEARCH PLAN

The overarching goal of this research was to examine and understand the effects of various parameters on the electrical properties of carbon black-filled polymer nanocomposites. A series of experiments were performed and analyzed to understand the formation of segregated networks and clarify the relationship between polymer matrix properties (microstructure, modulus, and particle size) and the electrical and mechanical properties of the resulting conductive composites. First, a segregated network composite was compared with a solution-processed composite to understand the advantages and limitations of the segregated network composite. Next, two important polymer matrix properties were studied: (1) particle size and (2) polymer matrix modulus.

6.1. Segregated Network vs. Random Dispersion

Two composites with similar chemical composition were produced with liquid-based processing. The resulting composites had very different final properties due to their differing microstructure. The segregated network composite, made with a poly(vinyl acetate) emulsion, showed dramatic changes in modulus and conductivity at low carbon black loading, while randomly dispersed composites exhibited more gradual changes. The percolation threshold concentration of the segregated network composite is 1.21 vol%, which is about seven times less than that of the solution-based composite. The SEM images of composite cross sections show that CB within the emulsion-based matrix

creates a conductive pathway at low concentration due to the excluded volume created by emulsion particles. The CB in the solution-processed composite is more uniformly dispersed. The modulus of these composite also exhibits similar behavior, with the emulsion-based system showing greater stiffness enhancement at low CB concentration.

6.2. Polymer-Filler Particle Size Ratio

Uniform surface coverage of a polymer particle by the filler is essential to study the effect of particle size ratio. Hyper-branched polyethylenimine (PEI) was covalently grafted to the surface of polyethylene (PE) particles in an effort to promote the growth of conductive thin films deposited using layer-by-layer (LbL) assembly. LbL films were then deposited using dilute aqueous mixtures containing carbon black stabilized with polyethylenimine or poly(acrylic acid). Deposition of carbon black-filled bilayers on PEI-grafted PE shows uniform surface coverage and strong bonding after just 2-bilayers, while neat polyethylene shows only patchy film growth and poor adhesion. After carbon black deposition, the electrical conductivities of films made by compression molding were compared. No conductivity was measured for films made with neat PE particles containing 2 and 4-bilayers, but the PEI-grafted system exhibits a conductivity of 0.01 S/cm. Plotting conductivity as a function of carbon black concentration revealed a percolation threshold below 0.1 wt% and a maximum conductivity of 0.2 S/cm with just 6 wt%. The empirically determined percolation threshold for the PEI-grafted system was compared with the Malliaris and Turner prediction [28] and the conducting behavior was

compared with Slupkowski's model [37]. The theoretical prediction suggests that the actual PTC for the PEI-grafted system may be lower than 0.002 wt%.

6.3. Polymer Matrix Modulus

Polymer matrix modulus had not been previously studied as a means to alter composite electrical properties because conventional composites are produced in the solution or melt states. In solution and melt processing the modulus of the polymer matrix can be disregarded. This is not the case for emulsion-based composites because they are produced with the polymer in its solid state during processing. Monodispersed emulsions having different glass transition temperature were synthesized to investigate the effect of the polymer matrix modulus on the electrical properties of segregated network composites. The emulsion with highest modulus at room temperature produced composites with the lowest percolation threshold concentration. The PTC for a composite made from a copolymer latex containing 50 wt% butyl acrylate and 50 wt% methyl methacrylate (BA5) is 1.5 vol%, while the PTC for BA7 (70wt% BA), which has lowest modulus, is 4.93 vol %. The microstructure of each composite shows significant differences in the level of CB dispersion within the polymer matrix. Higher modulus polymer particles push the CB more efficiently into the interstitial space between them, resulting in lower PTC. This modulus effect was confirmed by increasing the drying temperature, where the modulus of two emulsions (BA5 and BA6) were practically the same and the PTC for both composite is very similar.

6.4 Future Work

The segregated network approach is relatively mature (more than 30 years of research) and many studies have shown that it is one of the most effective ways to reduce the percolation threshold of polymer composites. Despite its potential, complexity of processing and lack of mechanical robustness hinders the use of segregated network composites for many useful applications. Using an emulsion polymer as the matrix can resolve these problems because the processing is relatively simple, requires little energy, and the final composites are mechanically robust. More studies are needed to establish processing rules for emulsion-based composites because it is a new system for conductive purpose. Some suggestions for future study, to develop a more fundamental understanding of these composites, are presented here.

6.4.1. Influence of Emulsion Particle Size on Composite Properties

The polymer particle size is expected to play an important role for emulsion-based composite properties. An emulsion with larger particle size should have a lower percolation threshold. The change in other properties, such as maximum conductivity and mechanical properties, are not as obvious. It is possible to adjust the particle size of emulsion particles by adjusting the stabilizer composition and reaction temperature [95,97-99]. When carbon black is then added to these emulsions with varying particle size, the effect of particle size ratio can be investigated. Furthermore, an empirical model to predict the electrical behavior of emulsion-based composite can be established.

6.4.2. Influence of Particle Size Distribution on Composite Properties

The particle size distribution is also an important parameter expected to change the electrical properties of these composites. In Chapter III, a commercial emulsion was used to create a segregated network composite with very low percolation threshold due to large average particle size and a wide particle size distribution. This system tends to show less change with drying temperature, relative to the monodisperse emulsions studied in Chapter V. By mixing and matching the particles of varying size from different monodisperse emulsions, the effect of the particle size distribution can be studied.

6.4.3. Transparent Conductive Polymer Composite

Conductive thin films with high transparency have attracted significant interest for the past decade. They can be used in many applications such as solar cells [100], displays [101], electrochromic windows [102], and organic light-emitting diodes (OLED) [103]. Currently, ceramic materials are most commonly used to create these films due to their transparency and high conductivity. Indium tin oxide [104], zinc oxide [105], indium gallium oxide [106] and cadmium tin oxide [107] are all used as transparent conductive oxides. More recently, single-walled carbon nanotubes were used to make transparent conductive films [108]. If nanoparticles of these materials can be combined with an emulsion polymer, the final composite could be transparent and conductive. In this dissertation, the emulsion polymer was shown to significantly reduce the percolation threshold due to its segregated microstructure. The fabrication process is also quite straightforward so the cost can be reduced significantly. Unfortunately, it is not easy to

make very thin films with an emulsion. A film with a thickness of less than 50 μm tends to have a rough surface. If the particle size of the emulsion is small and the distribution is narrow, it may be possible to create a very thin film with the emulsion polymer. Another issue associated with conductive composites is that the conductivity decreases dramatically as the thickness of the film decreases (due to a transition from 3-D to 2-D percolation). Further studies are needed to find an optimal thickness to achieve the best combination of the transparency and conductivity.

REFERENCES

- [1] Brodeur SA, Huebner W, Runt JP, Newnham RE. *J Mater Res* 1991;6:175.
- [2] Wan Y, Wen DJ. *Smart Mater Struct* 2004;13:983.
- [3] Kim YS, Ha SC, Yang Y, Kim YJ, Cho SM, Yang H, Kim YT. *Sensor Actuat B-Chem* 2005;108:285.
- [4] Koscho ME, Grubbs RH, Lewis NS. *Anal Chem* 2002;74:1307.
- [5] Das NC, Chaki TK, Khastgir D, Chakraborty A. *Adv Polym Tech* 2001;20:226.
- [6] Klason C, McQueen DH, Kubat J. *Macromol Symp* 1996;108:247.
- [7] Kale V, Moukwa M. *J Electrostat* 1996;38:239.
- [8] Lee GJ, Suh KD, Im SS. *Polym Eng Sci* 1998;38:471.
- [9] Feller JF, Linossier I, Levesque G. *Polym Advan Technol* 2002;13:714.
- [10] Tang H, Chen XF, Luo YX. *Eur Polym J* 1996;32:963.
- [11] Schueler R, Petermann J, Schulte K, Wentzel HP. *J Appl Polym Sci* 1997;63:1741.
- [12] Grunlan JC, Gerberich WW, Francis LF. *J Mater Res* 1999;14:4132.
- [13] Souza FG, Sena ME, Soares BG. *J Appl Polym Sci* 2004;93:1631.
- [14] Tchoudakov R, Breuer O, Narkis M, Siegmann A. *Polym Eng Sci* 1996;36:1336.
- [15] Levon K, Margolina A, Patashinsky AZ. *Macromolecules* 1993;26:4061.
- [16] Cheah K, Forsyth M, Simon GP. *J Polym Sci Pol Phys* 2000;38:3106.
- [17] Grunlan JC, Gerberich WW, Francis LF. *J Appl Polym Sci* 2001;80:692.
- [18] Kirkpatrick S. *Rev Mod Phys* 1973;45:574.

- [19] Thongruang W, Balik CM, Spontak RJ. *J Polym Sci Pol Phys* 2002;40:1013.
- [20] Sumita M, Sakata K, Hayakawa Y, Asai S, Miyasaka K, Tanemura M. *Colloid Polym Sci* 1992;270:134.
- [21] Breuer O, Tchoudakov R, Narkis M, Siegmann A. *J Appl Polym Sci* 1997;64:1097.
- [22] Feng JY, Chan CM, Li JX. *Polym Eng Sci* 2003;43:1058.
- [23] Foulger SH. *J Polym Sci Pol Phys* 1999;37:1899.
- [24] Bouchet J, Carrot C, Guillet J, Boiteux G, Seytre G, Pineri M. *Polym Eng Sci* 2000;40:36.
- [25] Yacubowicz J, Narkis M, Benguigui L. *Polym Eng Sci* 1990;30:459.
- [26] Wang YC, Anderson C. *Macromolecules* 1999;32:6172.
- [27] Kusy RP. *J Appl Phys* 1977;48:5301.
- [28] Malliaris A, Turner DT. *J Appl Phys* 1971;42:614.
- [29] Kusy RP, Corneliussen RD. *Polym Eng Sci* 1975;15:107.
- [30] Grunlan JC, Gerberich WW, Francis LF. *Polym Eng Sci* 2001;41:1947.
- [31] Scher H, Zallen R. *J Chem Phys* 1970;53:3759.
- [32] Grunlan JC, Mehrabi AR, Bannon MV, Bahr JL. *Adv Mater* 2004;16:150.
- [33] Ehrburgerdolle F, Lahaye J, Misono S. *Carbon* 1994;32:1363.
- [34] Etemad S, Quan X, Sanders NA. *Appl Phys Lett* 1986;48:607.
- [35] Hotta S, Rughooputh SDDV, Heeger AJ. *Synthetic Met* 1987;22:79.
- [36] Janzen J. *J Appl Phys* 1975;46:966.
- [37] Slupkowski T. *Phys Status Solidi A* 1984;83:329.

- [38] Bueche F. *J Appl Phys* 1972;43:4837.
- [39] Sumita M, Asai S, Miyadera N, Jojima E, Miyasaka K. *Colloid Polym Sci* 1986;264:212.
- [40] Wessling B. *Polym Eng Sci* 1991;31:1200.
- [41] Nielsen LE. *Ind Eng Chem Fund* 1974;13:17.
- [42] Mccullough RL. *Compos Sci Technol* 1985;22:3.
- [43] Huang JC. *Adv Polym Tech* 2002;21:299.
- [44] Miyasaka K, Watanabe K, Jojima E, Aida H, Sumita M, Ishikawa K. *J Mater Sci* 1982;17:1610.
- [45] Sumita M, Abe H, Kayaki H, Miyasaka K. *J Macromol Sci Phys* 1986;B25:171.
- [46] Fournier J, Boiteux G, Seytre G, Marichy G. *Synthetic Met* 1997;84:839.
- [47] Boiteux G, Fournier J, Issotier D, Seytre G, Marichy G. *Synthetic Met* 1999;102:1234.
- [48] Flandin L, Prasse T, Schueler R, Schulte K, Bauhofer W, Cavaille JY. *Phys Rev B* 1999;59:14349.
- [49] Zhang MY, Jia WT, Chen XF. *J Appl Polym Sci* 1996;62:743.
- [50] Huang JC, Wu CL. *Adv Polym Tech* 2000;19:132.
- [51] Sumita M, Sakata K, Asai S, Miyasaka K, Nakagawa H. *Polym Bull* 1991;25:265.
- [52] Gubbels F, Blacher S, Vanlathem E, Jerome R, Deltour R, Brouers F, Teyssie P. *Macromolecules* 1995;28:1559.
- [53] Mierczynska A, Friedrich J, Maneck HE, Boiteux G, Jeszka JK. *Cent Eur J Chem* 2004;2:363.

- [54] Asbeck WK, Vanloo M. *Ind Eng Chem* 1949;41:1470.
- [55] Patton TC. *Paint Flow and Pigment Dispersion*, 2nd ed. New York: Wiley, 1979.
- [56] Kim YS, Liao KS, Jan CJ, Bergbreiter DE, Grunlan JC. *Chem Mater* 2006;18:2997.
- [57] Bertrand P, Jonas A, Laschewsky A, Legras R. *Macromol Rapid Comm* 2000;21:319.
- [58] Decher G, Schlenoff JB. *Multilayer Thin Films-Sequential Assembly of Nanocomposite Materials*, Weinheim, Germany: Wiley-VCH, 2003.
- [59] Mermut O, Barrett CJ. *J Phys Chem B* 2003;107:2525.
- [60] Schoeler B, Poptoshev E, Caruso F. *Macromolecules* 2003;36:5258.
- [61] Sui ZJ, Salloum D, Schlenoff JB. *Langmuir* 2003;19:2491.
- [62] Tan HL, McMurdo MJ, Pan GQ, Van Patten PG. *Langmuir* 2003;19:9311.
- [63] Dubas ST, Schlenoff JB. *Macromolecules* 1999;32:8153.
- [64] Zhang HN, Ruhe J. *Macromolecules* 2003;36:6593.
- [65] Shiratori SS, Rubner MF. *Macromolecules* 2000;33:4213.
- [66] Choi J, Rubner MF. *Macromolecules* 2005;38:116.
- [67] McAloney RA, Sinyor M, Dudnik V, Goh MC. *Langmuir* 2001;17:6655.
- [68] Lee SH, Kumar J, Tripathy SK. *Langmuir* 2000;16:10482.
- [69] Tian SJ, Liu JY, Zhu T, Knoll W. *Chem Mater* 2004;16:4103.
- [70] Jiang CY, Markutsya S, Pikus Y, Tsukruk VV. *Nat Mater* 2004;3:721.
- [71] Zhang FX, Srinivasan MP. *Thin Solid Films* 2005;479:95.

- [72] Jan CJ, Walton MD, McConnell EP, Jang WS, Kim YS, Grunlan JC. *Carbon* 2006;44:1974.
- [73] Hiller J, Mendelsohn JD, Rubner MF. *Nat Mater* 2002;1:59.
- [74] DeLongchamp DM, Kastantin M, Hammond PT. *Chem Mater* 2003;15:1575.
- [75] Liu SQ, Kurth DG, Mohwald H, Volkmer D. *Adv Mater* 2002;14:225.
- [76] Farhat TR, Schlenoff JB. *Electrochem Solid St* 2002;5:B13.
- [77] Boulmedais F, Frisch B, Etienne O, Lavallo P, Picart C, Ogier J, Voegel JC, Schaaf P, Egles C. *Biomaterials* 2004;25:2003.
- [78] Grunlan JC, Choi JK, Lin A. *Biomacromolecules* 2005;6:1149.
- [79] Delcorte A, Bertrand P, Wischerhoff E, Laschewsky A. *Langmuir* 1997;13:5125.
- [80] Greene G, Tannenbaum R. *Appl Surf Sci* 2004;233:336.
- [81] Hougen LR. *Nature* 1960;188:577.
- [82] Carley JF, Kitze PT. *Polym Eng Sci* 1978;18:326.
- [83] Morra M, Occhiello E, Gila L, Garbassi F. *J Adhesion* 1990;33:77.
- [84] Nihlstrand A, Hjertberg T, Johansson K. *Polymer* 1997;38:3581.
- [85] Blais P, Carlsson DJ, Csullog GW, Wiles DM. *J Colloid Interf Sci* 1974;47:636.
- [86] Bergbreiter DE. *Prog Polym Sci* 1994;19:529.
- [87] Tao GL, Gong AJ, Lu JJ, Sue HJ, Bergbreiter DE. *Macromolecules* 2001;34:7672.
- [88] Bergbreiter DE, Boren D, Kippenberger AM. *Macromolecules* 2004;37:8686.
- [89] Bergbreiter DE, Simanek EE, Owsik I. *J Polym Sci Pol Chem* 2005;43:4654.

- [90] Lutkenhaus JL, Hrabak KD, McEnnis K, Hammond PT. *J Am Chem Soc* 2005;127:17228.
- [91] Foldes E, Toth A, Kalman E, Fekete E, Tomasovszky-Bobak A. *J Appl Polym Sci* 2000;76:1529.
- [92] Yu J, Zhang LQ, Rogunova M, Summers J, Hiltner A, Yu J. *J Appl Polym Sci* 2005;98:1799.
- [93] Chern CS, Hsu H. *J Appl Polym Sci* 1995;55:571.
- [94] Sperling LH. *Introduction to Physical Polymer Science*, 4th ed. Hoboken, New Jersey: Wiley, 2005 (Chapter VIII).
- [95] Grunlan JC, Ma Y, Grunlan MA, Gerberich WW, Francis LF. *Polymer* 2001;42:6913.
- [96] Agarwal N, Farris RJ. *Polym Eng Sci* 2000;40:376.
- [97] Unzueta E, Forcada J. *Polymer* 1995;36:4301.
- [98] Unzueta E, Forcada J, HidalgoAlvarez R. *Polymer* 1997;38:6097.
- [99] Tanrisever T, Okay O, Sonmezoglu IC. *J Appl Polym Sci* 1996;61:485.
- [100] Chopra KL, Paulson PD, Dutta V. *Prog Photovoltaics* 2004;12:69.
- [101] Hohnholz D, Okuzaki H, MacDiarmid AG. *Adv Funct Mater* 2005;15:51.
- [102] Granqvist CG, Azens A, Hjelm A, Kullman L, Niklasson GA, Ronnow D, Mattsson MS, Veszeli M, Vaivars G. *Sol Energy* 1998;63:199.
- [103] Kulkarni AP, Tonzola CJ, Babel A, Jenekhe SA. *Chem Mater* 2004;16:4556.
- [104] Granqvist CG, Hultaker A. *Thin Solid Films* 2002;411:1.
- [105] Major S, Chopra KL. *Sol Energ Mater* 1988;17:319.

- [106] Presley RE, Hong D, Chiang HQ, Hung CM, Hoffman RL, Wager JF. Solid State Electron 2006;50:500.
- [107] Coutts TJ, Young DL, Li X, Mulligan WP, Wu X. J Vac Sci Technol A 2000;18:2646.
- [108] Pasquier AD, Unalan HE, Kanwal A, Miller S, Chhowalla M. Appl Phys Lett 2005;87:

APPENDIX A
THERMAL AND MECHANICAL BEHAVIOR OF CARBON NANOTUBE-
FILLED LATEX*

A.1 Introduction

Single-walled carbon nanotubes (SWNTs) remain an interesting filler material for polymers due to their large aspect ratio; small diameter and relatively large length ($d \approx 1\text{nm}$ and $l \approx 1\ \mu\text{m}$), high elastic modulus ($\sim 1\ \text{TPa}$), high intrinsic electrical conductivity ($> 10^4\ \text{S/cm}$), and high thermal conductivity ($> 200\ \text{W/m}\cdot\text{K}$). SWNT-filled polymers are a unique class of composites due to their ability to achieve significant property enhancements with very low filler concentration. Significant improvements in thermal transport, electrical conductivity, and mechanical properties of polymers have been achieved with the addition of less than 1 wt% SWNTs. These types of composites are being studied for a variety of uses including actuators, electromagnetic interference (EMI) shielding, chemical sensing, and solar cells. Despite all of the progress that has been made with respect to properties and applications, processing of these composites remains a challenge. In an effort to further reduce the quantity of nanotubes required to achieve a given property enhancement, thereby making processing easier, latex has been used as the composite matrix starting material.

* Reprinted with permission from "Thermal and Mechanical Behavior of Carbon Nanotube-Filled Latex" by J. C. Grunlan and Y.-S. Kim *et al.*, 2006. *Macromolecular Materials and Engineering*, 291, 1035-1043. ©2006 WILEY-VCH Verlag GmbH & Co.

Aqueous polymer emulsions, or latexes, exist as microscopic solid polymer particles (typically 0.1 – 1 μm) suspended in water prior to film formation through coalescence . When combined with nano-sized filler, such as carbon nanotubes, the polymer particles create excluded volume that leads to a segregated network of filler and enhanced properties at very low concentration ($\ll 1$ wt%). For example, the percolation threshold for electrical conductivity was below 0.04 wt% SWNT for a thick film (>100 μm) composite made with a poly(vinyl acetate) (PVAc) latex . SWNT-filled composites of comparable thickness, made with traditional processing of a polymer solution or melt, typically show thresholds of 25 wt% or more . When multi-walled nanotubes (MWNTs) are used instead of SWNTs the threshold is even higher (> 1 wt%) due to their larger size. If similar enhancement in thermal conductivity could be realized with latex-based composites, there is potential for thermal interface materials with very low filler concentration.

Poor heat dissipation is the top problem facing microelectronics in terms of reliability and performance . Thermal stresses can warp a chip and thermal fatigue, due to rapid heating and cooling, destroys soldered joints. Thermally conductive polymer composites can be used as interface materials to dissipate heat before it can cause damage. These composites also find application in heat exchangers, appliances, and other machinery . High filler loadings (> 40 vol%) are typically required to achieve the appropriate level of thermal conductivity in these polymer composites , which presents a significant processing challenge and dramatically alters the polymer mechanical behavior. In the present work, the thermal and mechanical behavior of SWNT-filled

poly(vinyl acetate) latex-based composites are investigated. This system did not show the magnitude of thermal conductivity (k) improvement that was expected due to high thermal interface resistance associated with SWNTs, but the shape of the increase with nanotube concentration shows promise for other high aspect ratio fillers. Unlike filled polymers produced from melts or solutions, which show a nearly linear or exponential increase in thermal conductivity (k), the latex-based composite exhibits a sharp initial rise in thermal conductivity as a function of nanotube concentration. Furthermore, the combination of low thermal conductivity and relatively high electrical conductivity ($\rho \approx 5 \Omega \cdot \text{cm}$ with 4 wt% SWNT) may make this composite system a good candidate for thermoelectric applications. Other thermal properties, such as thermal diffusivity (α) and heat capacity (C_p), also show unique changes with nanotube concentration. Dynamic mechanical analysis (DMA) and differential scanning calorimetry (DSC) were also performed to evaluate the effects of the segregated nanotube network on mechanical behavior and glass transition temperature, respectively. Storage modulus above T_g was improved by an order of magnitude with the addition of only 2 wt% nanotubes, which may provide the basis for extending the usage temperature of a commodity polymer like poly(vinyl acetate).

A.2. Experimental

A.2.1. Materials

Poly(vinyl acetate) homopolymer latex (tradename Vinac XX210) was supplied by Air Products (Allentown, PA). This polymer emulsion is approximately 55 wt% solids in water with an average particle size of approximately 650 nm, although it is very polydisperse with particles ranging in size from 0.14 to 3.5 μm . The glass transition temperature (T_g) for this polymer is 34 $^{\circ}\text{C}$ and the minimum film formation temperature (MFFT) is approximately 15 $^{\circ}\text{C}$. Raw single-walled carbon nanotubes (SWNTs), containing 18 wt% iron impurity, were supplied by Rice University (Houston, TX). Gum arabic (GA), used to stabilize the SWNTs, and 1-dodecene, used for density determination of composites, were purchased from Aldrich (Milwaukee, WI).

A.2.2. Composite Preparation

Single-walled carbon nanotubes were ground into an aqueous solution, containing 2 wt% GA, with a mortar and pestle. After grinding to achieve a 1:1 SWNT:GA ratio, the mixture was sonicated for 20 minutes in a bath by Branson Ultrasonic Corporation (Danbury, CT). PVAc emulsion was then added to the GA-stabilized SWNT mixture to produce an aqueous pre-composite mixture. Blending of the pre-composite was done with an “F” style high-speed impeller blade, purchased from Paul N. Gardner (Pompano Beach, FL), attached to a drill press and operated at 3100 rpm for 15 minutes. The composite with the highest concentration of SWNTs (i.e.,

3wt%) was mixed first, followed by lower concentration mixtures created by further diluting the initial mixture with more emulsion and deionized water. These aqueous pre-composite mixtures were kept at a constant 10 wt% solids during processing. Solid composites were made by drying these aqueous mixtures within a 2 in.² plastic mold for 72 hours under ambient conditions. Dry composite films produced with this technique are $520 \pm 30 \mu\text{m}$.

A.2.3. Density Determination

Density of each film was calculated by measuring the mass and volume of composite pieces. These density values were a required input to calculate thermal conductivity. The mass was obtained using an analytical balance and volume was calculated by measuring the mass of a piece in air and in 1-dodecene and applying the Archimedes law, which states that the volume of a material is the difference between mass in air and mass in a reference liquid divided by the density of the reference liquid. Poly(vinyl acetate) absorbs many common solvents and water, but 1-dodecene ($\rho = 0.758 \text{ g/cm}^3$) is relatively incompatible and therefore a good solvent for density measurement. The mass of samples after immersion in 1-dodecene was measured to confirm that they did not absorb any solvent. Further analysis of the density data reveals some interesting points. Figure A.1 shows composite density as a function of SWNT volume percent. The data points represent the experimentally obtained values; however, a value for SWNT density had to be assumed to convert wt% to vol%. To make this assumption, three lines were constructed that represent density of the composite

specimens if the volume additivity law is assumed for the samples with assumed SWNT densities of 1.6, 1.7, or 1.8 g/cm³. The equation for density of a composite when volume additivity holds is:

$$\rho_{\text{composite}} = \rho_{\text{polymer}} \phi_{\text{polymer}} + \rho_{\text{nanotube}} \phi_{\text{nanotube}} \quad (\text{A.1})$$

where ρ is the density and ϕ is the volume fraction of a given component. Information about the composite microstructure from SEM images was used in conjunction with the data in Figure A.1 to obtain an appropriate SWNT density. SEM micrographs (Figure A.3) show these composites to have porosity, which mean the experimentally measured density values are expected to be below the additivity line. The only line in Figure A.1 that fits this criterion is for a SWNT density of 1.8 g/cm³. It should also be noted that the density of samples between 0.9 and 2.5 wt% SWNT forms a line that is steeper than any of the additivity lines in Figure A.1 (shown as a gray line). This suggests that voids formed by the addition of 0.9 wt% SWNT were filled with the addition of more nanotubes, up to 2.5 wt%. An initial nanotube network was created by the addition of 0.9 wt% SWNT, which is referred to as the pre-existing network. It is not clear whether a more extensive network is formed by the addition of nanotubes beyond 0.9 wt% or if these nanotubes simply agglomerate within the pre-existing network. At 3 wt% SWNT, the density decreases due to greater void formation in the composite (seen clearly in Figure A.3). Based upon this information, a SWNT density of 1.8 g/cm³ was chosen to

convert wt% to vol% in Table 1 and in the figures below. This value is larger than commonly accepted in the literature ($1.33 - 1.5 \text{ g/cm}^3$), but the nanotubes used here contain 18 wt% iron catalyst impurity that is believed responsible for this elevated value.

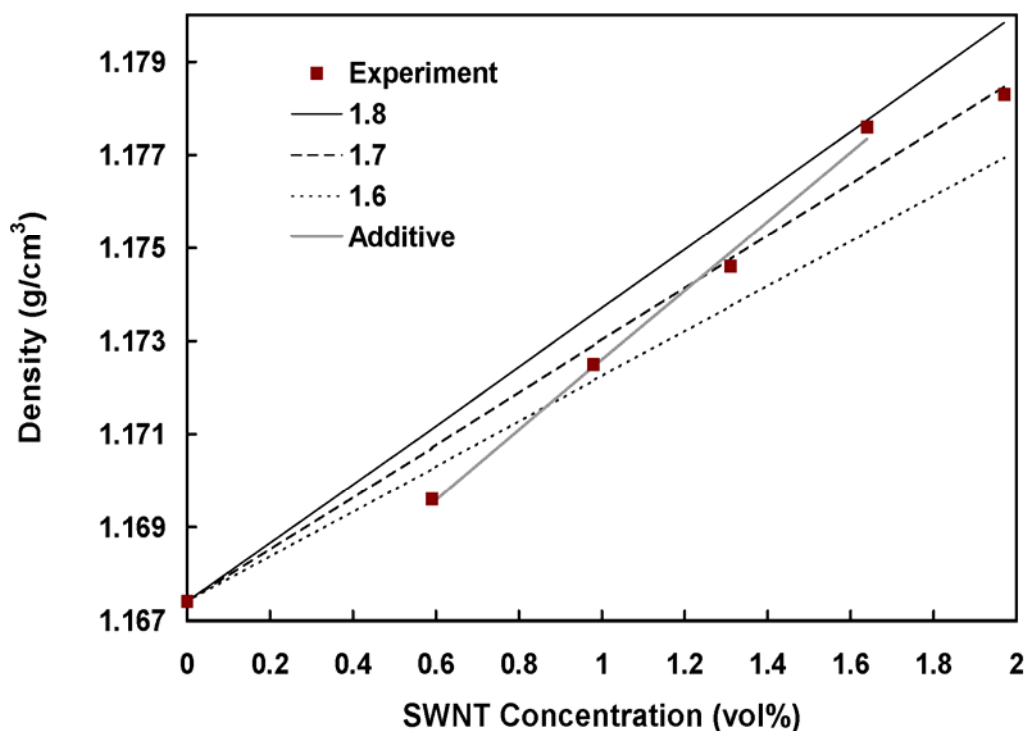


Figure A.1. Composite density as a function of single-walled carbon nanotube concentration in poly(vinyl acetate). Experimental data points are compared with density of model composites obeying volume additivity law with SWNT density of 1.6, 1.7, and 1.8 g/cm^3 . The thick gray line through the four middle points is a straight line fit ($R^2 > 0.99$) demonstrating that additivity is being obeyed.

A.2.4. Thermal Conductivity Measurement

Thermal diffusivity and specific heat of neat poly(vinyl acetate) (PVAc) and its composites with single walled carbon nanotubes (SWNTs) were measured at approximately 11 °C using a Holometrix Micro-Flash instrument, which uses the flash method. Circular samples, with a nominal diameter of 12 mm, were used for testing. The disks were sputtered with gold to make them reflective and sprayed with graphite to obtain uniform heat distribution on the surface. Sample thickness, before gold and graphite coating, was used to by the Holometrix software for calculation purposes. Thermal conductivity () was calculated using:

$$\kappa = \alpha \rho C_p \quad (\text{A.2})$$

where α is thermal diffusivity (cm^2/s), ρ is bulk density (g/cm^3), and C_p is specific heat ($\text{J}/\text{g}\cdot^\circ\text{C}$). Table A.1 shows the values of density, thermal diffusivity, specific heat, and thermal conductivity that were measured or calculated for the emulsion-based films with varying nanotube concentration.

Table A.1. Density and thermal properties of SWNT-filled latex films.

SWNT (wt%) ^{a)}	SWNT (vol%) ^{b)}	(g/cm ³)	(cm ² /s)	C _p (J/g·°C)	(W/m·K)
0	0	1.1674	0.00153	1.1837	0.21118
0.9	0.59	1.1696	0.00139	1.2816	0.20822
1.5	0.98	1.1725	0.00153	1.2308	0.22040
2.0	1.31	1.1746	0.00159	1.2243	0.22937
2.5	1.64	1.1776	0.00161	1.2294	0.23293
3.0	1.97	1.1783	0.00182	1.0603	0.22685

^{a)} Single-walled carbon nanotube wt% includes weight contributed by non-nanotube impurities.

^{b)} Nanotube vol% was calculated using the known density of the PVAc matrix and assuming a density of 1.8 g/cm³ for the SWNTs.

A.2.5. Thermal Analysis

Glass transition temperatures of the composite films were measured with a Q1000 Differential Scanning Calorimeter (DSC) by TA Instruments (New Castle, DE). Samples were scanned from 0 – 50 °C at 2 °C/minute. Composite storage modulus (E') was measured as a function of temperature with Q800 Dynamic Mechanical Analyzer (DMA) from TA Instruments. Films were cut into strips that were approximately 25 mm long and 3 mm wide. These strips were measured in tensile mode with amplitude of oscillation maintained between 8 and 10 μm. Temperature was raised from -10 – 160 °C, at a rate of 2 °C/minute, during testing.

A.3. Results and Discussion

A.3.1. Composite Microstructure

The use of a polymer emulsion (i.e., latex) as the matrix for the composite produces a microstructure that is unique relative to those obtained from solution or melt-based processing. Unlike these latter systems, the polymer in latex remains solid during all processing steps from mixing to drying into a composite film. Latex begins as microscopic polymer spheres (typically 0.1 – 1 μm in diameter) suspended in water with the aid of a stabilizer (e.g., surfactant). The carbon nanotubes are suspended with the latex with the help of gum Arabic, which stabilizes them in water. During drying, in the presence of the much smaller dimension filler material, a segregated network microstructure is formed due to excluded volume created by the polymer particles. In a solution or melt-based composite, filler particles can be randomly placed anywhere within the polymer matrix. In contrast, filler particles are restricted to the interstitial space between the much larger polymer particles in a latex-based composite. Figure A.2 schematizes the process of segregated network formation during drying. Some amount of interdiffusion occurs between the polymer particles as they become close-packed, which is a process known as coalescence. In the case of poly(vinyl acetate), full coalescence does not occur at room temperature due to its proximity to the minimum film formation temperature of PVAc. Even without perfect coalescence the composite films containing SWNTs are mechanically coherent and exhibit a highly segregated microstructure.

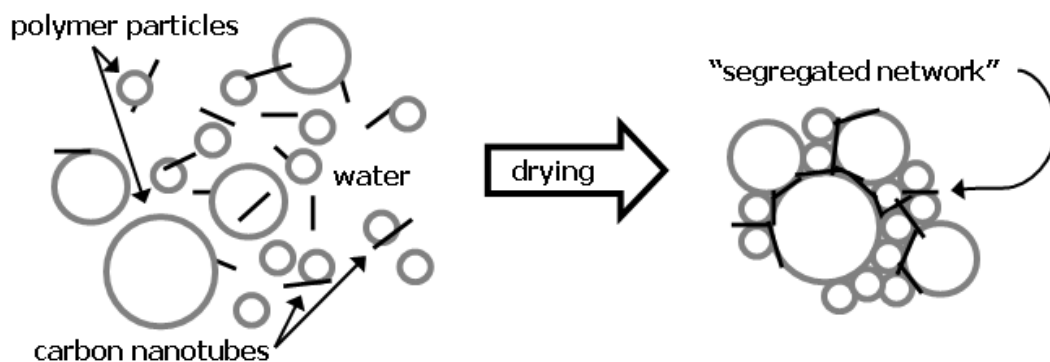


Figure A.2. Schematic illustration of the formation of a segregated network of carbon nanotubes during the drying of a water-based polymer emulsion. Boundaries between the polymer particles would disappear, in the image on the right, if the polymer emulsion were able to fully coalesce.

Figure A.3 shows SEM images of freeze-fractured poly(vinyl acetate) latex-based composites containing SWNTs. These images clearly show the segregated network microstructure described above. At a concentration of just 0.65 vol% SWNT an extended bundle of ropes is observed (see Fig. A.3(a)) and the system is known to be fully networked (i.e., above the percolation threshold). As the nanotube concentration increases from 0.9 to 3 wt% (0.59 to 1.97 vol%) the network becomes bulkier. Polymer particle coalescence appears to improve as the filler concentration increases. This phenomenon is not clearly understood, but has also been observed in carbon black-filled latex. Increasing levels of composite porosity also accompany higher nanotube concentrations. Pore formation is due to the inability of the solid polymer particles to envelop the filler, thereby creating microscopic voids between SWNTs that increase in size with increasing concentration. This effect, known as the critical pigment volume

concentration (CPVC) , is observed in all filled polymers. Eventually pores begin to connect with one another and relatively large-scale defects form, as shown in Figure A.3(d). In segregated network composites, porosity occurs at much lower filler concentrations due to the restricted volume in which the particles must pack .

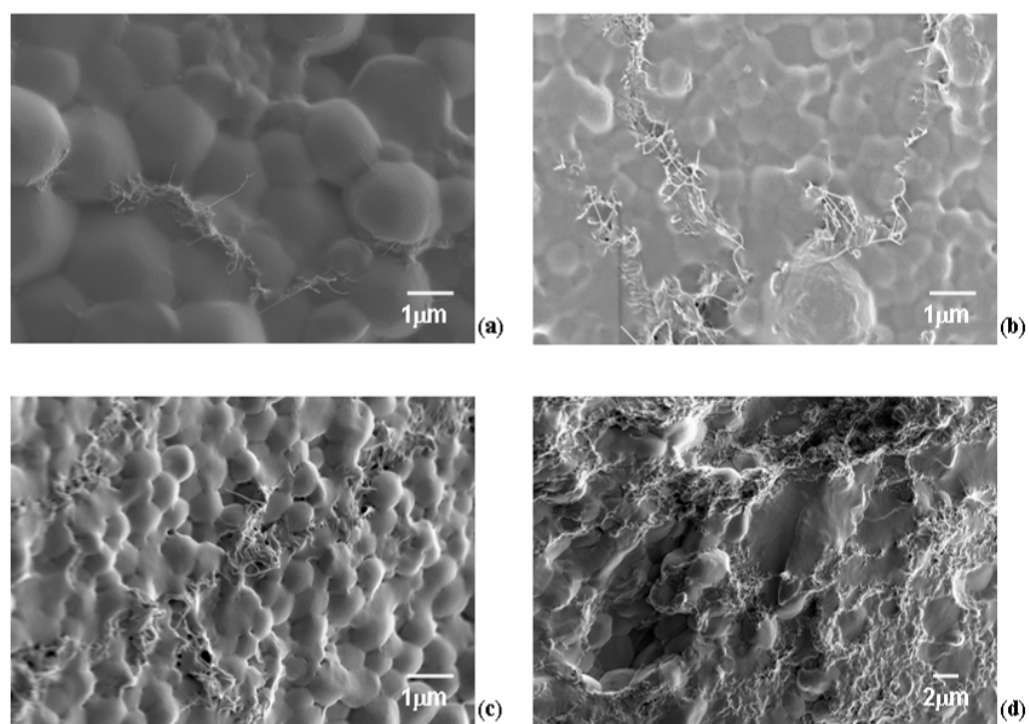


Figure A.3. Freeze-fractured cross-sections of dried poly(vinyl acetate) latex filled with 0.59 (a), 1.31 (b), and 1.97 vol% SWNT (c – d). The lower magnification image (d) highlights the extensive porosity present in the composite containing 1.97 vol% SWNT.

Density measurements (see Figure A.1) suggest that porosity does not grow significantly between SWNT concentrations of 0.9 and 2.5 wt%. The thick gray line that goes through the data points for 0.9 wt% to 2.5 wt% in Figure A.1 indicates that the density of these samples follows an additive rule. This straight line ($R^2 > 0.99$) has a slope that is steeper than those of lines constructed using 1.6, 1.7, and 1.8 g/cm³ as the densities of SWNT. This result suggests that the addition of SWNT (up to 2.5 wt%) fills in pre-existing nano-void space in the latex interstices that offsets any CPVC-related pore formation. At a concentration of 3 wt%, porosity becomes the more dominant factor as accessible interstitial space runs out. It seems as though carbon nanotubes tend to saturate these initially formed pathways before creating new ones. The amount of available interstitial volume and network growth in a given system will be affected by the size and distribution of latex particles, the polymer nanotube interaction, and the affinity of SWNTs for each other.

A.3.2. Thermal Behavior

The SEM micrographs in Figure A.3 suggest that the bundles of SWNT are present throughout the matrix but they are not mixed with the polymer at the molecular level. Figure A.4 shows reversible heat flow as a function of temperature for the series of SWNT-filled poly(vinyl acetate) composites. The vertical line drawn at 34°C highlights the glass transition temperature of neat PVAc, which is taken as the middle of the drop in heat flow.

Although the T_g fluctuates somewhat with the addition of nanotubes, it does not vary more than one or two degrees regardless of SWNT concentration. Composites with strong polymer-filler interactions should exhibit increasing T_g with filler concentration due to restricted motion of the polymer chains, but in this case T_g is essentially constant. This result confirms that there is little or no molecular level interaction between the PVAc matrix and carbon nanotubes. Gum Arabic stabilized nanotubes are expected to have a strong affinity for one another during drying, which further supports the idea of nanotubes first filling existing pathways prior to generating a more extensive network that would produce more undesirable contacts with the polymer matrix.

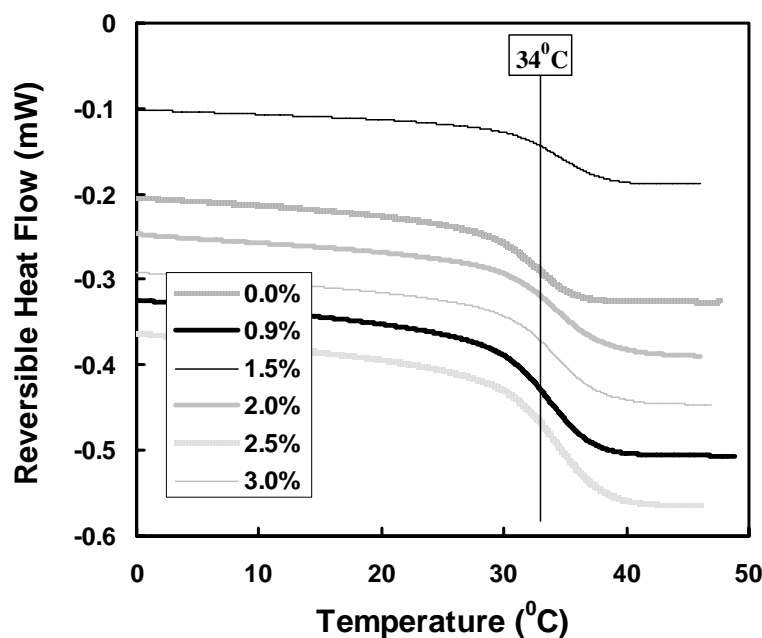


Figure A.4. Reversible heat flow as a function of temperature for composites with varying concentration of SWNT. All of the systems exhibit an inflection, that marks the glass transition temperature, within two degrees of 34°C.

Figure A.5 shows thermal diffusivity (α) and heat capacity (C_p) as a function of nanotube concentration. An increasing trend in thermal diffusivity is observed for all samples containing SWNT (see Table A.1). The initial drop in α relative to neat PVAc is likely due to porosity that was created by the addition of the nanotubes. The gradual increase in α from 0.59 to 1.64 vol% SWNT could be due to the increasing concentration of SWNT in a pre-existing network (formed in the 0.59 vol% sample) or due to the formation of a more extensive network. The density measurements shown in Figure A.1, combined with the fact that α is reaching a plateau at 1.64 vol% SWNT, suggests that thermal diffusivity is increasing due to the increase of nanotubes in a pre-existing network. The abrupt increase at 1.97 vol% SWNT could be due to formation of more networks in the sample. Heat capacity follows a similar trend, but decreases with nanotube concentration. The initial increase in C_p with the addition of 0.59 vol% SWNT is an unexpected result, but this may be due to the presence of water-soluble gum Arabic as a stabilizer. Increased porosity is the reason for the significant drop in C_p between 1.64 and 1.97 vol% SWNT. Thermal conductivity, calculated using Equation A.2, exhibits similar transitions to those seen in diffusivity and specific heat.

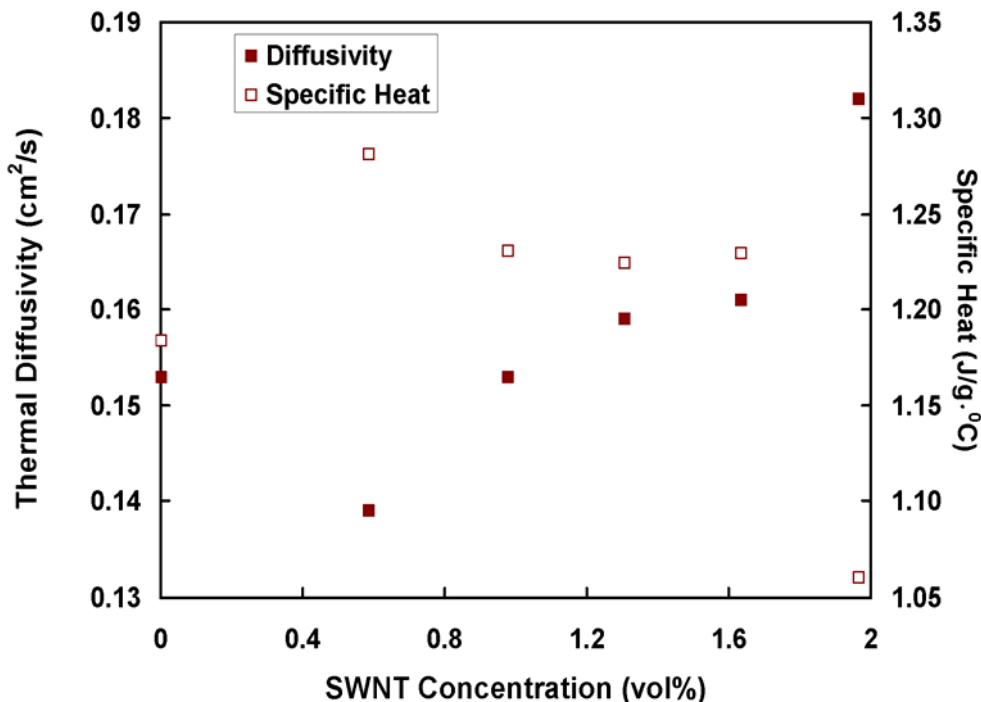


Figure A.5. Thermal diffusivity and specific heat capacity as a function of nanotube concentration in poly(vinyl acetate).

The variation of thermal conductivity with SWNT content is shown in Figure A.6. There is consistent increase in thermal conductivity with nanotube concentration following an anomalous decrease at the lowest SWNT concentration, similar to that seen in Table A.1 for thermal diffusivity. This initial drop in conductivity resembles the decrease in strength that is sometimes observed at very low volume fraction of fibers in a composite, known as the minimum fiber volume fraction (MFVF). This same effect has never been described for thermal conductivity, but is likely another result of porosity and poor interaction between filler and matrix (much like the anomalous jump in specific heat shown in Table A.1). A maximum κ is reached at 1.64 vol% SWNT, but is only

10% greater than that of the unfilled polymer matrix. This level of conductivity enhancement falls well below most theoretical predictions, assuming an intrinsic SWNT conductivity of 1000 W/m·K or more. Interfacial thermal resistance has been proposed as the reason for such a low κ value in nanotube-filled composites. In a latex-based system this thermal resistance is magnified by the need for an insulating stabilizing agent (i.e., gum Arabic) to disperse nanotubes in water. Despite the lack of significant improvement in thermal conductivity, the sharp increase as a function of nanotube loading is a unique trend that is due to the segregated network microstructure and could be better exploited with a high aspect ratio nano-filler with lower interfacial resistance (e.g., multi-walled nanotubes) or one that did not require a stabilizer. For example, single crystal alumina nanowires could potentially be stabilized in water by varying pH to generate a stabilizing surface charge. The eventual drop in κ is due to increasing levels of porosity in the composite and is also observed in composite modulus in the next section.

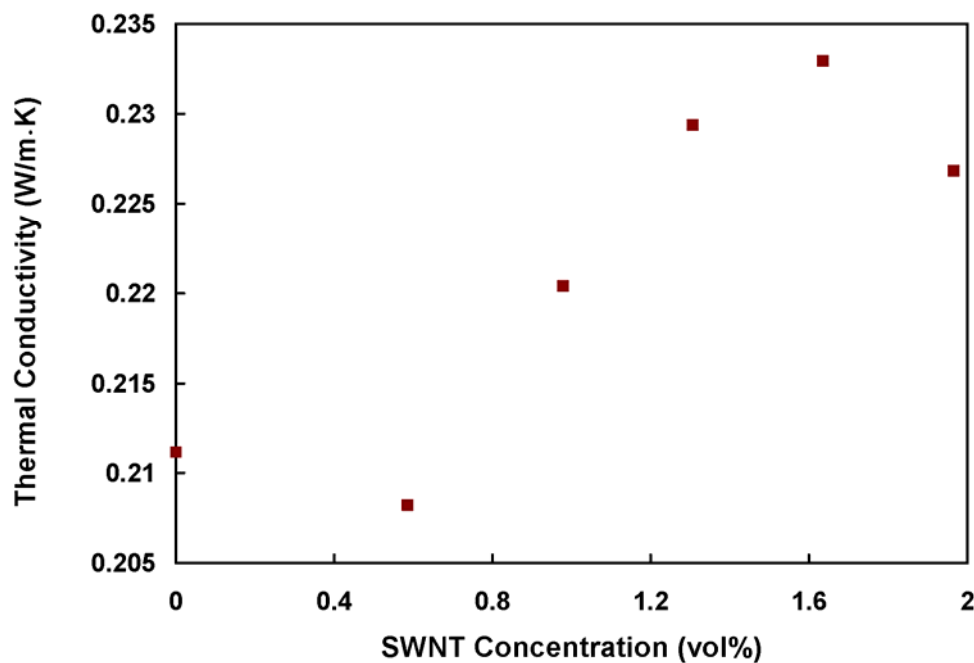


Figure A.6. Thermal conductivity as a function of nanotube concentration in poly(vinyl acetate).

A.3.3. Mechanical Properties

Figure A.7 shows how the storage modulus (E') changes as a function of SWNT concentration at 25 °C. E' increases to a maximum of 2.85 GPa at approximately 1 vol% SWNT before gradually declining as porosity develops in the composite. This 46% increase in storage modulus with such a small nanotube concentration is comparable to, and in some cases better than, modulus enhancements recently seen in solution or melt-based systems. These results are well predicted by the Halpin-Tsai model for randomly-oriented, short fiber composites :

$$E_{random} = \frac{3}{8}E_L + \frac{5}{8}E_T \quad (A.3)$$

where E_L is the elastic modulus for oriented short fibers in the longitudinal direction:

$$E_L = E_m \left(\frac{1 + (2l/d)\eta_L\phi_f}{1 - \eta_L\phi_f} \right) \quad (A.4)$$

and E_T is the elastic modulus for oriented short fibers in the transverse direction:

$$E_T = E_m \left(\frac{1 + 2\eta_T\phi_f}{1 - \eta_T\phi_f} \right) \quad (A.5)$$

where ϕ_f is the volume fraction of fibers, l is nanotube length, d is nanotube diameter, E_m is the poly(vinyl acetate) matrix modulus (experimentally determined to be 1.93 GPa), E_f is the nanotube modulus (assumed to be 1000 GPa), η_L is defined by:

$$\eta_L = \frac{E_f / E_m - 1}{E_f / E_m + (2l/d)} \quad (A.6)$$

and η_T is defined by:

$$\eta_T = \frac{E_f/E_m - 1}{E_f/E_m + 2} \quad (\text{A.7})$$

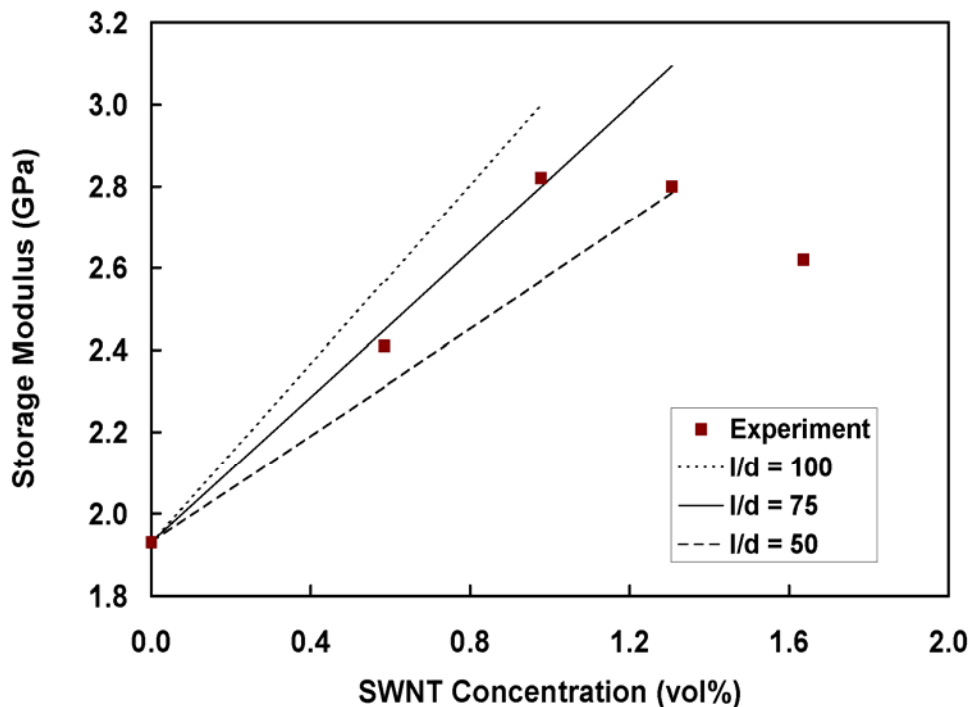


Figure A.7. Storage modulus as a function of single-walled carbon nanotube concentration in poly(vinyl acetate). Experimental data, measured at 25⁰C, is compared to the prediction of the Halpin Tsai model (Equations A.3 – A.7) for different nanotube length to diameter ratios.

In this case we are assuming that the elastic modulus and storage modulus are approximately equal, which is a reasonable approximation at room temperature . Furthermore, the effective SWNT l/d is a variable quantity determined by the composite microstructure. The best fit to the experimental data was found when a value of 75 was

used for the length to diameter ratio. While this is a small aspect ratio for individual nanotubes, it is not unreasonable in the present system due to the heavy aggregation that is caused during composite film formation. A highly magnified image of a nanotube cluster, within a composite containing 1.31 vol% SWNT, is shown in Figure A.8. From this image it is clear that the SWNT ropes have diameters of 30 – 40 nm, which would give an aspect ratio of 75 if the effective length is 2.25 – 3 μm .

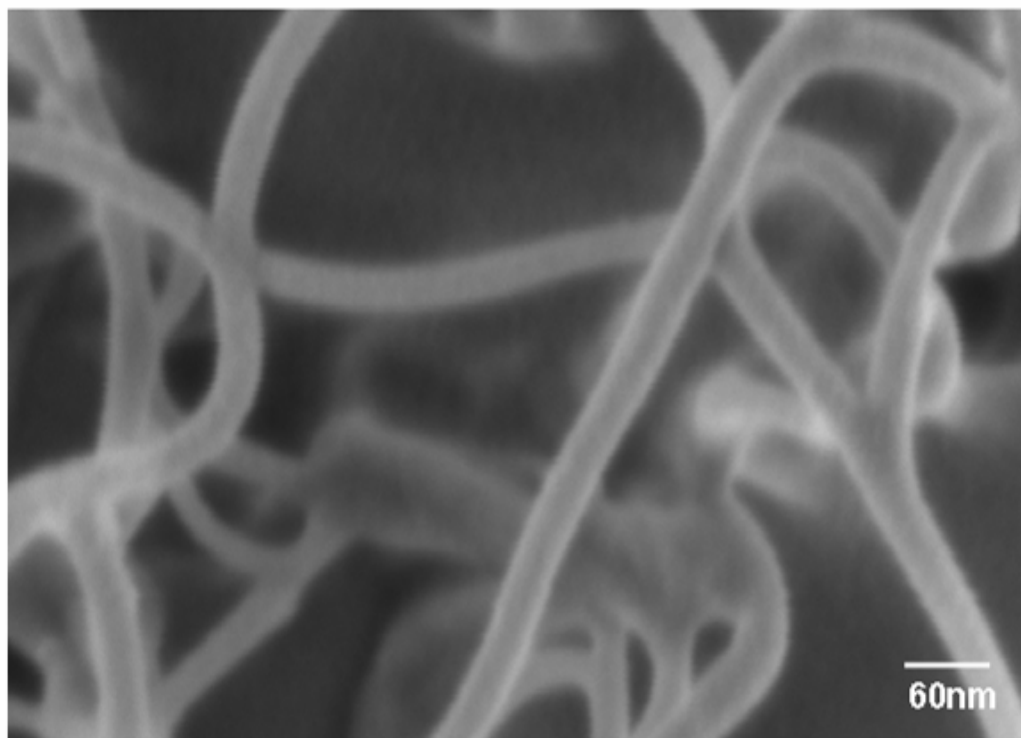


Figure A.8. High magnification freeze-fractured SEM image of cluster of SWNT ropes in composite containing 1.31 vol% nanotubes. Individual bundles are 30 – 40 nm in diameter based upon this representative image.

Modulus enhancement is much more significant above the glass transition temperature, as shown in Figure A.9. The overall trend is similar to that below the T_g of poly(vinyl acetate) (Fig. A.7), but the maximum increase in E' is an order of magnitude greater than that of unfilled PVAc, rising from 7.7 to 68.6 MPa with 1.31 vol% SWNT. This unprecedented result suggests that the segregated network of nanotubes remains largely intact at elevated temperatures. In non-segregated solution and melt-based systems the SWNT network is very fragile at these low concentrations and little or no modulus improvement with SWNT concentration would be expected due to network break up as the matrix thermally expands. This is in contrast to the latex-based composites, where extensive nanotube networking is already present at concentrations less than 1.5 vol%. Additionally, the effects of porosity appear to be postponed at this elevated temperature, resulting in a peak modulus at higher SWNT concentration relative to that at 25 °C. These results offer the possibility for commodity thermoplastics (e.g., PVAc, PMMA, PS, etc.) to be mechanically useful at temperatures well above T_g with only 1 – 1.5 vol% added filler.

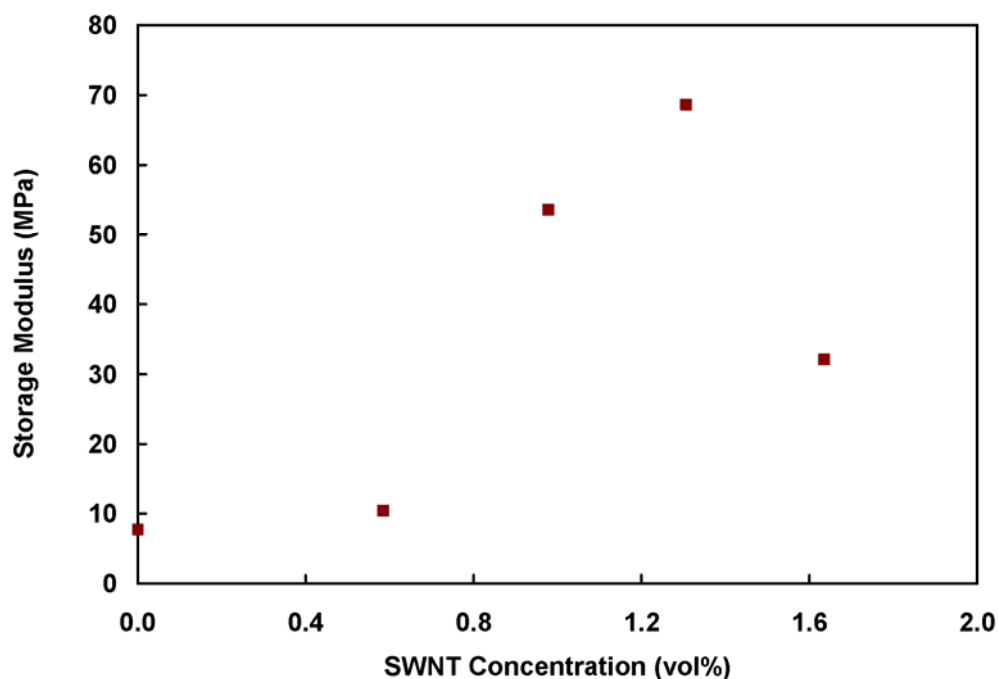


Figure A.9. Storage modulus as a function of single-walled carbon nanotube concentration in poly(vinyl acetate) measured at 60°C.

A.4. Conclusions

Mixing single-walled carbon nanotubes into a polymer emulsion produces a segregated network upon drying. This unique microstructure leads to transport and mechanical property enhancement at very low filler concentration. Density measurements suggest that the segregated network formed at low SWNT concentration progressively grows denser with further nanotube addition before eventually generating new pathways. The trend in thermal diffusivity appears to support this assertion. Thermal conductivity of this SWNT-PVAc composite system was well below that predicted by theory due to interfacial thermal resistance. Future work to improve κ will

focus on other types of high aspect ratio nanotubes and nanowires with lower interfacial resistance and/or better dispersion behavior in water without the use of a dispersing agent. Storage modulus showed good improvement with increasing SWNT concentration, especially above the glass transition temperature. At 25 °C (below T_g), composite modulus was well predicted by the Halpin-Tsai model. The thick nanotube network generated as a result of latex excluded volume appears to lessen the drop in modulus that occurs when the composite is heated beyond its glass transition temperature. This post T_g modulus enhancement was nearly an order of magnitude, making the composite transition from rubbery to leathery. Further study of this phenomenon could lead to extended use temperatures for latex systems containing small quantities of nanotubes. All of the properties studied showed an eventual degradation due to increasing levels of porosity as a function of SWNT concentration. In future studies, composites will be dried at elevated temperatures ($> T_g$), which should enhance latex coalescence and reduce porosity.

A.5. References

Agarwal N, Farris RJ. *Polymer Engineering and Science* 2000;40:376-390.

An KH, Jeong SY, Hwang HR, Lee YH. *Advanced Materials* 2004;16:1005-+.

Asbeck WK, Vanloo M. *Industrial and Engineering Chemistry* 1949;41:1470-1475.

Bandyopadhyaya R, Nativ-Roth E, Regev O, Yerushalmi-Rozen R. *Nano Letters* 2002;2:25-28.

- Bansal A, Yang HC, Li CZ, Cho KW, Benicewicz BC, Kumar SK, Schadler LS. *Nature Materials* 2005;4:693-698.
- Barrera EV. *Jom-Journal of the Minerals Metals & Materials Society* 2000;52:A38-A42.
- Bekyarova E, Davis M, Burch T, Itkis ME, Zhao B, Sunshine S, Haddon RC. *Journal of Physical Chemistry B* 2004;108:19717-19720.
- Benoit JM, Corraze B, Lefrant S, Blau WJ, Bernier P, Chauvet O. *Synthetic Metals* 2001;121:1215-1216.
- Biercuk MJ, Llaguno MC, Radosavljevic M, Hyun JK, Johnson AT, Fischer JE. *Applied Physics Letters* 2002;80:2767-2769.
- Borodin O, Smith GD, Bandyopadhyaya R, Bytner E. *Macromolecules* 2003;36:7873-7883.
- Bouchet J, Carrot C, Guillet J, Boiteux G, Seytre G, Pineri M. *Polymer Engineering and Science* 2000;40:36-45.
- Cadek M, Coleman JN, Ryan KP, Nicolosi V, Bister G, Fonseca A, Nagy JB, Szostak K, Beguin F, Blau WJ. *Nano Letters* 2004;4:353-356.
- Chen G, Dresselhaus MS, Dresselhaus G, Fleurial JP, Caillat T. *International Materials Reviews* 2003;48:45-66.
- Chesnokov SA, Nalimova VA, Rinzler AG, Smalley RE, Fischer JE. *Physical Review Letters* 1999;82:343-346.
- Correa RA, Nunes RCR, Franco WZ. *Polymer Composites* 1998;19:152-155.
- Du FM, Fischer JE, Winey KI. *Journal of Polymer Science Part B-Polymer Physics* 2003;41:3333-3338.

- Fu SJ, Wu PP, Han ZW. *Composites Science and Technology* 2002;62:3-8.
- Gaal PS, Thermitus MA, Stroe DE. *Journal of Thermal Analysis and Calorimetry* 2004;78:185-189.
- Grunlan JC, Gerberich WW, Francis LF. *Polymer Engineering and Science* 2001;41:1947-1962.
- Grunlan JC, Gerberich WW, Francis LF. *Journal of Applied Polymer Science* 2001;80:692-705.
- Grunlan JC, Grigorian A, Hamilton CB, Mehrabi AR. *Journal of Applied Polymer Science* 2004;93:1102-1109.
- Grunlan JC, Mehrabi AR, Bannon MV, Bahr JL. *Advanced Materials* 2004;16:150-+.
- Guo H, Sreekumar TV, Liu T, Minus M, Kumar S. *Polymer* 2005;46:3001-3005.
- Halpin JC, Kardos JL. *Polymer Engineering and Science* 1976;16:344-352.
- Hone J, Llaguno MC, Biercuk MJ, Johnson AT, Batlogg B, Benes Z, Fischer JE. *Applied Physics a-Materials Science & Processing* 2002;74:339-343.
- Huxtable ST, Cahill DG, Shenogin S, Xue LP, Ozisik R, Barone P, Usrey M, Strano MS, Siddons G, Shim M, Keblinski P. *Nature Materials* 2003;2:731-734.
- Kashiwagi T, Grulke E, Hilding J, Groth K, Harris R, Butler K, Shields J, Kharchenko S, Douglas J. *Polymer* 2004;45:4227-4239.
- Keddie JL. *Materials Science & Engineering R-Reports* 1997;21:101-170.
- Kim P, Shi L, Majumdar A, McEuen PL. *Physica B-Condensed Matter* 2002;323:67-70.
- King JA, Tucker KW, Meyers JD, Weber EH, Clingerman ML, Ambrosius KR. *Polymer Composites* 2001;22:142-154.

- Krupa I, Novak I, Chodak I. *Synthetic Metals* 2004;145:245-252.
- Kumlutas D, Tavman IH, Coban MT. *Composites Science and Technology* 2003;63:113-117.
- Kusy RP. *Journal of Applied Physics* 1977;48:5301-5305.
- Kymakis E, Alexandrou I, Amaratunga GAJ. *Journal of Applied Physics* 2003;93:1764-1768.
- Landi BJ, Raffaele RP, Castro SL, Bailey SG. *Progress in Photovoltaics* 2005;13:165-172.
- Landi BJ, Raffaele RP, Heben MJ, Alleman JL, VanDerveer W, Gennett T. *Nano Letters* 2002;2:1329-1332.
- Lei M, Francis LF, Scriven LE. *Journal of Coatings Technology* 2003;75:95-102.
- Levitsky IA, Kanelos P, Euler WB. *Journal of Chemical Physics* 2004;121:1058-1065.
- Lewis TB, Nielsen LE. *Journal of Applied Polymer Science* 1970;14:1449-&.
- Li XD, Gao HS, Scrivens WA, Fei DL, Xu XY, Sutton MA, Reynolds AP, Myrick ML. *Nanotechnology* 2004;15:1416-1423.
- Liao YH, Marietta-Tondin O, Liang ZY, Zhang C, Wang B. *Materials Science and Engineering a-Structural Materials Properties Microstructure and Processing* 2004;385:175-181.
- Lovell PA, El-Aasser MS. *Emulsion Polymerization and Emulsion Polymers*, New York: John Wiley & Sons, 1997.
- Manchado MAL, Valentini L, Biagiotti J, Kenny JM. *Carbon* 2005;43:1499-1505.

- Maxwell JC. A Treatise on Electricity and Magnetism, New York: Dover, 1954 (Chapter IX).
- Nan CW, Liu G, Lin YH, Li M. Applied Physics Letters 2004;85:3549-3551.
- Nan CW, Shi Z, Lin Y. Chemical Physics Letters 2003;375:666-669.
- Ng HY, Lu XH, Lau SK. Polymer Composites 2005;26:66-73.
- Nikolaev P, Bronikowski MJ, Bradley RK, Rohmund F, Colbert DT, Smith KA, Smalley RE. Chemical Physics Letters 1999;313:91-97.
- Ou YC, Yu ZZ, Vidal A, Donnet JB. Journal of Applied Polymer Science 1996;59:1321-1328.
- Ounaies Z, Park C, Wise KE, Siochi EJ, Harrison JS. Composites Science and Technology 2003;63:1637-1646.
- Pan N. Polymer Composites 1993;14:85-93.
- Potschke P, Bhattacharyya AR, Janke A, Pegel S, Leonhardt A, Taschner C, Ritschel M, Roth S, Hornbostel B, Cech J. Fullerenes Nanotubes and Carbon Nanostructures 2005;13:211-224.
- Qian D, Dickey EC, Andrews R, Rantell T. Applied Physics Letters 2000;76:2868-2870.
- Rahman GMA, Guldi DM, Cagnoli R, Mucci A, Schenetti L, Vaccari L, Prato M. Journal of the American Chemical Society 2005;127:10051-10057.
- Ramasubramaniam R, Chen J, Liu HY. Applied Physics Letters 2003;83:2928-2930.
- Rege K, Raravikar NR, Kim DY, Schadler LS, Ajayan PM, Dordick JS. Nano Letters 2003;3:829-832.
- Regev O, ElKati PNB, Loos J, Koning CE. Advanced Materials 2004;16:248-+.

- Roberts JA, Imholt T, Ye Z, Dyke CA, Price DW, Tour JM. *Journal of Applied Physics* 2004;95:4352-4356.
- Schlelling P, Shi L, Goodson K. *Materials Today* 2005;8:30-35.
- Seo MK, Park SJ. *Chemical Physics Letters* 2004;395:44-48.
- Sim LC, Ramanan SR, Ismail H, Seetharamu KN, Goh TJ. *Thermochimica Acta* 2005;430:155-165.
- Spinks GM, Xi BB, Truong VT, Wallace GG. *Synthetic Metals* 2005;151:85-91.
- Starr FW, Schroder TB, Glotzer SC. *Macromolecules* 2002;35:4481-4492.
- Stephan C, Nguyen TP, Lahr B, Blau W, Lefrant S, Chauvet O. *Journal of Materials Research* 2002;17:396-400.
- Thess A, Lee R, Nikolaev P, Dai HJ, Petit P, Robert J, Xu CH, Lee YH, Kim SG, Rinzler AG, Colbert DT, Scuseria GE, Tomanek D, Fischer JE, Smalley RE. *Science* 1996;273:483-487.
- Tsutsumi N, Takeuchi N, Kiyotsukuri T. *Journal of Polymer Science Part B-Polymer Physics* 1991;29:1085-1093.
- Weaver JC. *Journal of Coatings Technology* 1992;64:45-46.
- Weber EH, Clingerman ML, King JA. *Journal of Applied Polymer Science* 2003;88:112-122.
- Wong CP, Bollampally RS. *Journal of Applied Polymer Science* 1999;74:3396-3403.
- Xu YS, Luo XC, Chung DDL. *Journal of Electronic Packaging* 2000;122:128-131.
- Yu MF, Files BS, Arepalli S, Ruoff RS. *Physical Review Letters* 2000;84:5552-5555.

Zhang XF, Liu T, Sreekumar TV, Kumar S, Moore VC, Hauge RH, Smalley RE. Nano Letters 2003;3:1285-1288.

Zhou J, Deng SZ, Chen J, She JC, Xu NX. Chemical Physics Letters 2002;365:505-508.

Zweben C. 2001;2

(http://www.coolingzone.com/Guest/News/NL_APR_2001/Main.html).

VITA

Yeon Seok Kim was born in Suwon, Republic of Korea in 1973. He received his Bachelor of Science degree from Chung-Ang University, Seoul, Korea in 1998. After completing his B.S., he began his graduate studies at Purdue University in the field of the mechanical engineering and earned his M.S. degree in 2002. His master's coursework emphasis was on CAD and manufacturing. He completed his Ph. D. program at Texas A&M University in the Department of Mechanical Engineering under the supervision of Dr. Jaime Grunlan in 2007. His research interests include development and characterization of conducting polymer nanocomposites. His permanent address is: 103-901 Sunkyung APT, Wuman-Dong, Kyunggi-Do, Republic of Korea.